ADP-93-217/T135

Non-Perturbative Aspects of Hadron Structure Examined Through Deep-Inelastic Scattering

A.W.Thomas and W.Melnitchouk[1]

Department of Physics and Mathematical Physics, The University of Adelaide
Adelaide S.A. 5005 AUSTRALIA

ADP-93-217-T135
ADP-93-217-T135
Fermilab Library
0 1160 0032115 2
MAY 16 1994
LIBRARY

1 INTRODUCTION

Understanding the structure of the nucleon is clearly one of the most challenging problems in modern physics. Apart from its intrinsic interest, there is by now a broad appreciation of the role its internal structure plays in determining the properties of finite nuclei. While lattice devotees continue to work on the brute force solution of QCD, the range and sophistication of phenomenological models of hadron structure continues to grow. On the other hand, the tests usually applied to those models tend to be rather indirect. It is really only in the last ten years or so that deep-inelastic scattering data, which is our *only* direct view of the quarks inside hadrons, has been taken seriously as a source of useful information [1, 2].

In these lectures we shall outline some of the progress that has been made in using deep-inelastic scattering (DIS) to refine our knowledge of hadron structure. Of course, in order to be reasonably self-contained we need to devote the first few sections to the kinematics of DIS, the parton model and the standard machinery required to treat DIS within QCD – namely the operator product expansion and the renormalisation group. In sect.4 we turn to recent work which successfully connects the MIT bag model with the measured parton distribution functions. We shall see that a number of features of those distributions can be understood in terms of familiar physics required in almost all quark models. We also examine a recent development which treats the spinor structure of the composite nucleon seriously.

There has recently been quite a bit of interest in the role of the meson cloud of the nucleon in DIS. This is explained in detail in sect.5. Our discussion includes the reasons for preferring the infinite momentum frame for the calculation as well as a detailed comparison with recent data. In sect.6 we turn to some unexpected surprises which DIS experiments have revealed – including the apparent violation of the Gottfried sum rule, the proton "spin crisis", and the nuclear European Muon Collaboration (EMC) effect. All of these phenomena are rich in information about the non-perturbative structure of the nucleon, free or bound. Finally in sect.7 we make some concluding remarks.

[1]Address from 1 September 1993: Institut für Theoretische Physik, Universität Regensburg, D-93040 Regensburg, GERMANY

2 BASICS OF DEEP-INELASTIC SCATTERING

The elementary ideas of DIS can be found in many text books and reviews [3-10]. In this section our aim is simply to define our notation and collect together the essential formulae.

Consider the inclusive scattering of a high energy lepton (initial energy E, final energy E', and scattering angle θ) from a hadronic target (mass M and initial four-momentum p) as illustrated in Fig.1. The spacelike four-momentum transferred to the target is denoted q. For an unpolarised target the laboratory differential cross-section for electromagnetic scattering is calculated by contacting the lepton tensor $L_{\mu\nu}$ with the hadronic tensor $W^{\mu\nu}$:

$$W^{\mu\nu} = \tilde{g}^{\mu\nu} W_1 + \frac{\tilde{p}^\mu \tilde{p}^\nu}{M^2} W_2. \tag{1}$$

$$\tilde{g}^{\mu\nu} = -g^{\mu\nu} + \frac{q^\mu q^\nu}{q^2} \tag{2}$$

and

$$\tilde{p}^\mu = p^\mu - \frac{p\cdot q}{q^2} q^\mu, \tag{3}$$

and the two arbitrary functions W_1 and W_2 contain all the information we can learn about the target from such experiments. After contracting the tensors and integrating over phase space we find:

$$\frac{d^2\sigma}{dE'd\Omega} = \frac{4\alpha^2(E')^2}{q^4}\left[\cos^2\frac{\theta}{2}\frac{F_2}{\nu} + 2\sin^2\frac{\theta}{2}\frac{F_1}{M}\right]. \tag{4}$$

All of the information concerning the structure of the target is now contained in the structure functions F_1 ($= MW_1$) and F_2 ($= \nu W_2$, with $\nu = E - E'$ the photon energy in the laboratory frame) which can depend on at most two variables. It is most usual to choose those to be the Lorentz invariant quantities $Q^2 (= -q^2 > 0)$ and Bjorken x ($= -q^2/2p\cdot q = Q^2/2M\nu$).

For $\nu(\bar{\nu})$ scattering from an unpolarised target we find a third structure function, F_3, associated with parity violation:

$$\frac{d^2\sigma^{\nu(\bar{\nu})}}{dE'd\Omega} = \frac{G_F^2(E')^2}{2\pi^2}\left(\frac{M_W^2}{M_W^2+Q^2}\right)^2\left[\cos^2\frac{\theta}{2}\frac{F_2^{\nu(\bar{\nu})}}{\nu} + 2\sin^2\frac{\theta}{2}\frac{F_1^{\nu(\bar{\nu})}}{M} \pm \frac{E+E'}{M\nu}\sin^2\frac{\theta}{2}F_3^{\nu(\bar{\nu})}\right]. \tag{5}$$

Finally, for scattering of a polarised electron (or muon) from a polarised, spin-1/2 target there are (at least in principle) two more structure functions (g_1 and g_2) which can be measured. Denoting beam and target helicity with arrows top and bottom respectively we find:

$$\frac{d^2\sigma}{dE'd\Omega}\left(\rightrightarrows - \rightleftarrows\right) = \frac{4\alpha^2 E'}{M\nu Q^2 E}\left[(E + E'\cos\theta)g_1 - 2Mxg_2\right]. \tag{6}$$

(We note in passing some recent theoretical arguments [11] which imply a relationship between g_1 and g_2, but we shall not discuss these further here.) In the deep-inelastic regime Q^2 and ν are both very large ($Q^2 > 2$ GeV^2, $\nu > 1$ GeV) but $x \in (0,1)$. Clearly the second term on

the r.h.s. in equ.(6) will be negligible if g_1 and g_2 are of the same order. For this reason only g_1 has been measured so far. To determine g_2 one would need to work with a longitudinally polarised beam and a transversely polarised target. However, even then the cross-section is of order $(1/Q)$ times that given in equ.(6):

$$\frac{d^2\sigma}{dE'd\Omega}\left(\vec{\uparrow}-\vec{\downarrow}\right) = -\frac{4\alpha^2(E')^2}{M\nu Q^2 E}\left[g_1+\frac{2Eg_2}{E+E'}\right]\sin\theta. \tag{7}$$

In the late 1960s tremendous excitement was generated by the discovery at SLAC that the structure functions were almost independent of Q^2 over a very wide range. That is, they were functions of the single variable — Bjorken x. It is very easy to see that this is what one would expect if the nucleon contained a collection of elementary constituents (initially called partons by Feynman but later identified with quarks) with low mass, which do not interact strongly during the DIS collision.

For simplicity it is usual to consider this problem in a so-called infinite momentum frame – e.g. one where the nucleon has momentum $P \gg M$ in the z-direction so that its 4-momentum is $p = (P; 0, 0, P)$. Suppose a constituent with 4-momentum $yp = (yP; 0, 0, yP)$, where y is the "momentum fraction" of the nucleon carried by the constituent, absorbs the photon. Its final invariant mass squared will be:

$$(yp+q)^2 = y^2p^2 - Q^2 + 2y\ p\cdot q. \tag{8}$$

But $p^2 \ll Q^2$ and $p\cdot q$, and the invariant mass squared of the parton must be small (≈ 0) by assumption. Then we find $y = Q^2/2p\cdot q$ which was called Bjorken x above. Thus we see that under the assumptions of the parton model, only a parton with fraction x of the momentum of the nucleon can absorb the exchanged photon (or W-boson). In the case that the impulse approximation is valid, DIS structure functions then measure the number density of partons in the nucleon with momentum fraction x.

It is usual to define distributions $q^{\uparrow\downarrow}(x)$ which give the number density of quarks in the target with helicity parallel or anti-parallel to that of the target. For example, $u(x)xdx$ gives the fraction of momentum of u quarks *in the proton* with momentum between xP and $(x+dx)P$ in the infinite momentum frame (and with either helicity). By charge symmetry u also gives the distribution of d quarks in the neutron.

The structure functions mentioned earlier are directly related to these distribution functions. For an electromagnetic probe one finds:

$$F_1(x) = \frac{1}{4}\sum_q e_q^2(q^\uparrow(x)+q^\downarrow(x)) \tag{9}$$

$$F_2(x) = 2xF_1(x) \tag{10}$$

$$g_1(x) = \frac{1}{2}\sum_q e_q^2(q^\uparrow(x)-q^\downarrow(x)) \tag{11}$$

with e_q the charge in units of e of quark flavor q. Equation (10) is the Callan-Gross relation and relies on the partons having spin 1/2 and no transverse momentum (in the infinite momentum frame). In general we have

$$F_2 = 2xF_1\frac{1+R}{1+2Mx/\nu} \tag{12}$$

where R is the ratio of cross-sections for absorbing a longitudinal to that for a transverse photon. Experimentally R is small [12] ($\lesssim 0.1$) for all x, for $Q^2 \gtrsim 5$ GeV^2.

For neutrino scattering from an isoscalar target one finds

$$F_2^{(\bar{\nu})} = (u+\bar{u}+d+\bar{d}+s+\bar{s}), \tag{13}$$

which measures the total quark content of the proton. Even more important, by combining ν and $\bar{\nu}$ data one can measure the combination

$$F_3^{(\nu,\bar{\nu})} = (u-\bar{u}+d-\bar{d}), \tag{14}$$

which isolates the excess of quarks over antiquarks – i.e. the valence quark distribution of the nucleon. Clearly we would expect the sum rule (due to Gross and Llewellyn Smith)

$$\int_0^1 dx\ F_3^{(\nu,\bar{\nu})}(x) = 3 \tag{15}$$

to be obeyed. It will also be useful to define the n'th moment of a structure function like xF_3, F_2 or xF_1 as, e.g.

$$M_{3n} = \int_0^1 dx\ x^{n-2}\ [xF_3(x)]. \tag{16}$$

Initially the major experimental activity in this field was at SLAC, but for the past 10-15 years, the emphasis has shifted to the muon and neutrino beams of CERN and Fermilab. For a thorough summary of the experiments at these laboratories we refer to the recent review by Morfin [13]. While most of data has been been accumulated for Q^2 between 5 and 20 GeV^2 and x between 0.1 and 0.65, Q^2 as high as 200 GeV^2 and x as low as 10^{-4} (at HERA) have now been obtained. (The latter is particularly relevant for certain sum rules as we shall see.) Figure 2 illustrates the results typically obtained — "this experiment" is the CDHS neutrino experiment [14]. We note that the antiquarks, which form half of the sea of virtual pairs in the nucleon, are concentrated at low x ($x \lesssim 0.3$). The valence quarks (c.f. equ.(14)) dominate the large x region. There is impressive agreement between the weak and electromagnetic experiments once one allows for the appropriate charges. Actually the situation is a little worse than Fig.1 might suggest. Because of systematic errors, different muon data sets on the same target may differ by as much as 10–20%. These differences are typically within the quoted systematic errors. Again such differences can be important whenever an absolute measurement is required – e.g. in the spin sum rule.

It is clear from the analysis of the experimental data that even in the Bjorken region the structure functions have a weak Q^2-dependence, and therefore so do the distribution functions which we write as $q(x, Q^2)$. If one sticks to any one data set in order to (partially) avoid systematic errors, this variation of the structure functions (scaling violation) is essentially logarithmic. In order to understand it one must go beyond the naive parton model to QCD.

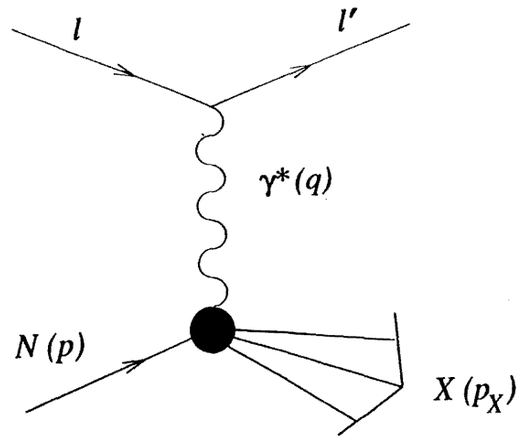

Figure 1: The deep-inelastic cross-section involves a sum over all (unobserved) final states, X.

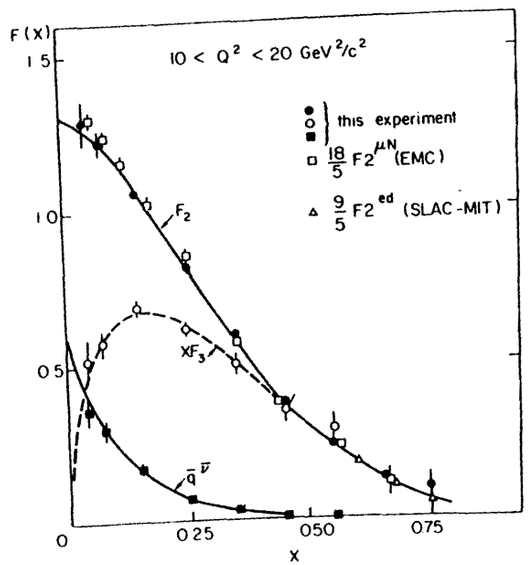

Figure 2: Summary of structure function data taken with neutrinos – from the CDHS group [14] – in comparison with data from electromagnetic probes.

3 PERTURBATIVE QCD

In developing a theoretical description of the deep-inelastic process shown in Fig.1 it is usual to assume that the wavefunction of the target has no high-momentum components (i.e. $p_T^2 \ll Q^2$). Thus any Q^2-dependence can only come from the lepton-quark scattering process. Scaling results if the quark is treated as point-like and the trivial Q^2-dependence of the Mott cross-section is factored out. On the other hand, in an interacting field theory, the lepton-quark scattering amplitude will involve radiative corrections, some of which add coherently (e.g. wave function and vertex renormalisation) while others are incoherent (e.g. bremmstrahlung). It is well known that such radiative processes lead to corrections which vary logarithmically with the appropriate cut-off scale — in this case Q^2.

For explicit calculations of these radiative corrections, we refer to some excellent texts [3-10]. It is particularly important from the point of view of application to other systems, that one can develop a very physical interpretation of this Q^2 variation. This is perhaps best expressed through Close's "onion skin" picture, whereby every time we increase Q^2, we increase the resolution at which we observe the structure of the target — hence revealing more and more of its previously virtual quarks and gluons. The mathematical description of the variation of the structure function of Q^2 is given by the Altarelli-Parisi equations. If one sticks to any one of the data sets mentioned above (in order to avoid systematic errors), the Q^2 variation of the structure functions is well described by these equations. However there are discrepancies between data sets and difficulties have also been encountered when trying to make a consistent fit to the EMC data on different nuclear targets.

The most rigorous approach to the calculation of structure functions, and the description of their Q^2 variation, comes through the operator product expansion and the renormalisation group. As these are also discussed in many texts, we highlight only those features needed for our main consideration, namely the prediction of structure functions from particular quark models.

3.1 The Operator Product Expansion

As electromagnetic DIS involves a total cross-section for lepton scattering with a single photon exchanged, the structure functions are proportional (through the optical theorem) to the imaginary part of the forward Compton amplitude for a photon of 4-momentum q. The Compton amplitude is written:

$$T_{\mu\nu} = i \int d^4z \, e^{iq\cdot z} \, \langle N|T(j_\mu(z) j_\nu(0))\,|N\rangle, \tag{17}$$

where j_μ is the electromagnetic current operator. The essential idea of the operator product expansion (OPE) is that one can expand the time-ordered product of the currents in what is essentially a generalisation of the familiar Taylor series. That is, one writes it as an infinite series, whose terms each involve a (possibly singular) function of z^2 times a local operator, in general involving $\bar{\psi}(0)$ and derivatives of $\psi(0)$, contracted with products of z^λ. It is crucial that this is an expansion of the operator which is therefore target independent.

Dropping Lorentz indices, for purposes of illustration, one has schematically:

$$T(j_\mu(z)j_\nu(0)) \;=\; \sum_{i,n} \tilde{C}_{i,n}(z^2)\; z_{\mu_1}\cdots z_{\mu_n}\; O_{i,n}^{\mu_1\cdots\mu_n} \tag{18}$$

where for example one might have an operator $O_{i,n}^{\mu_1\cdots\mu_n}$ of the form:

$$\bar{\psi}(0)\gamma^{\mu_1} D^{\mu_2}\cdots D^{\mu_n}\psi(0) \tag{19}$$

$$\bar{\psi}(0)\gamma^{\mu_1} D^{\mu_2}\psi(0)\bar{\psi}(0)\gamma^{\mu_3}\cdots D^{\mu_n}\psi(0) \tag{20}$$

and so on. Now ignoring renormalisation ψ has dimensions of [energy]$^{3/2}$, which is usually called simply dimension-3/2. Therefore the l.h s. of equ.(18) has dimension 6. Suppose the operator $O_{i,n}$ has dimension N_i, then $\tilde{C}_{i,n}$ must have dimension $6+n-N_i$. After Fourier transformation to give the Compton amplitude (equ.(17)) it will therefore behave like Q^{6+n-N_i}. Since $Q^2\to\infty$ in the Bjorken limit, the dominant operators will be those with the largest exponent, or the smallest value of $(N_i - n)$ — which is usually called "twist". One can easily check that the operator in equ.(19) is twist-2, while that in equ.(20) is twist-4. With a little thought one can see that twist-2 is the best that can be done, and therefore *DIS in the Bjorken limit will be entirely determined by twist-2 operators.*

The operator given in equ.(19) is called a singlet, twist-2 operator because it involves a trace over flavors. The only other twist-2, singlet operator involves the gluons:

$$g_{\alpha\beta} F^{\mu_1\alpha} D^{\mu_2}\cdots D^{\mu_{n-1}} F^{\mu_n\beta}. \tag{21}$$

One can also write down a set of non-singlet operators

$$\bar{\psi}(0)\gamma^{\mu_1} D^{\mu_2}\cdots D^{\mu_n}\lambda_i\psi(0), \tag{22}$$

where λ_i are the flavor-SU(3) matrices. For simplicity we shall concentrate on the non-singlet operators from now on.

In general the matrix elements of these operators must be of the form

$$\langle N|O_i^{\mu_1\cdots\mu_n}|N\rangle \;=\; p^{\mu_1}\cdots p^{\mu_n}\;\langle N|O_{i,n}|N\rangle. \tag{23}$$

Returning to equ.(17) we realise that the Fourier transform of z_μ is essentially q_μ/Q^2, which contracted with p^μ gives $1/x$. Thus we find that in the large-Q^2 limit, schematically (i.e. corresponding to equ.(18))

$$T \sim \sum_n C_n(Q^2)\; x^{-n}\;\langle N|O_n|N\rangle, \tag{24}$$

and we have incorporated an appropriate number of factors of Q^{-2} into the (n'th derivative of the) Fourier transform of $\tilde{C}_n$ to give C_n. The latter is easily seen to be dimensionless.

Finally, for the full electromagnetic case one finds

$$\begin{aligned} & i\int d^4z\; e^{iq\cdot z}\; T(j_\mu(z)j_\nu(0)) \\ = & \sum_{i,n}\Big[(g_{\mu\mu_1}g_{\nu\mu_2}Q^2 + g_{\mu_1\mu}q_\nu q_{\mu_2} + g_{\nu\mu_2}q_\mu q_{\mu_1} - g_{\mu\nu}q_{\mu_1}q_{\mu_2})C_{i,n}(Q^2) \\ + & \left(g_{\mu\nu} - \frac{q_\mu q_\nu}{q^2}\right) q_{\mu_1}q_{\mu_2}C^L_{i,n}(Q^2) \;- i\epsilon_{\mu\nu\alpha\beta}g^\alpha_{\mu_1}q^\beta q_{\mu_2}C^3_{i,n}(Q^2)\Big] \\ & \times q_{\mu_3}\cdots q_{\mu_n}\left(\frac{2}{Q^2}\right)^n O_i^{\mu_1\cdots\mu_n}. \end{aligned} \tag{25}$$

Here we have kept only the twist-2 operators, $C_{i,n}$ and $C^L_{i,n}$ correspond to the parity conserving transverse and longitudinal contributions respectively while $C^3_{i,n}$ is the parity violating term leading to F_3 in $\nu(\bar{\nu})$ scattering — c.f. equ.(5).

3.2 The Renormalisation Group

The arguments just presented must be modified in a field theory like QCD. The matrix element of the currents on the l.h.s. of equ.(25) must be renormalised, as must the matrix elements of the operators in the OPE on the r.h.s. This procedure introduces a new mass scale (or renormalisation scale), μ^2, upon which no physical results can depend. It is very important that the μ^2 dependence of the coefficient functions $C_{i,n}(Q^2,\mu^2,g^2(\mu^2))$ be chosen such that equ.(25) is true after renormalisation. From the practical point of view it is crucial that the OPE is an operator relationship which holds independent of the target. One can therefore calculate the μ^2 dependence for a simple target, such as a free quark. As this too is found in many texts [3-8] we just review it briefly.

Assuming that the operator O_n is multiplicatively renormalised by $Z^{-1}_{O_n}$, we define

$$\beta(g) \;=\; \frac{\partial g(\mu^2)}{\partial \ln\mu^2} \tag{26}$$

and

$$\gamma_{O_n} \;=\; \frac{\partial \ln Z_{O_n}}{\partial \ln\mu^2}. \tag{27}$$

(Note that we have dropped the label i for convenience.) We shall show below that the product $C_n(Q^2,\mu^2,g^2)\langle N|O_n|N\rangle$ is measurable and therefore cannot depend on μ^2. (It is proportional to the n'th moment of the DIS structure function defined in equ.(16)). For the present we write

$$\mu\frac{d}{d\mu}C_n\langle N|O_n|N\rangle \;=\; 0, \tag{28}$$

and hence (in an appropriate gauge)

$$\left(\frac{\partial}{\partial\ln\mu^2} + \frac{\partial g}{\partial\ln\mu^2}\frac{\partial}{\partial g} - \gamma_{O_n}\right) C_n(Q^2,\mu^2,g^2) \;=\; 0. \tag{29}$$

However we saw above that for twist-2 C_n is dimensionless and therefore can only depend on Q^2 as Q^2/μ^2. Therefore we can replace $\partial/\partial\ln\mu^2$ by $-\partial/\partial\ln Q^2$ and equ.(29) becomes

$$\left(\frac{\partial}{\partial\ln Q^2} - \beta(g(Q^2))\frac{\partial}{\partial g(Q^2)} + \gamma_{O_n}\right) C_n \;=\; 0. \tag{30}$$

The first two terms are easily identified as $-\beta(g(Q^2))d/dg(Q^2)$ so that equ.(30) implies

$$\frac{d\ln C_n}{dg(Q^2)} \;=\; \frac{-\gamma_{O_n}}{\beta}. \tag{31}$$

Finally we obtain:

$$C_n(Q^2,\mu^2,g^2(\mu^2)) \;=\; C_n(Q^2,Q^2,g^2(Q^2))\exp\left(-\int_{g(\mu^2)}^{g(Q^2)}\frac{\gamma}{\beta}dg'\right). \tag{32}$$

In practice one has a series expansion for $\gamma(g')$ and $\beta(g')$ to only a few terms. In the so-called leading order we have

$$\beta(g) = -\frac{\beta_0 g^3}{16\pi^2}, \qquad \gamma(g) = \gamma_0^n\frac{g^2}{16\pi^2}, \tag{33}$$

and

$$C_n(Q^2,Q^2,g^2(Q^2)) = 1. \tag{34}$$

Then the integral in equ.(32) is easily performed and we find

$$C_n(Q^2,\mu^2,g^2) \overset{L.O.}{=} \left(\frac{\alpha(Q^2)}{\alpha(\mu^2)}\right)^{d_0^n}, \tag{35}$$

and using the calculated value of β_0 (for N_f quark flavors) and γ_0^n, the anomalous dimension d_0^n is

$$d_0^n \;=\; \frac{\gamma_0^n}{2\beta_0} \;=\; \frac{4}{33-2N_f}\left(1-\frac{2}{n(n+1)}+4\sum_{m=2}^{n}m^{-1}\right). \tag{36}$$

3.3 The Moments of the Structure Functions

As we hinted above, there is a direct connection between the moments of the structure functions and the Compton amplitude which we have calculated so far. In fact as a function of ν for fixed Q^2, $T_{\mu\nu}$ has two cuts, (ν_{th},∞) corresponding to the physical region and $(-\infty,-\nu_{th})$ corresponding to crossed processes. In terms of x, again for fixed Q^2, the corresponding cuts run from (0,1) and (-1,0). Thus the dispersion relation for $T_{\mu\nu}$ at fixed Q^2 has the form

$$T_{\mu\nu}(x,Q^2) \;=\; \frac{1}{2\pi i}\left[\int_{-\infty}^{-\nu_{th}}+\int_{\nu_{th}}^{\infty}\right]\frac{d\nu'(disc)T_{\mu\nu}(x',Q^2)}{\nu'-\nu}. \tag{37}$$

Replacing ν' by x' and using the optical theorem to replace $\mathrm{Im}T_{\mu\nu}$ by the total cross-section, which is by definition the structure function, we find

$$T_{\mu\nu}(x,Q^2) \;=\; \sum_n x^{-n}\int_0^1 dx'(x')^{n-1}W_{\mu\nu}(x',Q^2). \tag{38}$$

Note that for the various terms in $T_{\mu\nu}$ (see equ.(25)) the sum over n is restricted to even or odd values depending on the crossing properties of the corresponding piece of $W_{\mu\nu}$.

Comparing equ.(38) with equ.(24) we see that the product of the coefficient function C_n and the operator matrix element is measurable. Indeed it is equal to the moment of the appropriate structure function as defined in equ.(16). Using the result of the above analysis based on

the OPE and the renormalisation group, we see that the Q^2 variation of the moments of the structure functions is given by perturbative QCD. To leading order one finds:

$$M_n(Q^2) \;=\; M_n(Q_0^2)\left(\frac{\alpha(Q^2)}{\alpha(Q_0^2)}\right)^{d_0^n}. \tag{39}$$

For fixed Q_0^2 it is then easily shown that

$$\ln M_n(Q^2) \;=\; \frac{d_0^n}{d_0^m}\ln M_m(Q^2) \;+\; \text{constant}, \tag{40}$$

and therefore a log-log plot of any two moments should be a straight line whose slope is predicted by QCD.

All of the above discussion of Q^2 evolution involves non-singlet operators. The Q^2 evolution of the operators given in equs.(19) and (21) is more complicated because they mix under renormalisation. While the corresponding analysis is not much more difficult (it involves a 2×2 matrix), it would divert us too much to explain it here. Instead we refer to the appropriate texts [3-8] — for example there is a concise summary in Table 2 of the review by Altarelli [9].

3.4 The Inverse Mellin Transform

Given an analytic continuation of a set of moments, $M_n(Q^2)$, there is a standard method for reconstructing the corresponding function — this is the Inverse Mellin Transform (IMT):

$$xF_3(x,Q^2) \;=\; \frac{1}{2\pi i}\int_{C-i\infty}^{C+i\infty}dn\; x^{1-n}M_{3n}(Q^2). \tag{41}$$

(Here C is chosen so that the integral exists.) If the moments can be written as a product, as in equ.(24) or (25):

$$M_{2n}(Q^2) \;=\; C_n(Q^2,\mu^2)\,\langle N|O_n(\mu^2)|N\rangle \tag{42}$$

then the IMT xF_3 is just a convolution of the IMT of C_n (denoted by $\mathcal{C}_3$) and $\langle N|O_n|N\rangle$ (denoted $\mathcal{F}_3$), viz:

$$xF_3(x,Q^2) \;=\; \int_x^1\frac{dy}{y}\,\mathcal{C}_3(x/y,Q^2,\mu^2)\,(y\mathcal{F}_3(y,\mu^2)). \tag{43}$$

This is an extremely important result. In particular, $\mathcal{C}_3$ is totally independent of the structure of the target — a property known as factorisation. Clearly if we can evaluate the structure function of the target at any renormalisation scale μ^2, equ.(43) allows us to calculate it at all higher values of Q^2. Higher order QCD corrections do not alter this result in principle, they just make $\mathcal{C}_3$ harder to compute. For this reason μ^2 cannot be too low.

4 RELATION TO SIMPLE QUARK MODELS

At last we have collected all the results necessary to understand how to relate quark models to QCD. (Of course, if one could use non-perturbative QCD (e.g. on the lattice) to calculate $\langle N|O_n(\mu^2)|N\rangle$ this would be unnecessary. However this is not feasible for more than a few moments at the present time — see for example Lissia et al. [15] and Sachrajda [16].) Since the models are only "QCD motivated", the connection cannot be rigorous. On the other hand we know of no sensible alternative to what is proposed here.

Apart from lattice technology, the only known technique for solving a bound state problem in field theory is to make quantum corrections about a classical solution. That is, one calculates radiative corrections at some renormalisation scale using perturbation theory and then solves (non-perturbative) classical equations of motion. One can then systematically add quantum corrections to the classical solutions. We assume that whatever quark model we are using represents just such a solution, renormalised at some scale μ^2. Although physically measurable quantities cannot depend on μ^2, the classical approximation may be better for some value. We treat the value of μ^2 appropriate to a given model, which we shall call Q_0^2, as a free parameter. If one can evaluate the twist-2 target matrix elements within the model, then through equ.(25) and (32) (or equivalently (42) and (43)), one can calculate the twist-2 structure function at all Q^2. Even though the twist-2 contribution may not be dominant at Q_0^2, the general considerations presented earlier (see the discussion of higher twist below equ.(20)) ensure that at high enough Q^2 it will eventually dominate.

The most convenient practical method for evaluating the twist-2 moments of the structure function of some target follows from important work by Jaffe [17]. However, his article which was entitled "parton distribution functions" involved no discussion of renormalisation group corrections, and the calculations in it were only made in the Bjorken limit. It would therefore not be surprising if the student were confused as to the connection between his parton distributions (e.g. calculated for some model) and experimental data. We shall make that connection quite clear.

Following ref.[17] we define a function $H(\alpha)$ (in the $A^+ = 0$ gauge):

$$H(\alpha) \;=\; \frac{M}{2\pi}\int_{-\infty}^{\infty} dz e^{-iM\alpha z}\langle N|T(\psi_+^\dagger(\xi^-)\psi_+(0))|N\rangle_c. \tag{44}$$

Here we understand a sum over the spins of the target ($|N\rangle$, mass M), c denotes a connected matrix element and $\psi_+(\xi^-)$ is an abbreviated notation for $\frac{1+\alpha^3}{2}\psi(z;0,0,-z)$.

To understand why the second field operator is evaluated at a point on the light-cone with respect to the first we recall equ.(17). In the target rest frame we can choose the photon four-momentum q to be $(\nu;0,0,-\nu-Mx)$ with $\nu\to\infty$. (Clearly Q^2 is $2M\nu x$.) The argument of the exponential in equ.(17) is $iq\cdot z$ which becomes $i[\nu(z^0+z^3)/2+Mxz^3]$. The rapid oscillations as $\nu\to\infty$ drive (z^0+z^3) to zero in the Bjorken limit and hence the process is light-cone dominated. (Causality implies that z_T^2 must be zero if we are to obtain a non-zero contribution to the connected matrix element.)

As a further matter of some practical importance, Jaffe has argued that the time-ordering in equ.(44) can be dropped. In particular, it was shown in ref.[17] that for a connected matrix

element involving field operators separated on the light-cone one can write either

$$\langle N|T(\psi_+^\dagger(\xi^-)\psi_+(0))|N\rangle_c \;=\; \langle N|\psi_+^\dagger(\xi^-)\psi_+(0)|N\rangle_c \tag{45}$$

or equivalently

$$\langle N|T(\psi_+^\dagger(\xi^-)\psi_+(0))|N\rangle_c \;=\; -\langle N|\psi_+(0)\psi_+^\dagger(\xi^-)|N\rangle_c. \tag{46}$$

The only reason for preferring one form to the other is calculational simplicity, because equ.(45) has no semi-disconnected contributions for $\alpha>0$ while the second form has none for $\alpha<0$. In general one can show that $H(\alpha)=0$ for $|\alpha|>1$, or alternatively that $H(\alpha)$ has support on (-1,+1).

The next step in establishing the significance of $H(\alpha)$ is to show that its n'th moment, A_n:

$$A_n \;=\; \int_{-1}^{+1} d\alpha\, \alpha^{n-1}\, H(\alpha) \tag{47}$$

is just $\langle N|O_{2,n}|N\rangle$ (see sect. 3.2 of ref.[17]) where $O_{2,n}$ is the local twist-2 operator of order n associated with the structure function $F_2^{(\nu)}$. Finally one has

$$F_2^{(\nu)}(x) \;=\; x\,(H(x)-H(-x)), \tag{48}$$

while

$$F_3^{(\nu,\bar\nu)}(x) \;=\; (H(x)+H(-x)). \tag{49}$$

Comparing with the parton model formulae in equs.(13) and (14) we identify $q(x)=H(x)$ and $\bar q(x)=-H(-x)$ for $x>0$.

Since, as explained earlier, we view the quark model which we use to evaluate $H(\alpha)$ as an approximate solution of the QCD equations at a renormalisation scale Q_0^2, we add the Q_0^2 label to q and $\bar q$. Using the relations (45) and (46) to simplify the calculation, we find therefore:

$$q(x,Q_0^2) \;=\; \frac{M}{2\pi}\int_{-\infty}^{\infty} dz e^{-iMxz}\langle N|\psi_+^\dagger(\xi^-)\psi_+(0)|N\rangle_c \tag{50}$$

and

$$\bar q(x,Q_0^2) \;=\; \frac{M}{2\pi}\int_{-\infty}^{\infty} dz e^{-iMxz}\langle N|\psi_+(\xi^-)\psi_+^\dagger(0)|N\rangle_c. \tag{51}$$

(In the last equation we used the translational invariance of the field operators to shift the argument ξ^- in $\psi_+^\dagger$ to $-\xi^-$ in ψ_+. We then changed the integration variable from z to $-z$.)

Before describing some numerical results obtained from equs.(50) and (51), some remarks must be made. Whereas we followed ref.[17] in taking the Bjorken limit ($Q^2\to\infty$) in order to obtain these parton distributions, the operator matrix elements needed in equ.(17) in order to reproduce data at some finite Q^2 should be evaluated at that Q^2. Although there is no rigorous proof yet, we believe that the difference between the exact results and the equations we use should be of order $1/Q^2$. (This is the case for the simple models which we have considered.) Effectively it amounts to a smearing of $\langle N|\psi_+^\dagger(z^0;0,0,z^3)\,\psi_+(0)|N\rangle$ about the point $z^0=-z^3$ by an amount of order $1/\nu$ (and therefore of $O(1/Q^2)$).

Since we only intend to compare our twist-2 predictions with data at high Q^2, it is consistent to ignore this correction. Indeed, from this point of view, equs.(50) and (51) are the twist-2 quark/parton distributions whose evolution is governed by perturbative QCD. In order to establish this result it is crucial that the renormalisation scale is not a momentum cut-off (c.f. ref.[18]). It is of course also crucial that the OPE has allowed us to factorise the target dependence from the Q^2 dependence of the quark-probe interaction.

4.1 The MIT bag

Starting from the usual expression for the twist-two quark distribution in equ.(50), one inserts a complete set of energy and momentum eigenstates between the field operators. For the nucleon itself and for the intermediate states we use translationally invariant Peierls-Yoccoz states. These will be two-quark (with mass in the region of $3M/4$) and three-quark + one-antiquark (with mass of order $5M/4$) states.

In the calculation of the antiquark distribution $\bar{q}(x, Q_0^2)$ (for which ψ and $\psi^\dagger$ are interchanged in equ.(50)) the dominant contribution is from a four-quark intermediate state (again with mass of order $5M/4$). One novel feature of this calculation is that it is quite clear that the nucleon has an intrinsic sea [19] — even in a model with just valence quarks, like the three-quark bag. Furthermore, as a result of the Pauli exclusion principle, this intrinsic sea will not be flavor symmetric [19]. Indeed we will find more $d\bar{d}$ pairs in the sea. (This is because, with two spins and three colors one can insert d quarks into five different 1s-states in a proton bag whereas there are only four states available for u quarks.) Clearly an asymmetry such as this will have important consequences for the Gottfried sum rule as discussed in sect.6.2.

The dominant piece of the valence quark distribution calculated from equ.(50) is that involving a two-quark intermediate state. This term is controlled by two parameters, the bag radius and the mass. For the latter it is important to take into account [20] the effect of gluon exchange which raises the mass of a pair of quarks with spin 1 and lowers that of a spin 0 pair so that the resultant splitting is 200 MeV.

Rather than using the model for the contribution to the valence distribution from $3q + \bar{q}$ intermediate states, we simply use a phenomenological term of similar shape (say $(1-x)^7$) with a normalisation chosen to ensure that we have three valence quarks. Under QCD evolution, this phenomenological term moves to small x so that there is no significant uncertainty for $Q^2 \gtrsim 5$ GeV^2 and $x \gtrsim 0.1$ [21, 22]. It is also worth noting that at small x we are sensitive to long-distance physics (the important values of z in equ.(50) are roughly up to order $(Mx)^{-1}$) which is difficult to handle in any phenomenological quark model, so it will be difficult to do better in the near future.

In Fig.3 we show a comparison between the valence quark distribution of the proton calculated for a bag radius of 0.8 fm and various phenomenological fits which will be loosely referred to as data. A priori we have no way to specify the bag scale μ. Instead it is determined by seeing how far one must evolve until the agreement with data at 10 GeV^2 is optimal. Clearly the overall description of the data is rather good. Only at very large values of x ($x \gtrsim 0.7$) is there a significant difference. At such values the struck quark will have a momentum greater

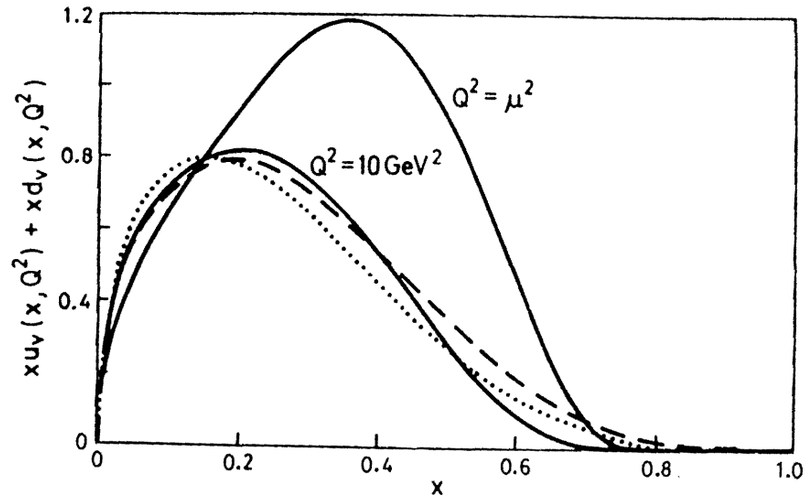

Figure 3: The valence quark distributions for the proton in the bag model ($R = 0.8$ fm) at the bag scale μ^2 (0.25 GeV^2) and at 10 GeV^2 (solid lines) [21, 22]. The dashed and dotted lines are the Duke-Owens [23] and MRS parametrisations [24] at 10 GeV^2.

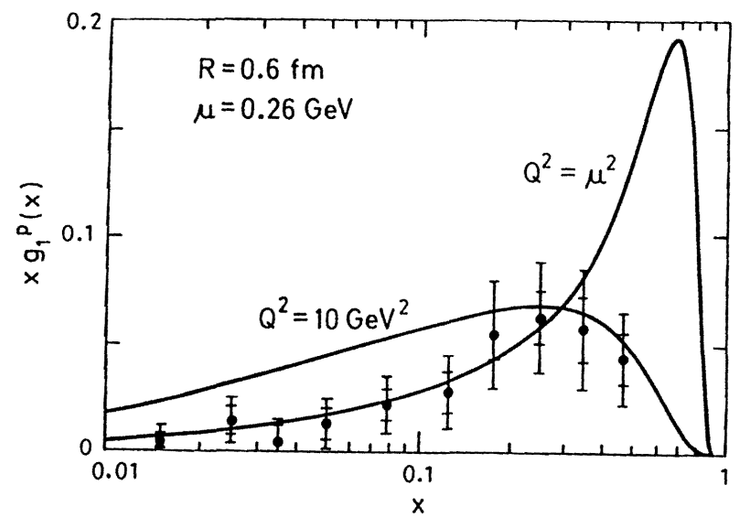

Figure 4: The valence quark distribution of the proton as in Fig.3 but for $R = 0.6$ fm [21, 22]. We have also included the fits of EHLQ [25] and DFLM [26].

than 1 GeV/c and one would expect to have to include the effect of correlations. There is an additional uncertainty associated with the use of leading order QCD, which may be less reliable for higher moments and hence large x.

On the other hand, the agreement with data for calculations with a bag radius of 0.6 fm are essentially perfect (see Fig.4). The improvement at large x is a consequence of the higher average momentum is the smaller cavity. Certainly it would be tempting to conclude that 0.6 fm is preferred. We choose not to draw that conclusion at this stage in view of the problems just cited. Instead we are content to observe that a bag radius in the range 0.6 to 0.8 fm gives a very good representation of the data. Particularly for the calculations at 0.6 fm the bag scale is rather low (e.g. 0.26 GeV in Fig.4). For $\Lambda_{QCD} = 0.2$ GeV, as used here, this gives a rather large value of $\alpha_s(\mu^2)$. Other phenomenological studies have used similar values in perturbative calculations of QCD evolution [27], but we would be more comfortable with μ closer to 0.7 or 0.8 GeV. This does seem to be a likely, desirable consequence of including the pionic corrections needed to preserve chiral symmetry [28, 29]. While we shall not pursue this discussion now, the effect of these pionic corrections on the Gottfried sum rule will be mentioned later.

Because the quark distributions measured in deep-inelastic scattering involve light-cone correlation functions, the energy of the struck quark is as important as its three-momentum. This is why, even for SU(6) wavefunctions for which the u and d quarks of all spin orientations have the same distribution of three-momentum, one finds important differences in $u^{\uparrow\downarrow}$ and $d^{\uparrow\downarrow}$ by including the first-order one-gluon-exchange corrections to the *energies* of the intermediate (diquark) states inserted in equ.(50) [20-22,30]. (The lowest mass diquark will give the hardest quark distribution.) In particular, in this unsophisticated model one can readily see that the ratio $d(x)/u(x)$ tends to zero for x going to one. As a consequence $F_{2n}/F_{2p} \to 1/4$ as $x \to 1$ [3]. Figure 5 shows the general agreement between the data for the d/u ratio and our calculations. Only at very large x is there any serious discrepancy and this may also be related to the absence of short-range correlations in the bag [31].

In Fig.6 we see that this same, simple physics, familiar from low energy spectroscopy, also leads to a quantitative understanding of the proton spin structure function, $g_{1p}(x)$. The crucial feature is that only a u quark with its spin parallel to that of the proton is accompanied by a low-mass spin-singlet pair of quarks (in an SU(6) proton). As a consequence $u^{\uparrow}$ is the dominant parton distribution at large x.

Of course, because we are using an SU(6) spin-flavor wavefunction, the integral of our g_{1p} agrees with the Ellis-Jaffe sum rule [33] — unlike the data [32]. A clear indication of this problem is the quantitative disagreement at intermediate x in Fig.6. One knows that a more sophisticated treatment of the proton wavefunction including gluonic and pionic corrections would improve the situation a little [34-36]. However, it is also known that the anomaly plays a critical role in the flavor singlet distribution [37-39] and this is still rather controversial [40]. We defer further discussion of this issue to sect.6.3.

Independent of the question of the Ellis-Jaffe sum rule, it would be extremely interesting to obtain data on the neutron spin-dependent structure function $g_{1n}(x)$. It is an exciting prediction of the bag model that g_{1n} should become positive at large x. However, a recent extension of that work to include pion corrections [29] has led us to question the sensitivity of this prediction

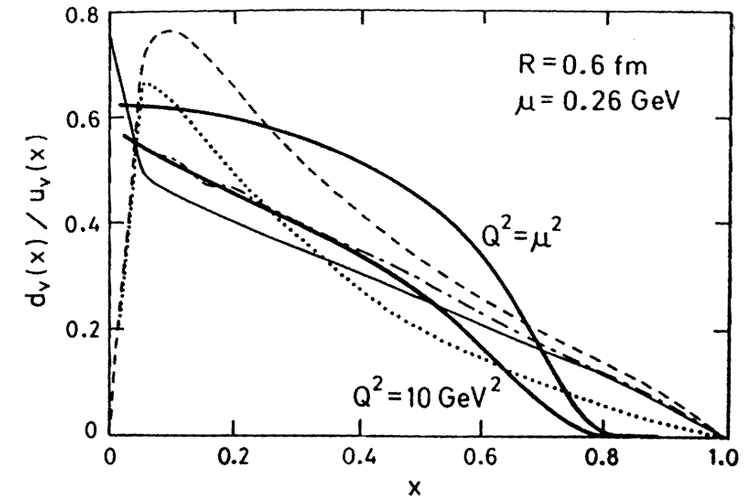

Figure 5: The bag model prediction for the d/u ratio calculated including the energy shift arising from one-gluon-exchange (heavy solid curves). For comparison we also show four fits to world data. The parameters are as for Fig.4.

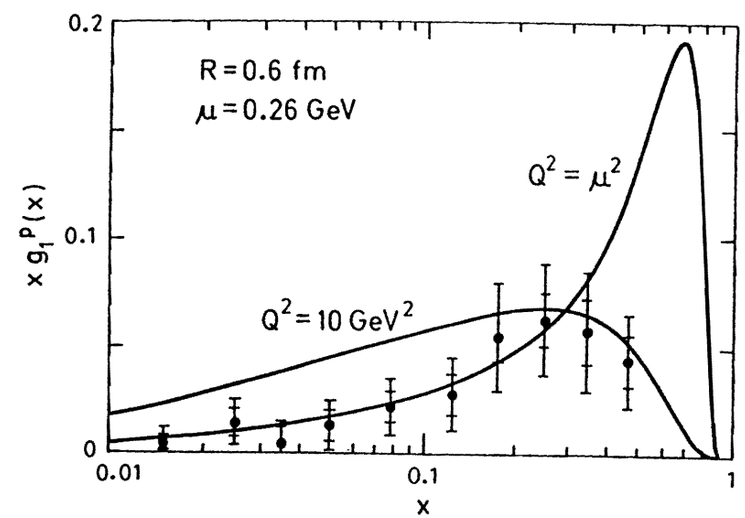

Figure 6: The spin-dependent structure function of the proton, g_{1p}, calculated in the bag model, in comparison with the data of EMC [32].

to small changes in the model. Morever, if the discrepancy between quark model calculations (e.g. Fig.6 above) and the data arises because of the axial anomaly, there could even be a change in the sign of g_{1n} at large x [41, 42].

4.2 Relativistic Models

The advantages of a model such as the one just discussed is its clear connection to hadron spectroscopy and low energy properties. One drawback, however, is the fact that the nucleon wavefunction used in equ.(50) is essentially non-relativistic – i.e. we need to use a technique like Peierls-Yoccoz to construct a state of total momentum zero. Here we outline some recent work in calculating nucleon quark distributions within a relativistic, covariant approach. Further details can be found in ref.[43] (see also ref.[44]).

To see how one can formulate the problem in a relativistic manner, we need to go back to the hadronic tensor $W_{\mu\nu}$, and in particular delve deeper into the Lorentz and Dirac structure of the truncated nucleon tensor, that is, one which has its fermion legs amputated. Because of the additional spinor degree of freedom the structure of the truncated tensor will necessarily be more complicated than that of the full nucleon tensor, $W_{\mu\nu}$. However, once we identify the relevant structures that contribute to the physical tensor in the Bjorken limit, we will be able to use these in a fully relativistic, covariant calculation of the nucleon structure function. The formalism developed here can also be extended to the case of off-mass-shell nucleons, since the truncated tensor will generally depend upon p^2 as well as q^2 and $p \cdot q$.

We can firstly observe that the nucleon tensor can be written [45]:

$$M\, W^{\mu\nu}(p,q) \;=\; \frac{1}{2}\mathrm{Tr}\left[(\not p + M)\, \widehat{W}^{\mu\nu}(p,q)\right] \tag{52}$$

where we have explicitly separated the nucleon spinors from the remaining interaction. In general, $\widehat{W}^{\mu\nu}$ must be constructed from the Lorentz tensors (Dirac scalars) $g^{\mu\nu}, p^\mu, q^\mu$ and Dirac matrices $I, \gamma^\mu, \sigma^{\mu\nu}, \gamma^\mu\gamma_5$ and γ_5. By parity considerations terms involving $\gamma^\mu\gamma_5$ or γ_5 will not contribute to the spin-averaged tensor. Furthermore, terms with $\sigma^{\mu\nu}$ will not contribute to $W^{\mu\nu}$. Therefore we can write [43]

$$\widehat{W}^{\mu\nu}(p,q) \;=\; \tilde{g}^{\mu\nu}\left(I\widehat{W}_T^0 + \not p\widehat{W}_T^1 + \not q\widehat{W}_T^2\right) + \cdots \tag{53}$$

where each of the functions on the right hand side is a scalar function of q^2, $p \cdot q$ and p^2: $\widehat{W}_T^i = \widehat{W}_T^i(p,q) = \widehat{W}_T^i(p^2, p\cdot q, q^2)$. Substituting equ.(53) into (52) and comparing with equ.(1), we see that the transverse structure function W_T ($W_T = W_1 = F_1/M$) can be written as a linear combination of three independent terms,

$$M\, W_T(p,q) \;=\; 2\, M\, \widehat{W}_T^0 \;+\; 2\, M^2\, \widehat{W}_T^1 \;+\; 2\, p\cdot q\, \widehat{W}_T^2. \tag{54}$$

We can calculate the functions $\widehat{W}_T^i$ explicitly by considering the "handbag" diagram, which represents the impulse approximation for quarks. As in the operator product expansion, this amounts to separating out the q^2-dependent part of $\widehat{W}^{\mu\nu}$ from the q^2-independent, non-perturbative part, which must be described by some model. To calculate the latter we need to

consider quark–nucleon vertices that transform as scalars or vectors under Lorentz transformations (since the intermediate spectator diquark state will have either spin 0 or 1, and we need to make an overall Lorentz scalar). It is straightforward to identify the form of the vertices that are allowed by Lorentz, parity and time-reversal invariance, however the specific momentum dependence has to be determined within a model. In general there will be many independent scalar and vector vertex functions. For simplicity we choose a specific form for the scalar (say $I\Phi^S$) and vector ($\gamma_\alpha\Phi^V$) vertices. Calculating the functions $\Phi^{S,V}$ from first principles amounts to solving the relativistic, many-body, bound-state problem, which present day technology does not yet allow, so in practice we use phenomenological input to constrain their functional form. Denoting the quark four-momentum and mass by k and m_q, respectively, we can take the vertex functions as

$$\begin{aligned} \Phi^S(k^2) &= N_S \frac{(k^2 - m_q^2)}{(k^2 - \Lambda_S^2)^2} \\ \Phi^V(k^2) &= N_V \frac{(k^2 - m_q^2)}{(k^2 - \Lambda_V^2)^{7/2}}, \end{aligned} \tag{55}$$

chosen to reproduce the correct large-x behaviour of the u and d quark distributions. The constants N_S and N_V are determined by the normalisation condition,

$$\int_0^1 dx\; q_0(x) \;=\; \int_0^1 dx\; q_1(x) \;=\; 1, \tag{56}$$

where $q_{0,1}$ are the distributions for a spin 0, 1 diquark state, respectively. Note that the above vertex functions incorporate the confinement mechanism, by removing the pole in the quark propagator which would have occurred at $k^2 = m_q^2$.

The result of this calculation is that each of the three functions $\widehat{W}_T^{0-2}$ contribute to W_T in the Bjorken limit [43]. This is extremely important if one wishes to discuss scattering from off-mass-shell nucleons. In particular, as shown in ref.[43], it is very unlikely that in scattering from a nuclear target one would obtain the same linear combination that occurs in the free case. As a consequence the usual approximation whereby the nuclear structure function is written as a convolution of a nucleon momentum distribution with the structure function of a free nucleon breaks down. For further details, including a fit to the free structure functions and application to the deuteron and nuclear matter, we refer to ref.[43].

5 ROLE OF THE MESON CLOUD

Simply on the basis of the Heisenberg uncertainty principle we know that the long range structure of the nucleon must involve a pion cloud. For example, the non-zero value for the neutron charge radius can be easily understood in terms of the emission from a neutron of a light, negatively charged virtual pion, $n \to p + \pi^-$. Furthermore, from PCAC, and from the tremendous successes of chiral quark models [46-49] we expect that the nucleon should have a pion cloud. In addition, because there is no scale at which chiral symmetry can be ignored, the nucleon properties will have pionic corrections at all Q^2.

The possible relevance of the extended pionic structure of the nucleon in high energy processes, such as deep-inelastic scattering, was first suggested by Sullivan in the early 1970s [50]. It was shown that the contribution to the inclusive $\gamma^* N$ cross-section from pion exchange between the virtual photon and the nucleon scales in the Bjorken limit. The reason for this is that, in contrast to processes such as exclusive pion-production which are suppressed by $O(1/Q^2)$ form factors, here it is the inelastic structure function of the pion itself that is probed.

Using this picture of the physical nucleon, it was later noticed [51] that the pion cloud could be responsible for generating an asymmetry between the $\bar{u}$ and $\bar{d}$ quark content of the proton, through the preferred proton dissociation into a neutron and π^+. Furthermore, DIS data on the momentum fractions carried by antiquarks were used to obtain an upper limit on this non-perturbative pionic component. More recently it has been hypothesised [52-56] that this asymmetry could account for some of the apparent discrepancy between the naive parton model prediction for the Gottfried sum rule [57] and its recently determined experimental value [58].

Since it has by far the smallest mass, the pion was the first meson whose contributions to the nucleon structure function were investigated [59, 60]. However, just as other mesons can be included to give corrections to low energy nucleon properties, such as the electromagnetic nucleon form factors or magnetic moments [61], an extended mesonic structure of the nucleon may also be relevant in DIS.

In this section we shall give a detailed account of the calculation of the virtual meson and baryon contributions to the nucleon structure functions. Furthermore, we will use recent DIS data to examine the extent to which such a picture may be relevant in high energy reactions.

The basic hypothesis of this model, in which the nucleon has internal meson and baryon degrees of freedom, is that the physical nucleon state (in an infinite momentum frame) can be expanded (in the one-meson approximation) in a series involving bare nucleon and two-particle meson—baryon states

$$|N\rangle_{\rm phys} = \sqrt{Z}\,\{|N\rangle_{\rm bare} + \sum_{MB}\int dy\; d^2\mathbf{k}_T\; g_{0_{MBN}}\; \phi_{MB}(y,\mathbf{k}_T)\;\; |M(y,\mathbf{k}_T);B(1-y,-\mathbf{k}_T)\rangle\;\}\,. \quad (57)$$

Here, $\phi_{MB}(y,\mathbf{k}_T)$ is the probability amplitude for the physical nucleon to be in a state consisting of a meson M and baryon B, having transverse momenta $\mathbf{k}_T$ and $-\mathbf{k}_T$, and carrying longitudinal momentum fractions y and $1-y$, respectively. Z is the bare nucleon probability. Although we shall work in the one-meson approximation, we shall include higher order vertex corrections to the bare coupling constants $g_{0_{MBN}}$. Illustrated in Fig.7 is the DIS of the virtual photon from the two-particle state $|M;B\rangle$. In Fig.7(a) the photon interacts with a quark or antiquark inside the exchanged meson, while in Fig.7(b) the scattering is from a quark in the baryon component of the physical nucleon.

According to equ.(57), the probability to find a meson inside a nucleon with momentum fraction y $(= k\cdot q/p\cdot q = k_+/p_+)$ is (to leading order in the coupling constant)

$$f_{MB}(y) \equiv Z\; g^2_{0_{MBN}} \int d^2\mathbf{k}_T\;\; |\phi_{MB}(y,\mathbf{k}_T)|^2\,. \quad (58)$$

This must also be the probability to find a baryon inside a nucleon with momentum fraction $1-y$. The baryon distribution function, $f_{BM}(y')$, where $y' = p'\cdot q/p\cdot q$, is probed directly

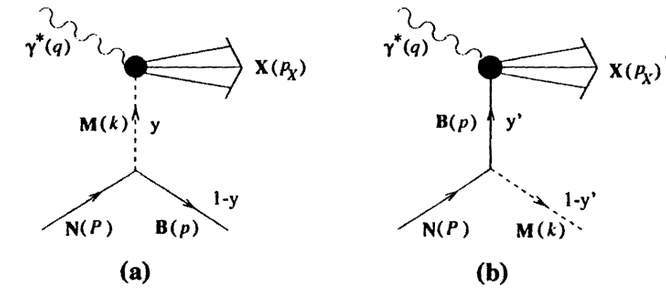

Figure 7: DIS from the virtual (a) meson and (b) baryon components of a physical nucleon.

through the process in Fig.7(b), and should be related to the meson distribution function by

$$f_{MB}(y) \;=\; f_{BM}(1-y) \quad (59)$$

for all y, if the above interpretation is valid. We also demand equal numbers of mesons emitted by the nucleon, $\langle n\rangle_{MB} = \int_0^1 dy\; f_{MB}(y)$, and virtual baryons accompanying them, $\langle n\rangle_{BM} = \int_0^1 dy'\; f_{BM}(y')$:

$$\langle n\rangle_{MB} \;=\; \langle n\rangle_{BM}. \quad (60)$$

This is just a statement of charge conservation. Momentum conservation imposes the further requirement that

$$\langle y\rangle_{MB} + \langle y\rangle_{BM} \;=\; \langle n\rangle_{MB} \quad (61)$$

where $\langle y\rangle_{MB} = \int_0^1 dy\; y\; f_{MB}(y)$ and $\langle y\rangle_{BM} = \int_0^1 dy'\; y'\; f_{BM}(y')$ are the average momentum fractions carried by meson M and the virtual baryon B, respectively. Equations (60) and (61), and in fact similar relations for all higher moments of $f(y)$, follow automatically from equ.(59).

In what follows we shall explicitly evaluate the functions f_{MB} and f_{BM}, and examine the conditions under which equ.(59) is satisfied. The results will be used to calculate the contributions to the nucleon structure function from the extended mesonic structure of the nucleon, which are expressed as convolutions of the functions $f(y)$ with the structure functions of the struck meson or baryon:

$$\delta^{(MB)}F_{2N}(x) \;=\; \int_x^1 dy\; f_{MB}(y)\; F_{2M}(x_M) \quad (62)$$

$$\delta^{(BM)}F_{2N}(x) \;=\; \int_x^1 dy'\; f_{BM}(y')\; F_{2B}(x_B) \quad (63)$$

with $x_M = x/y$ and $x_B = x/y'$. Note that equs.(62) and (63) are correct when physical (renormalised) meson—baryon coupling constants are used in the functions f_{MB} and f_{BM} (see sect.5.5 for a discussion on this point). By comparing against the experimental structure functions, we will ultimately test the reliability of the expansion in equ.(57), and also the relative importance of the states involving heavier mesons compared with the pion states.

5.1 Pions – Covariant Formulation

Let us firstly review the previous calculations of the contribution to F_{2N} from the pion cloud. Following the original method of Sullivan, the approach has been to simply treat the diagram in Fig.7(a) as a Feynman diagram. With a pseudoscalar πN coupling, $g_{\pi NN}\bar{u}(p)\, i\gamma_5 u(P)$, the contribution from this diagram to the hadronic tensor of the physical nucleon can be written

$$\delta^{(\pi N)}W^{\mu\nu}(P,q) = \int \frac{d^3\mathbf{p}}{(2\pi)^3(2p_0)} \frac{g^2_{\pi NN}(k^2)}{(k^2-m_\pi^2)^2} \frac{1}{2}\mathrm{Tr}\left[(\not{P}+M)\, i\gamma_5\, W^{\mu\nu}_\pi(k,q)\, (\not{p}+M)\, i\gamma_5\right] \quad (64)$$

where the hadronic tensor for the virtual pion is expressed as

$$W^{\mu\nu}_\pi = \tilde{g}^{\mu\nu}W_{1\pi} + \frac{\tilde{k}^\mu\tilde{k}^\nu}{m_\pi^2}W_{2\pi} \quad (65)$$

and where $g^2_{\pi NN}(k^2)$ is the interaction strength. [2] It is customary to isolate the k^2 dependence of $g^2_{\pi NN}(k^2)$ into the πNN form factor: i.e. $g^2_{\pi NN}(k^2) = g^2_{\pi NN}\, \mathcal{F}_{\pi N}(k^2)$, where $g_{\pi NN}$ is now the coupling constant at the pion pole ($\mathcal{F}_{\pi N}(-m_\pi^2) = 1$). We can obtain the contribution to the nucleon structure function W_1 (or W_2, by the Callan-Gross relation) by collecting $\tilde{g}_{\mu\nu}$ (or simply $g^{\mu\nu}$) terms on both sides of equ.(64) [62] to obtain an expression like that in equ.(62).

Performing the elementary trace gives a factor $2P\cdot p - 2M^2 = -k^2$, so that the distribution function of a virtual pion accompanied by a recoiling nucleon is [51, 60]

$$f_{\pi N}(y) = \frac{3g^2_{\pi NN}}{16\pi^2}\, y \int_{-\infty}^{k^2_{max}} dk^2\, \frac{\mathcal{F}^2_{\pi N}(k^2)(-k^2)}{(k^2-m_\pi^2)^2}. \quad (66)$$

Here, $k^2 = k^2_{max} - k_T^2/(1-y)$ is the 4-momentum squared of the virtual pion, with a kinematic maximum given by $k^2_{max} = -m^2y^2/(1-y)$, and k_T^2 is the pion transverse momentum squared. We have also included a factor 3 by taking account of the different charge states of the nucleon (namely 2 for the dissociation process $p \to n\pi^+$ and 1 for $p \to p\pi^0$). In a covariant formulation the form factor, $\mathcal{F}_{\pi N}$, parameterising the πNN vertex, at which only the pion is off-mass-shell, can only depend on k^2. In the literature this is most often parameterised by a simple monopole or dipole function,

$$\mathcal{F}_{\pi N}(k^2) = \left(\frac{\Lambda^2_{\pi N} - m_\pi^2}{\Lambda^2_{\pi N} - k^2}\right)^n \quad (67)$$

for $n = 1$ and 2, respectively.

Because we integrate over the recoiling particle's momentum, in principle we could also have contributions from processes where a baryon other than a nucleon (e.g. a Δ isobar) is left in the final state in Fig.7(a). It is expected that contributions from the higher mass baryons will be suppressed relative to the nucleon, since the maximum value of k^2 for which energy and momentum can be conserved when a higher mass baryon is produced decreases rapidly as the mass of the baryon increases. Nevertheless, the importance of the Δ-resonance is well known

[2] Since only tree diagrams are ever considered, the pseudoscalar interaction is equivalent to that with a pseudovector coupling $(f_{\pi NN}/m_\pi)\, \bar{u}(p)\, i\gamma_\alpha\gamma_5\, u(P)\, k^\alpha$, providing the coupling constants are related by $f_{\pi NN} = g_{\pi NN}\, (m_\pi/2M)$.

in pion physics. In any quark model the coupling to the N and Δ would enter on the same footing.

The process where the nucleon emits a pion and leaves behind an on-shell Δ was previously calculated in refs.[56, 63, 64], using the effective interaction $(f_{\pi N\Delta}/m_\pi)\, \bar{u}_\alpha(p)\, k^\alpha\, u(P)$, where $u_\alpha(p)$ is the spin-3/2 Rarita-Schwinger spinor-vector [65], which can be formed by combining the spin-1/2 Dirac spinor $u(p,s)$ with vectors $\epsilon_\alpha(\lambda)$:

$$u_\alpha(p,S) = \sum_m \left\langle \frac{3}{2}S \middle| 1m, \frac{1}{2}s \right\rangle \epsilon_\alpha(m)\, u(p,s). \quad (68)$$

The vectors ϵ_α can be parameterised, in a frame where $p = (p_0;\ \cos\varphi\sin\theta\ |\mathbf{p}|,\ \sin\varphi\sin\theta\ |\mathbf{p}|,\ \cos\theta\ |\mathbf{p}|)$, by

$$\begin{aligned} \epsilon_\alpha(0) &= \frac{1}{M_\Delta}(|\mathbf{p}|;\ \cos\varphi\sin\theta\ p_0,\ \sin\varphi\sin\theta\ p_0,\ \cos\theta\ p_0) \\ \epsilon_\alpha(\pm1) &= \frac{1}{\sqrt{2}}(0;\ \mp\cos\varphi\cos\theta + i\sin\varphi,\ \mp\sin\varphi\cos\theta - i\cos\varphi,\ \pm\sin\theta). \end{aligned} \quad (69)$$

The energy projection operator for the Rarita-Schwinger spinor-vector is [66]

$$\sum_S u_\alpha(p,S)\bar{u}_\beta(p,S) = \Lambda_{\alpha\beta}(p) \quad (70)$$

where

$$\Lambda_{\alpha\beta}(p) = (\not{p}+M_\Delta)\left(-g_{\alpha\beta} + \frac{\gamma_\alpha\gamma_\beta}{3} + \frac{\gamma_\alpha p_\beta - \gamma_\beta p_\alpha}{3\, M_\Delta} + \frac{2\, p_\alpha p_\beta}{3\, M_\Delta^2}\right). \quad (71)$$

Equation (71) can be verified by using the explicit parameterisation in equ.(69). Using this projection operator, we can therefore proceed to evaluate the $\pi\Delta$ trace factor, which in this case is

$$\frac{1}{2}\mathrm{Tr}\left[\Lambda_{\alpha\beta}(p)\, k^\alpha k^\beta\, W^{\mu\nu}_\pi(k,q)\, (\not{p}+M)\right] \quad (72)$$

and arrive at the distribution function for a pion with a Δ recoil:

$$f_{\pi\Delta}(y) = \frac{4}{3}\frac{f^2_{\pi N\Delta}}{16\pi^2\, m_\pi^2}\, y \int_{-\infty}^{k^2_{max}} dk^2\, \frac{\mathcal{F}^2_{\pi\Delta}(k^2)}{(k^2-m_\pi^2)^2} \frac{[(M+M_\Delta)^2-k^2]^2\,[(M-M_\Delta)^2-k^2]}{6\, M_\Delta^2} \quad (73)$$

where now the kinematic upper limit on k^2 is $k^2_{max} = -(M_\Delta^2 - (1-y)\, M^2)\, y/(1-y)$. Note that a dipole function for the $\pi N\Delta$ form factor is necessary to suppress contributions from large $|k^2|$.

Contributions from higher-mass baryon resonances can all be computed from the formulae given above because the lower lying states all have spin 1/2 or 3/2. For the (spin 1/2) Roper resonance, which with a mass $M_R = 1440$ MeV is the next heaviest state after the Δ, the trace factor is

$$\frac{1}{2}\mathrm{Tr}\left[(\not{P}+M)\, i\gamma_5\, (\not{p}+M_R)\, i\gamma_5\right] = -k^2 + (M_R - M)^2. \quad (74)$$

With a πNR coupling constant of $g^2_{\pi NR}/4\pi \approx 5.4$ the integral over y of the pion distribution function for a recoil Roper resonance comes to about 10% of that with a nucleon recoil for the

same cut-off parameter. Furthermore, the pion distribution function with a Roper recoil appears at somewhat smaller y than $f_{\pi N}$ or $f_{\pi\Delta}$, which means that the convolution in equ.(62) with the Roper distribution function will only be potentially relevant at very small x. Furthermore, because the Roper has the same quantum numbers as the nucleon, its inclusion as an incoherent contribution is somewhat less justified. In what follows we shall therefore restrict ourselves to the nucleon and Δ baryons only.

In order to conserve momentum and charge, we must also allow for the incident photon to scatter from the recoiling N or Δ after a pion has been emitted, Fig.7(b). Previous attempts at calculating the contributions from these processes within a covariant framework were made by several authors, including Hwang et al. [55], Mulders et al. [44], and Dmitrašinović et al. [67], although all obtained different results. Partly because there is less phenomenological experience with so-called sideways form-factors (where the nucleon, rather than the pion, is off-mass-shell) some early work [52, 56, 68] simply defined $f_{N\pi}(y')$ through equ.(59). However, this is unsatisfactory from a theoretical point of view, and ideally we should be able to verify explicitly that within our model the functions $f_{\pi N}$ and $f_{N\pi}$ satisfy equ.(59). In historical terms, it was the careful examination of this process that opened up a whole Pandora's box of problems, and led to the realisation of the terminal shortcomings of the covariant convolution model. This issue was dealt with more deeply in ref.[43], but let us briefly summarise the origin of the problem.

Clearly the treatment of DIS from an interacting nucleon is considerably more involved than that from a free nucleon. As we saw in the previous section, the truncated nucleon tensor $\widehat{W}_N^{\mu\nu}$. which enters this calculation can be written as a linear combination of three independent terms. Initial calculations [44] assumed that only the term involving the operator $\not{q}$ was relevant. For pointlike nucleons this operator would indeed be the only one present, just as it is for a point-like quark inside a nucleon [69]. Treating the diagram in Fig.7(b) as a Feynman diagram, the contribution to the on-shell nucleon tensor from DIS off the virtual (structured) nucleon with a pion in the final state can be written

$$\begin{aligned}\delta^{(N\pi)}W^{\mu\nu}(P,q) &= g_{\pi NN}^2 \int \frac{d^3\mathbf{k}}{(2\pi)^3(2k_0)} \frac{\mathcal{F}_{N\pi}^2(p^2)}{(p^2-M^2)^2} \\ &\quad \times \frac{1}{2}\mathrm{Tr}\left[(\not{P}+M)\, i\gamma_5\, (\not{p}+M)\, \widehat{W}_N^{\mu\nu}(p,q)\, (\not{p}+M)\, i\gamma_5\right] \qquad (75)\end{aligned}$$

with the tensor $\widehat{W}_N^{\mu\nu}(p,q)$ as defined in equ.(53). Using only the operator $\not{q}$ leads to the virtual nucleon distribution function of ref.[44], namely

$$f_{N\pi}(y') = \frac{3g_{\pi NN}^2}{16\pi^2}\, y' \int_{-\infty}^{p^2_{max}} dp^2\, \frac{\mathcal{F}_{N\pi}^2(p^2)}{(p^2-M^2)^2}\left(-m_\pi^2 - \frac{1-y'}{y'}(p^2-M^2)\right) \qquad (76)$$

where $p^2 = p^2_{max} - p_T^2/(1-y')$ is the 4-momentum squared of the virtual nucleon, with the upper limit now given by $p^2_{max} = M^2y' - m_\pi^2 y'/(1-y')$, and p_T^2 denotes the nucleon's transverse momentum squared. Apart from possible differences in the form factors, equs.(66) and (76) are clearly related by an interchange $y' \leftrightarrow 1-y$.

The large-$|p^2|$ suppression for the $N\pi N$ vertex is introduced by the form factor $\mathcal{F}_{N\pi}$, which

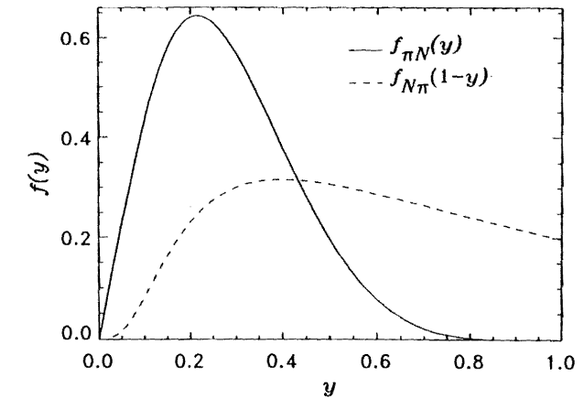

Figure 8: Distribution functions $f_{\pi N}(y)$ and $f_{N\pi}(1-y)$ with dipole form factors, and cut-offs $\Lambda_{\pi N} = 1$ GeV and $\Lambda_{N\pi} = 1475$ MeV chosen to give $\langle n\rangle_{\pi N} = \langle n\rangle_{N\pi} = 0.235$.

is usually parameterised by a monopole or dipole function [44, 70, 71]

$$\mathcal{F}_{N\pi}(p^2) = \left(\frac{\Lambda_{N\pi}^2 - M^2}{\Lambda_{N\pi}^2 - p^2}\right)^n \qquad (77)$$

for $n = 1$ and 2, respectively. However to satisfy equ.(60), the cut-off parameter $\Lambda_{N\pi}$ will in general have to be different from the cut-off $\Lambda_{\pi N}$ regulating the πNN vertex form factor in equ.(66), and a different $\Lambda_{N\pi}$ again to satisfy equ.(61). Furthermore, because the k_T^2 and p_T^2 dependence in the form factors in equs.(67) and (77) are clearly different, the calculated distribution functions $f_{\pi N}$ and $f_{N\pi}$ will in general not satisfy equ.(59). In Fig.8 we plot $f_{\pi N}(y)$ and $f_{N\pi}(1-y)$ for dipole form factors, and cut-offs $\Lambda_{\pi N} = 1$ GeV and $\Lambda_{N\pi} = 1475$ MeV, respectively (to give the same values for $\langle n\rangle_{\pi N}$ and $\langle n\rangle_{N\pi}$, namely ≈ 0.235. Clearly the shapes are quite different, the most obvious difference being that $f_{N\pi}(1-y)$ is finite at $y = 1$.

By using only one operator $\not{q}$ in equ.(75) we are of course assuming that the entire structure function of the virtual nucleon can be represented by the function $\widehat{W}_T^2$ in equ.(53). In the model calculation of the nucleon structure function in ref.[43] it was shown (using the simple quark–nucleon relativistic vertex functions described in sect.4.2), that generally one has non-zero scaling contributions from other functions as well. Furthermore, choosing a different operator form for $\widehat{W}_N^{\mu\nu}$ can also lead to unphysical results. For example, with an operator involving I rather than $\not{q}$ the trace factor in equ.(75) is proportional to $-m_\pi^2$ (i.e. negative) [67].

Problems also arise for the emission of scalar mesons, for which the trace factor in $f_{N\sigma}(y')$ for the structure $\not{q}$ is $4M^2 - m_\sigma^2 + (M^2-p^2)(1-y')/y'$, which is clearly related to the trace in $f_{\sigma N}(y)$ (namely $k^2 + 4M^2$) when written in terms of the transverse momentum squared. For an operator I, the trace factor in $f_{N\sigma}(y')$ is $2p^2 + 2M^2 - m_\sigma^2$, which not only violates baryon number conservation but also leads to an unphysical (negative) cross-section. For the DIS from

a virtual Δ component, these same difficulties will also be present, since the Δ hadronic tensor will have a non-trivial spinor structure, similar to that for the nucleon.

These are the first hints of problems with the covariant approach to calculating DIS processes involving virtual nucleons. Indeed, the convolution formula in equ.(63) appears to be a very special case that cannot be easily obtained from the above considerations. The prescription of ignoring some of the structures in $\widehat{W}_N^{\mu\nu}$ is clearly unsatisfactory, as in principle all should be used. Another important assumption in the covariant convolution model is that the dependence of the virtual meson and baryon structure functions in equs.(62) and (63) on the particles' invariant mass squared is negligible. The argument usually made is that the vertex form factor suppresses contributions from the far off-mass-shell configurations (i.e. for $|k^2| \gtrsim 10\ M^2$ [56]). However, strictly speaking, in this approach even the identification of the off-shell structure functions themselves is not very clear. Some suggestions about how to relate the off-shell functions to the on-shell ones were made [72, 73] in the context of DIS from nuclei, although these were more *ad hoc* prescriptions rather than theoretical derivations. More importantly, a covariant treatment of DIS from virtual nucleons essentially involves both nucleon and antinucleon degrees of freedom. In contrast to this, the Fock state expansion in equ.(57), and in particular the interpretation of $f(y)$ as meson and baryon probability functions, is only meaningful in the IMF. Thus, simply put, the difficulties encountered in trying to obtain sensible results from the covariant calculation of $f(y)$ result from an incompatibility of the covariant formalism with the initial hypothesis that the physical nucleon state can be expanded as in equ.(57). The challenge is therefore to formulate the problem self-consistently, using a single formalism. Since we would like to study the relevance of the virtual meson cloud of the nucleon, the most economical solution would be to keep the Fock state expansion in equ.(57), and reformulate the rest of the problem in time-ordered perturbation theory (TOPT), where equ.(57) is well defined. In fact, an early calculation of the function $f_{\pi N}(y)$ in TOPT was performed some time ago by Güttner et al. [74], in the context of pion electroproduction. More recently the merits of this approach were expounded by Zoller [75], who demonstrated that the distribution functions for the πN and $\pi\Delta$ states calculated in this fashion satisfied equ.(59).

5.2 Pions – TOPT in the IMF

An alternative to the use of covariant Feynman diagrams, in the form of "old-fashioned" time-ordered perturbation theory in the IMF, was proposed some time ago by Weinberg [76] for scalar particles. This was later extended by Drell, Levy and Yan [77] to the πN system in DIS. The main virtues of this approach are that off-mass-shell ambiguities in the structure functions of virtual particles can be avoided, and that the meson and baryon distribution functions can be shown to satisfy equ.(59) exactly. We firstly review the results for the pion cloud, and then compare these with the previous, covariant calculations.

In the time-ordered theory the analogue of Fig.7(a) will now involve two diagrams in which the pion moves forwards and backwards in time, Fig.9. However, in a frame of reference where the target nucleon is moving fast in the z direction with longitudinal momentum $P_L(\to \infty)$,

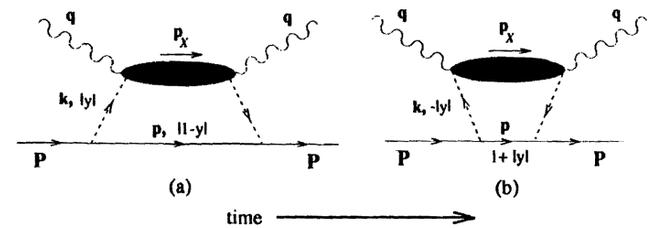

Figure 9: Time-ordered diagrams for pions moving (a) forwards and (b) backwards in time. Time is increasing from left to right.

only that diagram involving a forward moving pion gives a non-zero contribution. In the IMF the target nucleon of momentum $\mathbf{P} = (0_T, P_L)$ has energy

$$P_0 = P_L + \frac{M^2}{2P_L} + O\left(\frac{1}{P_L^2}\right). \tag{78}$$

Following Weinberg [76] we write the pion 3-momentum as

$$\mathbf{k} = y\,\mathbf{P} + \mathbf{k}_T \tag{79}$$

where $\mathbf{k}_T \cdot \mathbf{P} = 0$, and conservation of momentum demands that the recoil nucleon momentum is

$$\mathbf{p} = (1-y)\,\mathbf{P} - \mathbf{k}_T. \tag{80}$$

Since all particles are on their mass shells the energies of the intermediate meson and baryon must be

$$k_0 = |y|\,P_L + \frac{k_T^2 + m_\pi^2}{2\,|y|P_L} + O\left(\frac{1}{P_L^2}\right) \tag{81}$$

$$p_0 = |1-y|\,P_L + \frac{k_T^2 + M^2}{2\,|1-y|P_L} + O\left(\frac{1}{P_L^2}\right). \tag{82}$$

For forward moving particles, Fig.9(a), y and $1-y$ are positive, and applying the rules of TOPT [76] the contribution to the hadronic tensor of the physical nucleon can be written

$$\delta^{(\pi N)}W^{\mu\nu}(P,q) = \int \frac{d^3\mathbf{k}}{(2\pi)^3(2p_0)(2k_0)^2}\frac{g_{\pi NN}^2(k)}{(P_0-p_0-k_0)^2} \times\frac{1}{2}\mathrm{Tr}\left[(\not p + M)\,i\gamma_5\,W_\pi^{\mu\nu}(p,q)\,(\not p + M)\,i\gamma_5\right]. \tag{83}$$

The energy denominator in equ.(83) can be rewritten as $(P_0 - p_0 - k_0) = (M^2 - s_{\pi N})/2P_L$, where

$$s_{\pi N} = s_{\pi N}(k_T^2, y) = (p_0 + k_0)^2 - (\mathbf{p}+\mathbf{k})^2 = \frac{k_T^2 + m_\pi^2}{y} + \frac{k_T^2 + M^2}{1-y} \tag{84}$$

is the centre of mass energy squared of the intermediate πN state. Changing the variables of integration from $d^3\mathbf{k}$ to dy and dk_T^2, all powers of P_L are seen to cancel when combined with

the vertex factors, $(2p_0)^{-1}$ and $(2k_0)^{-2}$, leading to a result that is P_L-independent. Equating coefficients of $g_{\mu\nu}$, we find that the π distribution function with an N recoil is

$$f_{\pi N}(y) = \frac{3g^2_{\pi NN}}{16\pi^2}\int_0^\infty \frac{dk_T^2}{(1-y)\,y}\frac{\mathcal{F}^2_{\pi N}(s_{\pi N})}{(M^2-s_{\pi N})^2}\left(\frac{k_T^2+y^2M^2}{1-y}\right) \tag{85}$$

which means that the result of equ.(66) is reproduced, form factor aside. Obviously because here all particles are on-mass-shell, we cannot use the same k^2-dependent form factor as in the covariant case. In the time-ordered calculation, it is quite natural to choose the form factor to be a function of the centre of mass energy squared of the πN system, $s_{\pi N}$, as was done by Zoller [75]. For the functional form of $\mathcal{F}_{\pi N}(s_{\pi N})$ we choose a dipole parameterisation,

$$\mathcal{F}_{\pi N}(s_{\pi N}) = \left(\frac{\Lambda^2+M^2}{\Lambda^2+s_{\pi N}}\right)^2 \tag{86}$$

normalised so that the coupling constant $g_{\pi NN}$ has its standard value at the pole ($\mathcal{F}(M^2)=1$). Previously, in refs.[75, 78] an exponential function was used

$$\mathcal{F}_{\pi N}(s_{\pi N}) = \exp\left(\frac{M^2-s_{\pi N}}{\Lambda_e^2}\right), \tag{87}$$

although ref.[75] in addition followed an unconventional normalisation.

For a backward moving meson, Fig.9(b), y is negative, and in this case the energy denominator becomes $(P_0-p_0-k_0) = 2yP_L + O(1/P_L)$. Therefore in the $P_L\to\infty$ limit this time-ordering is suppressed by a power of $1/P_L^4$, and so does not contribute.

For an interacting nucleon with a pion recoil, the contribution to the nucleon hadronic tensor is

$$\begin{aligned}\delta^{(N\pi)}W^{\mu\nu}(P,q) &= \int \frac{d^3\mathbf{p}}{(2\pi)^3(2p_0)^2(2k_0)}\frac{g^2_{\pi NN}(p)}{(P_0-p_0-k_0)^2}\\ &\quad\times\frac{1}{2}\mathrm{Tr}\left[(\not P+M)\,i\gamma_5\,(\not p+M)\,\widehat{W}^{\mu\nu}_N(p,q)\,(\not p+M)\,i\gamma_5\right].\end{aligned} \tag{88}$$

The kinematics here are similar to those described above, namely the nucleon and pion move with 3-momenta

$$\mathbf{p} = y'\,\mathbf{P}-\mathbf{k}_T \tag{89}$$

$$\mathbf{k} = (1-y')\,\mathbf{P}+\mathbf{k}_T \tag{90}$$

and have energies

$$p_0 = |y'|\,P_L + \frac{k_T^2+M^2}{2\,|y'|P_L} + O\left(\frac{1}{P_L^2}\right) \tag{91}$$

$$k_0 = |1-y'|\,P_L + \frac{k_T^2+m_\pi^2}{2\,|1-y'|P_L} + O\left(\frac{1}{P_L^2}\right) \tag{92}$$

respectively. Then direct evaluation of the trace in equ.(88) gives

$$\begin{aligned}&2\,(2P\cdot p - 2M^2)\left[\tilde{g}^{\mu\nu}\left(2M\widehat{W}^0_T + 2M^2\widehat{W}^1_T + 2p\cdot q\,\widehat{W}^2_T\right) + \ldots\right]\\ &= 2\,(2P\cdot p - 2M^2)\,\tilde{g}^{\mu\nu}\,W_{1N}(p,q) + \cdots\end{aligned} \tag{93}$$

where now the exact on-shell nucleon structure function appears, and automatically factorises.

For a backward moving nucleon, y' is negative, and $2P\cdot p - 2M^2 = -4y'P_L^2 + O(1/P_L)$, so that the numerator becomes large in the $P_L\to\infty$ limit. Technically this is due to the "badness" of the operator γ_5, which mixes upper and lower components of the nucleon spinors. The energy denominator here is $(P_0-p_0-k_0) = 2y'P_L + O(1/P_L)$, and when squared and combined with the $1/P_L^2$ from the integration and vertex factors, the contribution from this diagram vanishes when P_L is infinite. Therefore we need only evaluate the diagram with the forward moving nucleon, which gives the result

$$f_{N\pi}(y') = \frac{3g^2_{\pi NN}}{16\pi^2}\int_0^\infty \frac{dk_T^2}{(1-y')\,y'}\frac{\mathcal{F}^2_{N\pi}(s_{N\pi})}{(M^2-s_{N\pi})^2}\left(\frac{k_T^2+(1-y')^2M^2}{y'}\right) \tag{94}$$

with

$$s_{N\pi}(k_T^2,y') = s_{\pi N}(k_T^2,1-y') = \frac{k_T^2+M^2}{y'} + \frac{k_T^2+m_\pi^2}{1-y'}. \tag{95}$$

Notice that the integrand is identical to that in equ.(76), when p^2 there is written in terms of p_T^2 (or k_T^2), except perhaps for the form factor. It was shown in [75] that within this approach there is an explicit symmetry between the processes in which the intermediate pion and the intermediate nucleon are struck if the form factor in $f_{N\pi}$ is taken to be

$$\mathcal{F}_{N\pi}(s_{N\pi}) = \mathcal{F}_{\pi N}(s_{\pi N}). \tag{96}$$

Then as long as the same cut-off mass parameter is used in both vertex functions, equ.(59) is automatically satisfied. [3] In Fig.10 we plot the function $f_{\pi N}(y)$ evaluated in the IMF, with both the y-dependent exponential, equ.(87), and dipole, equ.(86), form factors, and compare this with the function evaluated in the covariant approach, with the k^2-dependent dipole form factor in equ.(67). In order to make the comparison meaningful the cut-offs have been chosen to yield the same pion multiplicity $\langle n\rangle_{\pi N}$ ($\simeq 0.235$), for which the cut-offs are $\Lambda_{\pi N} = 1$ GeV, $\Lambda_e = 1380$ MeV and $\Lambda = 1425$ MeV. With the y-dependent exponential form factor $f_{\pi N}(y)$ is a little broader and peaks at around $y = 0.3$, compared with $y\simeq 0.2$ for the covariant convolution model with a dipole form factor. The y-dependent dipole form factor yields a distribution which is a little broader still. The consequence of this will be that the convolution of $f_{\pi N}(y)$ with F_{2M} for the y-dependent form factors will have a slightly smaller peak and extend to marginally larger x (see sect.5.4).

The processes involving DIS from $\pi\Delta$ states can also be calculated in the IMF, although some care must be taken when describing the $\pi N\Delta$ interaction vertex in TOPT. Namely, in TOPT the relevant vertex is $\bar{u}_\alpha(p)\,(P-p)^\alpha\,u(P)$, rather than $\bar{u}_\alpha(p)\,k^\alpha\,u(P)$ as in the covariant theory, where of course the two are (trivially) identical. Using the same formalism as for calculating $f_{\pi N}$, and with the kinematics as given by equs.(78) to (82), but with $M\to M_\Delta$, we find that the pion distribution function with a Δ left in the final state is:

[3] The form factor in equ.(86) may also reduce the number of free parameters in models of NN or $N\bar{N}$ scattering [79], where currently different form factors are necessary for the meson- and baryon-exchange diagrams.

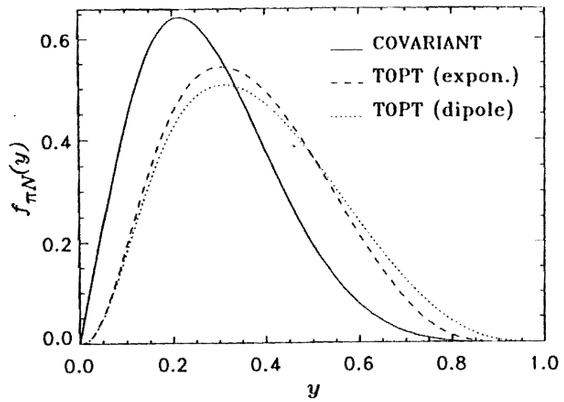

Figure 10: Distribution functions $f_{\pi N}(y)$ evaluated using covariant and time-ordered perturbation theory. The covariant function is as in Fig.8. The TOPT functions are evaluated with exponential and dipole form factors, with cut-offs $\Lambda_e = 1380$ MeV and $\Lambda = 1425$ MeV, respectively, to give the same value for $\langle n \rangle_{\pi N} = 0.235$.

$$f_{\pi\Delta}(y) = \frac{4}{3}\frac{f^2_{\pi N\Delta}}{16 m_\pi^2 \pi^2}\int_0^\infty \frac{dk_T^2}{(1-y)}\frac{\mathcal{F}^2_{\pi\Delta}(s_{\pi\Delta})}{y\,(s_{\pi\Delta}-M^2)^2} \times \frac{[k_T^2+(M_\Delta-(1-y)M)^2]\,[k_T^2+(M_\Delta+(1-y)M)^2]^2}{6\,M_\Delta^2\,(1-y)^3} \tag{97}$$

where $s_{\pi\Delta} = s_{\pi N}(M \to M_\Delta)$, and we take the same functional form for the $\pi N\Delta$ form factor as for the πNN form factor in equ.(86).

For an interacting Δ with a pion recoil we need additional information on the truncated Δ hadronic tensor, which in this case will involve additional Lorentz indices stemming from the fact that the Δ has spin 3/2. For an on-shell Δ the hadronic tensor can be represented as [80]:

$$W_\Delta^{\mu\nu}(p,q) = \frac{1}{4}\mathrm{Tr}\left[\Lambda_{\alpha\beta}(p)\,\widehat{W}_\Delta^{\mu\nu\alpha'\beta'}(p,q)\right] \tag{98}$$

with $\Lambda^{\alpha\beta}(p)$ the Δ energy projector given in equ.(71). Assuming the simplest structure for the truncated Δ tensor, namely [75]

$$\widehat{W}_\Delta^{\mu\nu\alpha\beta}(p,q) = -g^{\alpha\beta}\,\widehat{W}_\Delta^{\mu\nu}(p,q) \tag{99}$$

where $\widehat{W}_\Delta^{\mu\nu}$ has the same Dirac and Lorentz structure as the truncated nucleon tensor, gives the result

$$W_\Delta^{\mu\nu}(p,q) = 2\left(M_\Delta\widehat{W}_\Delta^0 + M_\Delta^2\widehat{W}_\Delta^1 + p\cdot q\widehat{W}_\Delta^2\right)\tilde{g}^{\mu\nu} + \cdots \tag{100}$$

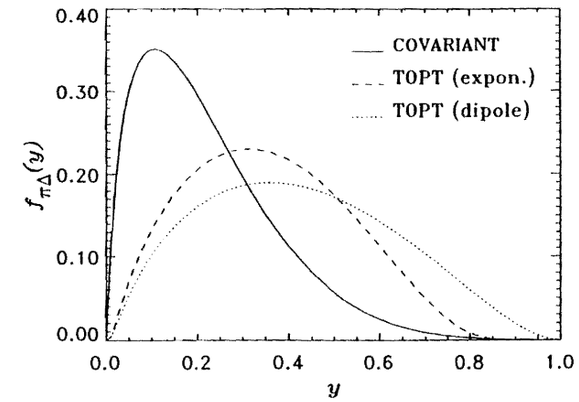

Figure 11: Distribution functions $f_{\pi\Delta}(y)$ evaluated using covariant and time-ordered perturbation theory. The covariant function is evaluated with a dipole form factor with cut-off mass $\Lambda_{\pi\Delta} = 1$ GeV. The TOPT functions have exponential and dipole form factors, with cut-offs $\Lambda_e = 1565$ MeV and $\Lambda = 1512$ MeV, respectively, to give the same value for $\langle n \rangle_{\pi N} = 0.114$.

so that by comparing coefficients of $g^{\mu\nu}$ we can use the term in parentheses to define the on-shell Δ structure function. Utilising the form equ.(99) for the truncated Δ tensor, we can then evaluate the trace

$$\begin{aligned}&\frac{1}{2}\mathrm{Tr}\left[(\not{P}+M)\,(P-p)_\alpha\,\Lambda^{\alpha\alpha'}(p)\;\widehat{W}_{\mu\nu\alpha\beta}(p,q)\,\Lambda^{\beta'\beta}(p)\;(P-p)_\beta\right]\\ &= \frac{1}{6\,M_\Delta^2\,y'^3}\left(k_T^2+(M_\Delta-y'M)^2\right)\left(k_T^2+(M_\Delta+y'M)^2\right)^2\\ &\quad\cdot\left((2M_\Delta\widehat{W}_\Delta^0+M_\Delta^2\widehat{W}_\Delta^1+p\cdot q\widehat{W}_\Delta^2)\,\tilde{g}_{\mu\nu}+\cdots\right)\end{aligned} \tag{101}$$

so that the on-shell Δ structure function factorises to give equ.(63), with the virtual Δ distribution function given by

$$f_{\Delta\pi}(y') = \frac{4}{3}\frac{f^2_{\pi N\Delta}}{m_\pi^2\,16\pi^2}\int_0^\infty \frac{dk_T^2}{(1-y')}\frac{\mathcal{F}^2_{\Delta\pi}(s_{\Delta\pi})}{y'\,(s_{\Delta\pi}-M^2)^2} \times \frac{[k_T^2+(M_\Delta-y'M)^2]\,[k_T^2+(M_\Delta+y'M)^2]^2}{6\,M_\Delta^2\,y'^3}. \tag{102}$$

Clearly this is related to $f_{\pi\Delta}(y)$ by equ.(59) if $\mathcal{F}_{\pi\Delta}(s_{\pi\Delta}) = \mathcal{F}_{\Delta\pi}(s_{\Delta\pi})$, where $s_{\Delta\pi} = s_{\pi\Delta}(M \to M_\Delta)$.

In Fig.11 we compare the function $f_{\pi\Delta}(y)$, calculated in the IMF, with the function given by equ.(73). The k^2-dependent form factor in the covariant formulation is a dipole form ($\Lambda_{\pi\Delta} = 1$ GeV), while the $s_{\pi\Delta}$-dependent form factors are dipole ($\Lambda = 1512$ MeV) and exponential ($\Lambda_e = 1565$ MeV), with all functions normalised to give the same $\langle n \rangle_{\pi\Delta} (\approx 0.114)$. Whereas for $f_{\pi N}(y)$ the y-dependent form factors produced a slight hardening of the distributions when

compared with the covariant form factor, here we see a marked difference between the two calculations, in which the distributions calculated in the IMF are considerably broader and extend to larger y.

Having found a useful method for obtaining the pion distributions in a self-consistent manner, we next apply the TOPT/IMF formalism to non-pseudoscalar mesons. As we shall see the difficulties encountered in attempting to compute the contributions from vector mesons make the covariant approach to this problem very problematic, and from a technical point of view the vector mesons can only be handled adequately in the IMF. From a physical point of view, our aim will be to test the relevance or otherwise of the higher mass meson states in the physical nucleon. We focus primarily on the vector mesons, but also briefly re-examine the importance of kaons in the time-ordered formalism.

5.3 Heavier Mesons

The importance of vector mesons in nuclear physics is well known. In the context of meson exchange models of the NN force in nuclear physics, it has long been realised that vector mesons play a vital role [79,81-86]. For example, the isovector ρ meson provides some cancellation of the tensor force generated by π meson exchange. On the other hand, the isoscalar ω meson, through its large vector coupling, is responsible for the short range NN repulsive force, and also provides most of the spin-orbit interaction. Traditionally it has been necessary to use hard vector meson—nucleon form factors in order to fit the NN phase shifts [79]. However, alternative approaches have recently been developed in which the NN data can be fitted with quite soft form factors [86-88].

¿From another direction, the vector meson dominance model of the elastic electromagnetic nucleon form factors, in which an isovector photon couples to the nucleon via a ρ meson, provides a natural explanation of the dipole Q^2 behaviour of the γNN vertex function. Recent analyses [86] have shown that a ρNN vertex parameterised by a soft monopole form factor ($\Lambda_{\text{monopole}} \sim 800$ MeV) provides a good description of the Q^2 dependence of the Dirac and Pauli form factors. The effect of vector mesons upon nucleon electromagnetic form factors has also been explored [61, 89] in the cloudy bag model [47], and in various soliton models [90].

In previous calculations [55], the vector meson distributions were evaluated within a covariant framework, but with the assumption that the vector meson and nucleon intermediate states were on-mass-shell. In this section we extend the analysis of pions in sect.5.2 to the vector meson sector. Specifically, we shall demonstrate that the vector meson functions, calculated within the TOPT/IMF formalism, can be made to satisfy the relation equ.(59) exactly.

For the effective VNN interaction we include both a vector, $g_{VNN}\ \bar{u}(p)\gamma^\alpha\epsilon_\alpha u(P)$, and a tensor, $f_{VNN}/(4M)\ \bar{u}(p)\ i\sigma^{\alpha\beta}[(P_\alpha - p_\alpha)\epsilon_\beta - (P_\beta - p_\beta)\epsilon_\alpha]u(P)$, coupling, where $V = \rho$ or ω, and $\epsilon_\alpha(\lambda)$ is the polarisation vector for a spin 1 meson with helicity λ. In the calculation of the vector meson distributions in ref.[78] the tensor coupling was taken to be $\sim \bar{u}(p)i\sigma^{\alpha\beta}k_\alpha\epsilon_\beta u(P)$ [79]. In our treatment of the $\pi\Delta$ states in the previous section, the derivative interaction was constructed from baryon momenta, $P_\alpha - p_\alpha$, rather than from the pion momentum k_α. For overall consistency in calculating contributions from all the meson-baryon states, we therefore

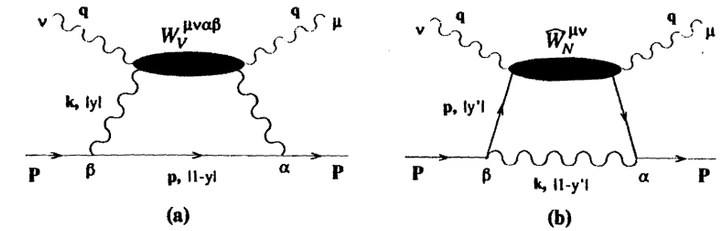

Figure 12: Time-ordered diagrams for the DIS from (a) vector mesons and (b) nucleons with recoil vector mesons, that are non-zero in the IMF.

use the above interaction for the tensor VNN vertex also [91]. In both cases, however, one can explicitly verify that the probability conservation condition, equ.(59), is satisfied [78].

The contribution from the diagram with backward moving vector mesons is suppressed in the IMF by the energy denominators, just as for pions. Therefore we only need to evaluate the diagram with forward moving vector mesons, which gives the following contribution to the nucleon hadronic tensor

$$\begin{aligned}\delta^{(VN)}W^{\mu\nu}(P,q) &= \int \frac{d^3\mathbf{k}}{(2\pi)^3(2p_0)(2k_0)^2}\frac{1}{(P_0-p_0-k_0)^2} \\ &\times\frac{1}{2}\sum_{\lambda,\lambda'}\mathrm{Tr}\Big[(\not{P}+M)\ \Big(g_{VNN}(k)\ \gamma^{\alpha'} + \frac{f_{VNN}(k)}{4M}2i\sigma^{\alpha''\alpha'}\ (P_{\alpha''}-p_{\alpha''})\Big) \\ &\cdot(\not{p}+M)\ \epsilon^*_{\alpha'}(\lambda)\epsilon_\alpha(\lambda)\ \ W_V^{\mu\nu\alpha\beta}(k,q)\ \ \epsilon^*_\beta(\lambda')\epsilon_{\beta'}(\lambda') \\ &\cdot\Big(g_{VNN}(k)\ \gamma^{\beta'} + \frac{f_{VNN}(k)}{4M}2i\sigma^{\beta''\beta'}\ (P_{\beta''}-p_{\beta''})\Big)\Big]\ . \quad (103)\end{aligned}$$

Evaluating the trace gives

$$\Big(g^2_{VNN}(k)\ A_{\alpha\beta}\ +\ f^2_{VNN}(k)\ B_{\alpha\beta}\ +\ g_{VNN}(k)\ f_{VNN}(k)\ C_{\alpha\beta}\Big) \quad (104)$$

where

$$\begin{aligned}A_{\alpha\beta} &= (P-p)^2\ g_{\alpha\beta}\ +\ 2\ (P_\alpha p_\beta\ +\ p_\alpha P_\beta) \\ B_{\alpha\beta} &= (P-p)^2\ g_{\alpha\beta}\ -\ (P_\alpha P_\beta + p_\alpha p_\beta)\ -\ \frac{1}{2}(P_\alpha - p_\alpha)(P_\beta - p_\beta)\ +\ \frac{P\cdot p}{2M^2}(P_\alpha + p_\alpha)(P_\beta + p_\beta) \\ C_{\alpha\beta} &= 2\ (P-p)^2\ g_{\alpha\beta}\ -\ (P_\alpha - p_\beta)\ (P_\beta - p_\alpha) \quad (105)\end{aligned}$$

are the VNN vertex trace factors for the vector, tensor and vector–tensor interference couplings, respectively. For an on-mass-shell vector meson, the spin 1 tensor $W_V^{\mu\nu\alpha\beta}$, symmetric under the interchange of $\mu \leftrightarrow \nu$ and $\alpha \leftrightarrow \beta$, is given by

$$W_V^{\mu\nu\alpha\beta}(k,q)\ =\ \Big(\tilde{g}^{\mu\nu}\ W_{1V}(k,q)\ +\ \frac{\tilde{k}^\mu\ \tilde{k}^\nu}{m_V^2}\ W_{2V}(k,q)\Big)\ \tilde{g}^{\alpha\beta}. \quad (106)$$

This form guarantees that the vector current is conserved, $k_{\alpha(\beta)}W_V^{\mu\nu\alpha\beta} = 0 = q_{\mu(\nu)}W_V^{\mu\nu\alpha\beta}$. Furthermore, it reproduces the correct unpolarised on-shell spin 1 tensor when contracted with

the meson polarisation vectors ($\epsilon_{\alpha(\beta)}$) and summed over the V helicity, λ [92]:

$$\begin{aligned} W_V^{\mu\nu}(k,q) &= \sum_\lambda \epsilon_\alpha^*(\lambda,k)\ \epsilon_\beta(\lambda,k)\ W_V^{\mu\nu\alpha\beta}(k,q) \\ &= \left(-g_{\alpha\beta} + \frac{k_\alpha k_\beta}{k^2}\right) W_V^{\mu\nu\alpha\beta}(k,q) \qquad (107) \\ &\propto \tilde{g}^{\mu\nu}\ W_{1V}(k,q) + \frac{\tilde{k}^\mu\ \tilde{k}^\nu}{m_V^2}\ W_{2V}(k,q). \end{aligned}$$

In the case of DIS from a vector particle emitted by a nucleon, we contract the spin 1 tensor $W_V^{\mu\nu\alpha\beta}$ with the VNN vertex trace factors in equ.(105). Equating coefficients of $g^{\mu\nu}$ in equ.(103), and using the same IMF kinematics as for the πN system, except with $m_\pi \to m_V$, together with the Callan-Gross relation for the nucleon and vector meson, enables the contribution to F_{2N} from vector mesons to be written as a convolution of the vector meson distribution function $f_{VN}(y)$ with the on-shell vector meson structure function $F_{2V}(x/y)$, as in equ.(62), where now

$$\begin{aligned} f_{VN}(y) &= \frac{c_V}{16\pi^2}\int_0^\infty \frac{dk_T^2}{(1-y)\,y}\frac{\mathcal{F}_{VN}^2(s_{VN})}{(M^2-s_{VN})^2} \\ &\times\Bigg\{ g_{VNN}^2\left(\frac{(k_T^2+y^2M^2+m_V^2)\,(k_T^2+y^2M^2+(1-y)^2m_V^2)}{y^2(1-y)m_V^2} + \frac{k_T^2+y^2M^2}{1-y} - 4M^2\right) \\ &+ g_{VNN}\ f_{VNN}\left(-\frac{(k_T^2+y^2M^2-(1-y)m_V^2)^2}{2(1-y)^2)m_V^2} + \frac{4\,(k_T^2+y^2M^2)}{(1-y)}\right) \\ &+ f_{VNN}^2\left(\frac{(2-y)^2\ (k_T^2+y^2M^2+(1-y)m_V^2)^2\,(k_T^2+(4(1-y)+y^2)M^2)}{16y^2(1-y)^3M^2m_V^2}\right. \\ &\quad - \frac{(k_T^2+y^2M^2)\,(k_T^2+(-4(1+y)+y^2)M^2)}{4(1-y)^2M^2} \\ &\quad \left. - \frac{(k_T^2+y^2M^2+(1-y)^2m_V^2)^2}{2y^2(1-y)^2m_V^2} - \frac{(k_T^2+y^2M^2+m_V^2)^2}{2y^2m_V^2}\right)\Bigg\} \qquad (108) \end{aligned}$$

where $c_V = 1 + 2\delta_{V\rho}$ is the isospin factor (here δ is the Kronecker-δ symbol). The VN centre of mass energy squared is $s_{VN} = s_{\pi N}(m_\pi \to m_V)$, and we take the same form factor for both the vector and tensor couplings, $g_{VNN}(s_{VN}) = g_{VNN}\ \mathcal{F}_{VN}(s_{VN})$ and $f_{VNN}(s_{VN}) = f_{VNN}\ \mathcal{F}_{VN}(s_{VN})$, with $\mathcal{F}_{VN}(s_{VN})$ defined analogously to equ.(86).

For the vector meson recoil process, we evaluate the distribution function $f_{NV}(y')$ using the full spinor structure of $\widehat{W}_N^{\mu\nu}$ given in equ.(53):

$$\begin{aligned} \delta^{(NV)}W^{\mu\nu}(P,q) &= \int \frac{d^3\mathbf{p}}{(2\pi)^3(2p_0)^2(2k_0)}\frac{1}{(P_0-p_0-k_0)^2} \\ &\times\frac{1}{2}\sum_\lambda \mathrm{Tr}\Bigg[(\not{P}+M)\left(g_{VNN}(p)\ \gamma^\alpha + \frac{f_{VNN}(p)}{4M}2i\sigma^{\alpha'\alpha}(P_{\alpha'}-p_{\alpha'})\right)(\not{p}+M)\ \widehat{W}_N^{\mu\nu}(p,q)\ (\not{p}+M) \\ &\quad\cdot\left(g_{VNN}(p)\ \gamma^\beta + \frac{f_{VNN}(p)}{4M}2i\sigma^{\beta'\beta}(P_{\beta'}-p_{\beta'})\right)\epsilon_\alpha^*(\lambda)\epsilon_\beta(\lambda)\Bigg]. \qquad (109) \end{aligned}$$

Performing the contractions over the indices α,β leads to the convolution integral of equ.(63), with the nucleon distribution function $f_{NV}(y')$ with a vector meson recoil given by equ.(108)

but with $y \to 1-y'$, with $s_{NV}(k_T^2,y') = s_{VN}(k_T^2,1-y')$. Again, we have evaluated only the diagram with forward moving nucleons which is non-zero in the IMF. Thus we can prove that the probability distributions for the VN intermediate states are related by $f_{NV}(y') = f_{VN}(1-y')$.

One should observe that the trace factor inside the braces in $f_{VN}(y)$ is divergent in the limit $y \to 0$. To illustrate one of the problems with the covariant approach to calculating f_{VN}, consider a form factor which behaves like $\exp[y\ (M^2 - s_{VN})]$. Since $k^2 = -(k_T^2+M^2y^2)/(1-y)$, this form factor corresponds to a k^2-dependent covariant form factor proportional to $\exp[k^2 - m_V^2]$. With such a form factor, $\delta^{(VN)}F_{2N}(x)$ would approach a finite value as $x \to 0$, much like a perturbative sea distribution. However, there are several problems with accepting such a result, the most obvious of which is that it would violate charge and momentum conservation very badly, since $f_{NV}(y') \to 0$ for $y' \to 1$ and $\to$ constant as $y' \to 0$ when the same form factor is used for the diagram where the nucleon is struck (i.e. a form factor which in the covariant formalism corresponds to $\exp[p^2 - M^2]$). Furthermore, it would lead to a gross violation of the Adler sum rule, which integrates the flavor combination $u - \bar{u} - d + \bar{d}$, and such a violation has not been observed in the range $1 < Q^2 < 40$ GeV^2 [93]. This gives further evidence for the preference of the IMF approach together with the y-dependent form factor in equ.(86) or (87).

To complete our discussion of vector mesons, we give the results for the functions describing the $V\Delta$ states. We saw in the previous section that the contributions from the $\pi\Delta$ states were certainly not negligible in comparison with the πN components of the physical nucleon. For the vector mesons, we would also like to examine whether the Δ isobar is of any importance. Since the ω meson is isoscalar, the only vector meson able to couple to a nucleon and Δ is the ρ, and for this we use a pseudovector coupling [79], $(f_{\rho N\Delta}/m_\rho)\ \bar{u}(P)\ i\gamma_5\gamma^\alpha u^\beta(p)\ ((P-p)_\alpha\epsilon_\beta - (P-p)_\beta\epsilon_\alpha)$. Again, we drop those diagrams which give order $1/P_L^4$ contributions in IMF (i.e. for backward moving ρ mesons or Δ). The contribution from scattering from a ρ meson with a Δ recoil is obtained by evaluating the following trace:

$$\begin{aligned} &\frac{1}{2}\sum_{\lambda,\lambda'}\mathrm{Tr}\Big[(\not{P}+M)\ i\gamma_5\gamma^\alpha\ \Lambda^{\alpha'\beta'}(p)\ \left((P-p)_\alpha\epsilon_{\alpha'}^*(\lambda)\epsilon_{\alpha''}(\lambda)\ -\ (P-p)_{\alpha'}\epsilon_\alpha^*(\lambda)\epsilon_{\alpha''}(\lambda)\right) \\ &\quad\cdot W_\rho^{\mu\nu\alpha''\beta''}(k,q)\ i\gamma_5\gamma^\beta\ \left((P-p)_{\beta'}\epsilon_{\beta''}^*(\lambda')\epsilon_\beta(\lambda')\ -\ (P-p)_\beta\epsilon_{\beta''}^*(\lambda')\epsilon_{\beta'}(\lambda')\right)\Big] \qquad (110) \end{aligned}$$

where $W_\rho^{\mu\nu\alpha\beta}$ is the ρ meson structure tensor, as given in equ.(106). The resulting probability distribution to find a ρ in the physical nucleon with a Δ recoil is therefore

$$\begin{aligned} f_{\rho\Delta}(y) &= \frac{4}{3}\frac{f_{\rho N\Delta}^2}{m_\rho^2\ 16\pi^2}\int_0^\infty \frac{dk_T^2}{(1-y)\,y}\frac{\mathcal{F}_{\rho\Delta}^2(s_{\rho\Delta})}{(M^2-s_{\rho\Delta})^2} \\ &\times\Bigg\{-\frac{4\ MM_\Delta}{3}\left(2M_\Delta^2 + MM_\Delta + 2M^2\right) - \frac{4\ MM_\Delta}{3m_\rho^2}((P-p)\cdot k)^2 \\ &\quad - \frac{4}{3m_\rho^2}\left(M_\Delta^2(P\cdot k)^2 + M^2(p\cdot k)^2\right) + \frac{4\ P\cdot p}{3}\left(2M_\Delta^2 + 4MM_\Delta + M^2\right) \qquad (111) \\ &\quad + \frac{4\ P\cdot p}{3m_\rho^2}(p\cdot k)^2\left(1 - \frac{M^2}{M_\Delta^2}\right) - 4\ (P\cdot p)^2\left(1 - \frac{2P\cdot k\ p\cdot k}{3m_\rho^2M_\Delta^2} - \frac{P\cdot p}{3M_\Delta^2}\right)\Bigg\} \end{aligned}$$

with the kinematics as given in equs.(78) through (82), except with $m_\pi \to m_\rho$ and $M \to M_\Delta$.

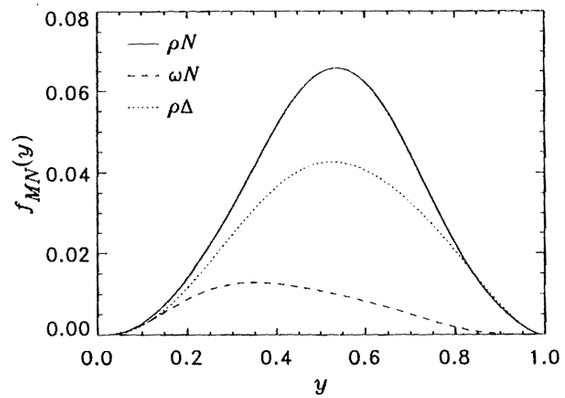

Figure 13: Vector meson distribution functions in the nucleon. The (dipole) form factor cut-off is $\Lambda = 700$ MeV for all curves.

For the DIS off a virtual Δ with a ρ meson recoil, we need to evaluate the trace

$$\frac{1}{2}\sum_{\lambda}\mathrm{Tr}\left[(\not{P}+M)\; i\gamma_5\gamma_\alpha\; \left((P-p)^\alpha\epsilon^{\alpha'*}(\lambda)-(P-p)^{\alpha'}\epsilon^{\alpha*}(\lambda)\right)\right.$$
$$\cdot\Lambda_{\alpha'\alpha''}(p)\;\widehat{W}_\Delta^{\mu\nu\alpha''\beta''}(p,q)\;\Lambda_{\beta''\beta'}(p)$$
$$\left.\cdot\; i\gamma_5\gamma_\beta\;\left((P-p)^{\beta'}\epsilon^{\beta}(\lambda)-(P-p)^{\beta}\epsilon^{\beta'}(\lambda)\right)\right] \qquad (112)$$

It's then straightforward to show, using the kinematics of equs.(89) to (92) that $f_{\Delta\rho}(y') = f_{\rho\Delta}(1-y)$, when the form factors satisfy $\mathcal{F}_{\rho\Delta}(s_{\rho\Delta}) = \mathcal{F}_{\Delta\rho}(s_{\Delta\rho})$.

In Fig.13 we show the vector meson distribution functions $f_{\rho N}$, $f_{\omega N}$ and $f_{\rho\Delta}$ as a function of y, for the dipole form factor of the form in equ.(86), with $\Lambda = 700$ MeV in all cases. The dominant contributions come from the tensor (derivative) couplings, which is reflected in the larger ρN and $\rho\Delta$ distributions in comparison with the ωN. Also, the vector distribution functions tend to peak at slightly larger y values ($y \sim 0.5$) in comparison with the πN and $\pi\Delta$ functions.

To conclude this discussion of heavy mesons we consider the DIS process involving the kaon cloud of the nucleon using the time-ordered formalism in the IMF (noting, however, that the role of kaons was first examined by Signal and Thomas [94] within a covariant approach). Through the proton dissociation processes $p \to K^0\Sigma^0(\Lambda^0)$ and $p \to K^+\Sigma^-$, the virtual photon will probe the quark structure of the virtual strange mesons and hyperons. Such a process will naturally generate a non-perturbative strange quark component of the nucleon, as well as a different antistrange sea, thereby breaking SU(3) flavor symmetry of the sea in the process.

Taking a pseudoscalar coupling for the KNH vertex, where the hyperon $H = \Sigma$ or Λ, the kaon distribution function is similar to the pion distribution function $f_{\pi N}(y)$, except the mass

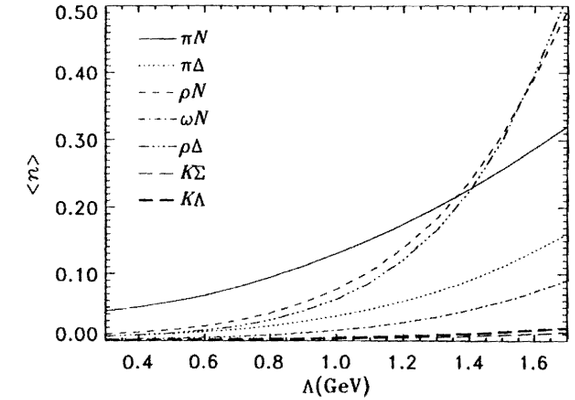

Figure 14: Calculated average meson multiplicities in the nucleon, as a function of the (dipole) meson-nucleon form factor cut-off.

of the recoil state is now different,

$$f_{KH}(y) \;=\; c_H\,\frac{g_{KNH}^2}{16\pi^2}\int_0^\infty \frac{dk_T^2}{(1-y)\,y}\,\frac{\mathcal{F}_{KH}^2(s_{KH})}{(M^2-s_{KH})^2}$$
$$\times\left(\frac{k_T^2+y^2M^2+(M_H-M)(M_H-(1-2y)M)}{1-y}\right) \qquad (113)$$

where the isospin factor is $c_H = 1 + 2\delta_{H\Sigma}$. Similarly for the DIS from a strange baryon with a spectator K, repeating the calculation of sect.5.2, we find that the hyperon distribution function $f_{HK}(y')$ is given by the right hand side of equ.(113) with $y \to 1-y'$, thereby satisfying equ.(59) exactly. Numerically, the kaon distributions are much smaller than the vector meson distributions, and can for practical purposes be dropped from the analysis.

The relatively small size of the kaon contributions is also clear from Fig.14, where we compare the average number of all mesons considered, $\langle n\rangle_{MB}$, as a function of the dipole form factor cut-off Λ. For relatively small cut-off masses, $\Lambda \lesssim 0.7$ GeV, the dominant contribution is from the πN component. However, the rapid growth with Λ of the ρ meson multiplicities and momentum fractions means that for large Λ ($\gtrsim 1.2-1.3$ GeV) the vector mesons become as important numerically as pions. In fact, the strong k_T dependence in $f_{\rho N}(y)$ and $f_{\rho\Delta}(y)$ implies that for $\Lambda \gtrsim 1.4$ GeV $\langle n\rangle_{\rho N}$ actually exceed $\langle n\rangle_{\pi N}$.

Note that for the πN component, $\Lambda = (600, 1000, 1400)$ MeV corresponds to an exponential cut-off $\Lambda_e \simeq (580, 1130, 1360)$ MeV, and a covariant dipole form factor cut-off $\Lambda_{\pi N} \simeq (590, 760, 980)$ MeV for the same $\langle n\rangle_{\pi N}$. In many nuclear physics calculations quite hard form factors of the k^2-dependent type are often used, for example in NN potential models, where cut-offs of the order of 1.5—2 GeV are typical. Clearly such large cut-offs would imply an extremely large number of pions and an even larger number of vector mesons. Whether or not

it is reasonable to accept such large heavy meson components in nucleon DIS is debatable, but obviously we would like some data to tell us whether this is so.

Up until now the cut-off Λ has been a free parameter. Indeed, because quantities such as the average number of mesons in the nucleon are not directly (or unambiguously) extracted from experiment, we cannot draw any conclusions about the size of Λ from the functions $f_{MB}(y)$ alone. However, we may be able to restrict the range of allowable values of Λ by comparing the calculated meson and baryon contributions with the experimental structure functions, or quark distributions. This is where we turn our attention next.

5.4 Nucleon Quark Distributions

With the functions f_{MB} and f_{BM} now calculated, we are able to compute the contributions to the quark and antiquark distributions of the proton from the DIS from its virtual meson and baryon components. The total contribution to a quark distribution in the proton from this process is

$$\delta q(x) = \sum_{M,B} \left(\delta^{(MB)}q(x) + \delta^{(BM)}q(x)\right) \tag{114}$$

and similarly for the antiquark distribution. Using the Clebsch-Gordan coefficients for the various charge states of the meson-baryon combinations we can easily obtain the individual flavor distributions. For example, for DIS from virtual π or ρ mesons we have contributions

$$\begin{aligned}
\delta^{(\pi/\rho\ N)}u(x) &= \int \frac{dy}{y} f_{\pi/\rho\ N}(y)\left(\frac{1}{3}u^{\pi^0}(x_M) + \frac{2}{3}u^{\pi^+}(x_M)\right) = \int \frac{dy}{y} f_{\pi/\rho\ N}(y)\frac{5}{6}V^M(x/y) \\
\delta^{(\pi/\rho\ N)}d(x) &= \int \frac{dy}{y} f_{\pi/\rho\ N}(y)\left(\frac{1}{3}d^{\pi^0}(x_M) + \frac{2}{3}d^{\pi^+}(x_M)\right) = \int \frac{dy}{y} f_{\pi/\rho\ N}(y)\frac{1}{6}V^M(x_M) \\
&\text{etc.}
\end{aligned} \tag{115}$$

Similar expressions can be deduced for other mesons based solely on SU(3) symmetry. For simplicity we have assumed here the same meson valence quark distribution $V^M(x_M)$ for all mesons (sea components of the meson distributions themselves are not included),

$$\begin{aligned}
u^{\pi^+/\rho^+} &= \bar{d}^{\pi^+/\rho^+} = 2u^{\pi^0/\rho^0/\omega} = 2\bar{u}^{\pi^0/\rho^0/\omega} = 2d^{\pi^0/\rho^0/\omega} = 2\bar{d}^{\pi^0/\rho^0/\omega} \\
&= u^{K^+} = d^{K^0} = \bar{s}^{K^+} = \bar{s}^{K^0} = V^M
\end{aligned} \tag{116}$$

and have used SU(3) flavor symmetry to obtain the others.

In practical applications, for V^M we can use the experimental pion valence distribution, which has been determined from Drell-Yan proton—pion scattering [95-97]. The pion valence quark distribution was found to be consistent with a behaviour $xV^M(x) \sim x^{0.44}(1-x)^{0.89}$ at $Q^2 \sim 4$ GeV^2 [95]. This is in fairly good agreement with the behaviour expected from large-x ($\sim (1-x)$) counting rules [98] and small-x ($\sim x^{1/2}$) Regge behaviour [99]. It was also found in [100] that the ratio of kaon to pion valence quark distributions was consistent with unity over most of the x range, although dropping slightly at large x, $V^K/V^\pi \sim (1-x)^{0.18\pm0.07}$. Unfortunately, the vector meson valence distribution has not yet been determined experimentally. As a first approximation it may seem reasonable to assume that its x-dependence resembles that of the

π meson. Deviations from this may be expected on theoretical grounds, if one assumes that a spin flip for one of the quarks in a spin 1 meson induces an additional power of $(1-x)$ at large x [98].

For the diagrams with a meson spectator the contributions from DIS from the virtual baryon B can be obtained in a similar way. For example, the change in the u quark distribution of the proton is:

$$\begin{aligned}
\delta^{(N\ \pi/\rho)}u(x) &= \int \frac{dy'}{y'} f_{N\ \pi/\rho}(y')\left(\frac{1}{3}u^p(x_B) + \frac{2}{3}u^n(x_B)\right) = \int \frac{dy'}{y'} f_{N\ \pi/\rho}(y')\left(\frac{1}{3}u(x_B) + \frac{2}{3}d(x_B)\right) \\
&\text{etc.}
\end{aligned} \tag{117}$$

Again, for simplicity, we relate all of the baryon quark distributions to those of the proton. For the neutron this is trivial if one assumes charge symmetry. Since the Δ has spin and isospin 3/2, from the SU(6) quark model we expect that the valence spectator diquark will always have spin and isospin of 1. Using this fact we can relate the valence quark distributions in the Δ to the d quark distribution in the proton (since the spectator uu diquark in the proton has the same quantum numbers), $u^{\Delta^{++}} = \frac{3}{2}u^{\Delta^+} = 3d^{\Delta^+} = 3d$, with the distributions for the other charge states obtained from isospin symmetry. Similarly for the Σ and Λ hyperons, according to SU(3) flavor symmetry we would expect $s^{\Sigma^+} = d$ and $u^{\Sigma^+} = 2q^{\Sigma^0} = 2q^\Lambda = u$.

For our numerical results we use experimentally determined coupling constants, all of which are referred to the nucleon pole. For the πNN coupling we use the recently determined value $g^2_{\pi NN}/4\pi = 13.6$ [101], which is marginally smaller than the "traditional" value [102]. The vector meson—nucleon couplings are obtained from analyses of πN scattering data, $g^2_{\rho NN}/4\pi = 0.55$, $f_{\rho NN}/g_{\rho NN} = 6.1$ [103], and $g^2_{\omega NN}/4\pi = 8.1$, $f_{\omega NN}/g_{\omega NN} = 0$ [104]. For the kaon-hyperon-nucleon couplings we use $g^2_{KN\Lambda}/4\pi = 13.1$ and $g^2_{KN\Sigma}/4\pi = 3.7$, as in ref.[94] (although this $KN\Sigma$ coupling is somewhat larger than the ones determined from KN forward dispersion relations [105] or in some hyperon—nucleon potentials [106], however even so the strange contributions are still very small). Finally, we use the quark model to relate the $\pi N\Delta$ and $\rho N\Delta$ couplings to other experimentally measured ones [107], $f^2_{\pi N\Delta} = (72/25)f^2_{\pi NN}$, and $f^2_{\rho N\Delta} = (f^2_{\pi N\Delta}/f^2_{\pi NN})\, g^2_{\rho NN}\, (m_\rho/2M)^2\, (1 + f_{\rho NN}/g_{\rho NN})^2$.

Apart from the coupling constants, the only other parameters in the model are the meson-baryon form factor cut-offs, Λ. The initial idea about how one might use DIS data to constrain Λ was to compare $\langle y\rangle_{MB}$ with the measured momentum fractions carried by the antiquarks [51]. Even more stringent constraints can be achieved by demanding that the shape of the meson exchange contributions to $\bar{q}(x)$ (i.e. $\delta^{(MB)}\bar{q}(x)$) are consistent with the shape of the experimental antiquark distribution.

As mentioned in the previous section, the fact that the old $f_{\pi N}(y)$ calculated in a covariant framework peaked more sharply and at smaller y compared with the $f_{\pi N}$ calculated in the IMF means that the quark distributions in equs.(115), (117) will also peak at smaller x for the covariant k^2-dependent form factor. Because the TOPT/IMF formulation generally gives broader antiquark distributions, the limits on the cut-offs will be more severe than for the covariant case, since at intermediate x ($x \gtrsim 0.2$) the TOPT/IMF distributions are still large compared with the experimental data.

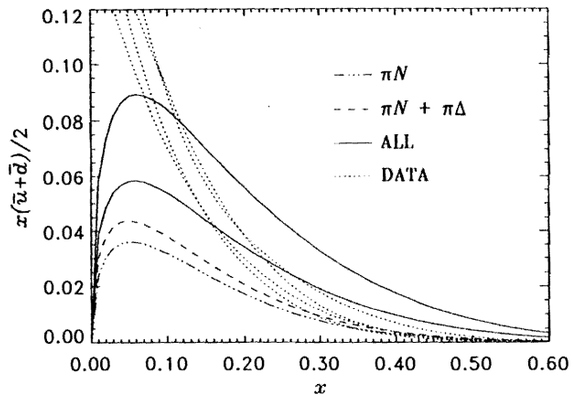

Figure 15: Proton SU(2) flavor antiquark distributions for DIS on the various meson–baryon components of the nucleon. The dot-dashed and dashed curves represent the contributions from πN and $\pi N + \pi\Delta$ states, respectively, for $\Lambda = 700$ MeV. The solid curves are the total contributions from all meson–baryon states, for $\Lambda = 700$ MeV (lower curve) and 900 MeV (upper curve). The data, indicated by the dotted lines, are from refs.[108, 109].

Figure 15 shows the contributions to the SU(2) antiquark distribution $x(\bar{u}+\bar{d})/2$ from all of the meson–baryon components of the nucleon, for $\Lambda = 700$ and 900 MeV – in equ.(86). This is compared with recent empirical data (as parameterised by Morfin and Tung [109], Owens [108], Eichten et al. [25] and Diemoz et al. [26]) for $(\bar{u}+\bar{d})/2$ at $Q^2 = 4$ GeV^2. Also shown are the calculated results (for $\Lambda = 700$ MeV) for the πN and $\pi N + \pi\Delta$ states alone. Clearly the SU(2) $\bar{q}$ content of the nucleon is well saturated for $\Lambda \approx 700$ MeV in the intermediate-x region when all meson–baryon components are included. The main contributions in this region come from the ρN and $\rho\Delta$ states, since the distribution functions $f_{\rho N(\Delta)}(y)$ generally extend to larger y compared with the pion distributions. As mentioned above, one uncertainty in the treatment of the vector meson contributions arises from the fact the structure function for a spin 1 meson may deviate at large x from the behaviour observed for the pion structure function. The effect on the ρN contribution to $x(\bar{u}+\bar{d})/2$ of including an extra power of $(1-x)$ in the ρ meson structure function is a slightly softer distribution, so that this would allow for a marginally larger cut-off mass when comparing against the data in Fig.15. If only the πN states are included, slightly harder form factors could also be accommodated, with $\Lambda \approx 1$ GeV. In either case, for the πNN vertex this corresponds to a dipole form factor cut-off in the covariant formulation of $\Lambda_{\pi N} \sim 700 - 800$ MeV (to give the same value of $\langle n\rangle_{\pi N} \sim 0.10 - 0.15$), which is still considerably smaller than that used by many authors.

5.5 Renormalisation, Incoherence

A subtle, but nonetheless important, point that needs to be made concerns the renormalisation of the total quark distributions in the presence of mesons. The meson and baryon exchange diagrams in Fig.7 describe physical processes (inclusive baryon and meson leptoproduction) whose cross-sections involve physical (renormalised) coupling constants. When integrated over the recoil particles' momenta these yield the inclusive DIS cross-sections, which are proportional to the total quark (and antiquark) distributions

$$q(x) \;=\; Z\, q_{\rm bare}(x) \;+\; \sum_{M,B} \left(\delta^{(MB)}q(x) \;+\; \delta^{(BM)}q(x)\right). \tag{118}$$

Therefore $\delta^{(MB)}q(x)$ and $\delta^{(BM)}q(x)$, and the convolution integrals in equs.(62) and (63), are expressed in terms of renormalised coupling constants contained in the functions $f_{MB}(y)$ and $f_{BM}(y')$. In equ.(118) we also identify the bare nucleon probability

$$Z \;=\; 1 \;-\; \sum_{M,B} \langle n\rangle_{MB} \tag{119}$$

chosen such that the baryon number and momentum sum rules are satisfied. We emphasise that all quantities in equs.(118) and (119) are evaluated using renormalised coupling constants.

We could, of course, choose to work at a given order in the bare coupling constant, and explicitly verify that the various sum rules are satisfied. For example, to lowest order (g_0^2) the total quark distributions would be [29]

$$q(x) \;=\; Z\left\{q_{\rm bare}(x) \;+\; \sum_{M,B}\left(\delta^{(MB)}q_{(0)}(x) \;+\; \delta^{(BM)}q_{(0)}(x)\right)\right\} \qquad \text{(order } g_0^2\text{)} \tag{120}$$

with

$$Z \;=\; \left(1 + \sum_{M,B}\langle n_{(0)}\rangle_{MB}\right)^{-1} \qquad \text{(order } g_0^2\text{)} \tag{121}$$

where the subscript (0) indicates that the functions $f(y)$ are evaluated using bare couplings. Equations (118) and (119) are easily recovered since the bare couplings, to this order, are defined by $g_0^2 = g_{\rm ren}^2/Z$. It would, however, be inconsistent to use (120) and (121) with renormalised coupling constants, especially with large form factor cut-offs. As long as the form factors are soft, the difference between the bare and renormalised couplings is not very large. However, with large cut-off masses the bare couplings would need to be substantially bigger than the physical ones. (In fact, the form factor cut-off dependence of the bare πN coupling constant in the cloudy bag model [48] showed some 40% difference for very hard form factors — or small bag radii, ~ 0.6 fm.) In addition, with large values of Λ the higher order diagrams involving more than one meson in the intermediate state would become non-negligible, and the initial assumption that the series in equ.(57) can be truncated at the one-meson level would be seriously in doubt. Fortunately, we need not consider the multi-meson contributions, since Fig.15 clearly demonstrates the difficulty in reconciling the empirical data with quark distributions calculated with such large cut-offs.

Finally, we need to make some additional comments regarding the justification of our calculation in terms of an incoherent summation of cross-sections (rather than amplitudes) for the various meson exchange processes. A possible breakdown of incoherence may arise when there are different exchange processes leading to the same final state. For nucleon final states, because of the pseudoscalar nature of the πNN vertex, there will be no interference between π meson and vector meson exchange. Furthermore, no mixing will take place between the ω and ρ exchange configurations due to their different isospins. In fact, all of the meson exchange processes with a recoil N considered in this analysis can be added incoherently. For a Δ recoil, the only mesons coupling to N and Δ are the π and ρ, but since they have different G-parities, interference effects from these will again be excluded. However, the possibility exists in the pion exchange process that the decay products of a Δ recoil, namely π and N, may mix with the state containing an N recoil together with a π from the hadronic debris X of the shattered exchanged pion. Interference between the πN and $\pi\Delta$ states could therefore occur if the π from the debris had very low momentum, enabling the combined system to have an invariant mass squared $\sim M_\Delta^2$. However the vast majority of semi-inclusive meson events in lepton–nucleon DIS are those with high momentum mesons (slow hadrons are almost exclusively baryons), so that the probability of interference arising from such processes will not be large. A similar argument can be given for the potential interference from hyperon decay into $N\pi$.

For the baryon exchange processes, the requirement of the same recoil meson eliminates interference from most states, except from DIS off N and Δ with π (or ρ) in the final state, and from DIS off a Σ^0 and Λ^0 with a K^+ recoil. For the latter, the different isospin quantum numbers of the $\Lambda(I=0)$ and $\Sigma(I=1)$ rule out interference, just as for the ρN and ωN states. A similar argument can be made for excluding interference contributions from $N(I=1/2)$ and $\Delta(I=3/2)$ exchange. Once again, the fact that the decay products of the recoil mesons have low momentum, while the pions from the baryonic debris are fast, will again reduce the size of any interference effects.

Therefore we see that by considering only the lowest lying meson and baryon states (i.e. by excluding resonances having the same quantum numbers as the mesons and baryons considered here) we can avoid potential problems with interference, and certainly for the values of Λ allowed by the data, the only relevant states are those with the lowest masses.

6 CHALLENGING PROBLEMS

It is a widely held belief that the best laid plans of mice and men often go astray! This is at least as true of DIS as of any other field of study. In this section we study several topical examples which have generated a great deal of excitement (and consternation!). The first concerns the nature of the sea of $q\bar{q}$ pairs in the nucleon. According to perturbative QCD these are generated from gluons which in turn carry no flavor information. As a consequence one expects to find equal numbers of $u\bar{u}$ and $d\bar{d}$ pairs. The Gottfried sum rule was built on this idea. Yet recent results from the New Muon Collaboration (NMC) at CERN have confirmed earlier hints that the sum rule is badly violated. Clearly this is more than a curiosity — it contains fundamental

information about the non-perturbative structure of the nucleon. We explore some of the ideas proposed to explain the result in sects.6.1 and 6.2.

Spin-dependent measurements have often been the graveyard of otherwise successful theories. In DIS this would probably be a fair summary of the situation immediately after the discovery by the EMC of a violation of the Ellis-Jaffe sum rule. This result, which was initially christened the proton "spin crisis", has since led to important advances in our understanding of how the U(1) axial anomaly is realised. Although the dust has not yet settled, and a lot more experimental and theoretical work is needed, we outline the current situation in sect.6.3.

Our final outstanding problem, dealt with in sect.6.4, is the old nuclear EMC effect – the variation of nuclear structure functions. At various stages over the past decade it has seemed like the problem was understood. This is certainly not the case – even now. However, we have reached a stage of illumination where we can at least say that the physics required in a decent theoretical treatment is now known.

6.1 Flavor asymmetry

One of the more interesting observations that can be made within the meson model is that it predicts that contributions from DIS off virtual mesons and baryons to the u, d and s quark (and the corresponding antiquark) distributions in the proton (equs.(115), (117)) will be different. Because the contributions to s and $\bar{s}$ from DIS from kaons and hyperons are very much smaller than those from the non-strange mesons and baryons to the u and d distributions (mainly because $m_K \gg m_\pi$) we see that the meson model produces significant SU(3) flavor symmetry violation. Furthermore, it is apparent that the contributions to the u and d (and $\bar{u}$ and $\bar{d}$) quark distributions themselves are not the same, so that SU(2) flavor symmetry of the proton sea is also broken. In the case of the pion cloud, the simple origin of this is asymmetry is the predominance of the dissociation process $p \to n\pi^+$ over $p \to p\pi^0$. In the former, the π^+ valence quark content is $d\bar{u}$, while in the latter the ratio of $\bar{u}$ to $\bar{d}$ quarks is the same. This process certainly respects isospin symmetry, which simply says that the dissociation $p \to n\pi^+$ is as likely as $n \to p\pi^-$, or at the quark level, $u \to d(u\bar{d})$ is as likely in the proton as $d \to u(d\bar{u})$ in the neutron. But it clearly implies an excess of $\bar{d}$ quarks in the proton, and an equal excess of $\bar{u}$ quarks in the neutron.

If the masses of quarks were identical (i.e. SU(3) flavor symmetry limit) then the ratio of strange to non-strange antiquark distributions in the proton would be 1:2. From neutrino experiments (at $Q^2 \sim 4$ GeV^2) the measured ratio was found to be about 1:4 [14], which can be understood semi-quantitatively from the heavier mass of the strange quark. On the other hand, because charge symmetry is such a good symmetry in strong interaction physics, it was naively expected that SU(2) flavor symmetry of the sea would be an excellent approximation. Indeed, this expectation has been built into almost all of the analyses of the nucleon structure function data. The main reason for believing this has been the simple picture, motivated by perturbative QCD, in which the mechanism for producing antiquarks is gluon splitting into $q\bar{q}$ pairs. However, unless isospin symmetry is genuinely violated (by giving a non-zero mass

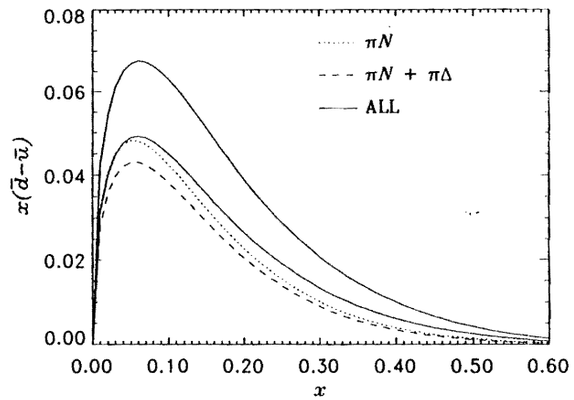

Figure 16: Calculated $\bar{d} - \bar{u}$ difference from the various meson-baryon states. For the dotted, dashed and lower solid curves a dipole form factor cut-off of $\Lambda = 700$ MeV is used, while the upper solid curve is calculated with $\Lambda = 900$ MeV.

difference between the u and d quarks), the perturbative process $g \to q\bar{q}$ should be SU(2) flavor symmetric, as the gluons of QCD are flavor-blind. Therefore a $\bar{d} - \bar{u}$ difference cannot be produced by perturbative QCD. Actually, this statement should be qualified by saying that at lowest order in α_S there is no asymmetry. A higher order perturbative QCD calculation of $\bar{d} - \bar{u}$ was performed some time ago by Ross and Sachrajda [110], who found a non-zero result for this difference, although the absolute value was very small. This means that the calculated $\bar{d} - \bar{u}$ difference will essentially be preserved in QCD evolution. But the fact that we get a non-zero $\bar{d} - \bar{u}$ difference in the meson-baryon model is not surprising, since this is a non-perturbative model, and its predictions are not in conflict with QCD, nor with isospin symmetry.

In Figs.16 and 17 we plot the $\bar{d} - \bar{u}$ difference, and the ratio $(\bar{d} - \bar{u})/(\bar{d} + \bar{u})$, respectively, calculated within the meson-exchange model of the nucleon. Fig.16 shows that the inclusion of $\pi\Delta$ states (with $\Lambda = 700$ MeV) eliminates some of the $\bar{d}$ excess, since here the dominant process is $p \to \Delta^{++}\pi^-$, which at the quark level, $d \to u(d\bar{u})$, is seen to produce a $\bar{u}$ excess. However, adding the vector meson components (lower solid curve) restores the original $\bar{d}$ excess at small x, and enhances the excess at larger x. At larger values of Λ ($= 900$ MeV) the $\bar{d} - \bar{u}$ difference is larger still (upper solid curve), although the ratio $(\bar{d} - \bar{u})/(\bar{d} + \bar{u})$ is smaller, Fig.17. On similar grounds the processes $p \to K^0\Sigma^+$ and $p \to K^+\Sigma^0(\Lambda)$ will introduce not only a different strange quark content of the proton than a non-strange, but also a different $\bar{s}$ distribution as well. However, because of the very small magnitude of the strange contributions it will be difficult for these effects to be observed in DIS experiments in the near future.

Of course the idea of an asymmetric proton sea is not a new one. The earliest, and perhaps most obvious, suggestion for why we should expect $\bar{u} \neq \bar{d}$ was made by Feynman and Field [111]. As mentioned in sect.4.1, because the proton has an unequal number of valence u and

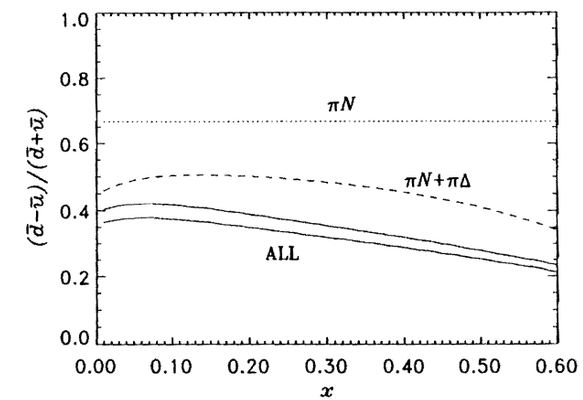

Figure 17: Ratio of the difference and sum of the calculated SU(2) antiquark distributions in the proton. The cut-off for the dotted, dashed and upper solid curves is $\Lambda = 700$ MeV, while the lower solid curve is calculated with $\Lambda = 900$ MeV.

d quarks, by the Pauli exclusion principle we would therefore expect creation of additional $q\bar{q}$ pairs inside the proton to be sensitive to the number of quarks of each flavor already in the proton. Since there are 2 valence u quarks in the proton compared with only 1 valence d quark, we therefore expect a larger $\bar{d}$ sea since $u\bar{u}$ pair creation will be suppressed relative to $d\bar{d}$. In ref.[111] the $\bar{d}$ and $\bar{u}$ distributions were parameterised by $x\bar{d} = 0.17(1-x)^7$ and $x\bar{u} = 0.17(1-x)^{10}$, see Fig.18. With these, the integrated difference is $\int dx(\bar{d} - \bar{u}) = 0.057$.

An early calculation of the u and d sea quark probabilities in the proton, incorporating the effects due to the Pauli principle, was made by Donoghue and Golowich [112] using the MIT bag model. However, this involved calculating the one-gluon-exchange induced $q\bar{q}$ admixture in the proton wavefunction. This is quite a different effect from that discovered in the recent work of Signal and Thomas [19] when calculating the of quark distribution functions in the MIT bag (see sect.4.1). Their work suggested a quantitative method of calculating the intrinsic sea associated with the different vacuum structure of the bag from that in free space. They also showed that the Pauli exclusion principle implied a $\bar{d} - \bar{u}$ difference as well. In particular these intrinsic antiquark distributions arose only from 4 q intermediate bag states. Thus the $\bar{d}$ distribution required the intermediate state to consist of 2 u and 2 d quarks, while DIS from a $\bar{u}$ quark implied a $3u + 1d$ intermediate state, which, because of the Pauli principle, has a smaller probability. Furthermore, in ref.[19] the $\bar{d}$ excess associated with the Pauli effect was equal to the d excess and satisfied the condition

$$\int_0^1 dx\ \bar{d}_{\rm excess}(x) = \int_0^1 dx\ (d_{\rm sea}(x) - u_{\rm sea}(x)) = \int_0^1 dx\ p_N(x) \equiv \mathcal{P}_N. \qquad (122)$$

Here, $p_N(x)$ denotes the piece of the valence quark distribution associated with a four quark intermediate state (all in a $1s$ state), while $1 - \mathcal{P}_N$ is the integral over the distribution function

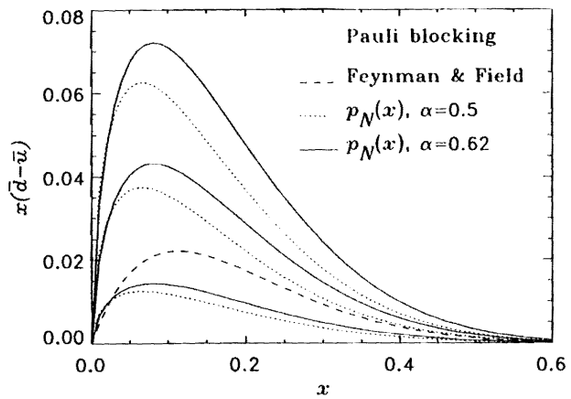

Figure 18: Difference between $\bar{d}$ and $\bar{u}$ quark distributions in the proton, for the Feynman and Field parameterisation [111], and a parameterisation of the function $p_N(x) \sim x^{0.62}(1-x)^7$, with normalisation $\mathcal{P}_N = 0.05, 0.15$ and 0.25.

associated with a two quark intermediate state. In ref.[19] the calculated distributions were found to peak at $x \sim 1 - M_{int}/M$, where M_{int} is the mass of the intermediate spectator state. Since the 4-quark intermediate states have mass greater than M, the antiquark distributions will peak at negative x. Therefore in the physical region ($x \geq 0$), $p_N(x)$ should resemble a typical sea quark distribution, namely be finite at $x = 0$ while dropping rapidly to zero by $x \sim 0.2 - 0.3$. For simplicity, we can parameterise the large-x behaviour by a $p_N(x) \propto (1-x)^7$ form [25, 56]. On theoretical grounds, we can also expect that due to the lack of Regge $f - A_2$ exchange degeneracy, at small x the $\bar{d} - \bar{u}$ difference should be proportional to $p_N(x) \sim x^\alpha$, where $\alpha(\simeq 0.5)$ is the Regge intercept [113, 99]. The overall normalisation $\mathcal{P}_N$ was calculated in ref.[52] to be less than about 0.25 for bag radii $R \lesssim 0.8$ fm.

In Fig.18 we compare the Feynman & Field parameterisation with the function $p_N(x)$, normalised so that $\mathcal{P}_N = 0.05, 0.15$ and 0.25. Also shown is the effect of using a slightly more singular small-x behaviour, $\alpha = 0.62$, as suggested by the NMC data on $F_{2p} - F_{2n}$ [58].

Unfortunately at the present time there are not sufficient data on $\bar{d} - \bar{u}$ to make definitive conclusions about these various mechanisms for SU(2) flavor symmetry breaking. However, there have been a number of interesting suggestions for experiments that could directly probe the light sea quark content of the proton, and we briefly review these now.

Recently it was suggested by Martin, Stirling and Roberts [114] that one could learn about the SU(2) sea by observing the W-boson asymmetries in $p\bar{p}$ collisions, $p\bar{p} \to W^\pm X$. The simple idea is that a $u(d)$ quark in a proton interacts with a $\bar{d}(\bar{u})$ antiquark in an antiproton to produce a $W^+(W^-)$ boson. Because the $u(\bar{u})$ quark in the proton (antiproton) carries more momentum (lies at larger x) than the $d(\bar{d})$ quark, $W^+(W^-)$ bosons will be predominantly produced in the proton (antiproton) direction. However, in addition there will be $W^+(W^-)$-bosons produced

by the annihilation of $\bar{d}(\bar{u})$ quarks in the proton with $d(u)$ quarks in the antiproton. Thus at large energies the asymmetry in the W-boson rapidity (y_W) distribution

$$A(y_W) = \frac{\sigma^+ - \sigma^-}{\sigma^+ + \sigma^-} = \frac{u(x_1)d(x_2) + \bar{d}(x_1)\bar{d}(x_2) - d(x_1)u(x_2) - \bar{d}(x_2)\bar{d}(x_1)}{u(x_1)d(x_2) + d(x_1)u(x_2) + d(x_1)u(x_2) + \bar{d}(x_2)\bar{d}(x_1)}, \tag{123}$$

where $\sigma^\pm = d\sigma/dy_W(W^\pm)$, would be sensitive to the antiquark distributions in the proton. Here, $x_{1,2} = M_W/\sqrt{s}\exp(\mp y)$, s is the centre of mass energy squared, and the W-boson rapidity is defined by $y_W = (1/2)\ \ln(q_-/q_+)$, with q the W-boson momentum. Furthermore, since only left-handed quarks (right-handed antiquarks) couple to W-bosons, in the resulting $W \to e\nu$ decay the electron (positron) distribution will generally follow the direction of the incoming proton (antiproton). It was suggested in [114] that the experimental $e^\pm$ asymmetry, $A(y_e) = (d\sigma/dy_{e^+}(y_{e^+}) - d\sigma/dy_{e^-}(y_{e^-}))/(d\sigma/dy_{e^+}(y_{e^+}) + d\sigma/dy_{e^-}(y_{e^-}))$, could then serve as an independent check on the $\bar{u}$ and $\bar{d}$ distributions in the proton. The claim in ref.[114] was that their existing parameterisations with no SU(2) flavor asymmetry are consistent with the data on $A_e(y_e)$ taken at the Collider Detector at Fermilab (CDF) [115]. However, the error bars in this experiment are quite large, and the data at present will have difficulty in discriminating between SU(2) flavor symmetric parameterisations, and those with a small $\bar{d} - \bar{u}$ difference, such as that suggested by the meson model in the previous section. On the other hand, a large $\bar{d} - \bar{u}$ difference, such as that arising from the meson model with large form factor cut-offs Λ, may well introduce a detectable difference.

In another experiment, performed some than 10 years ago by the E288 Collaboration at FNAL [116], the slope of the rapidity distribution for proton-nucleus Drell-Yan production was measured, and found to be sensitive to the $\bar{u}/\bar{d}$ ratio. In that experiment, the quantity

$$\frac{d}{dy} \ln\left(s\frac{d^2\sigma}{d\sqrt{\tau}dy}\right)_{y=0} \tag{124}$$

was measured as a function of $\sqrt{\tau}$, where $\tau = M^2_{l^+l^-}/s$. It was found that a parameterisation with $\bar{d} > \bar{u}$ improved the quality of the fit [117]. However, since the analysis of this experiment required the quark and antiquark distributions in the nucleus, any conclusions reached about the nucleon sea distributions were obviously dependent upon any nuclear assumptions made. In fact, it was later shown by Ericson and Thomas [118] that a similar improvement in the fit could be made by assuming a small difference between the $\bar{q}$ distributions in the nucleon and in a nucleus.

Proton-nucleus Drell-Yan production was also studied recently by the E772 Collaboration at Fermilab. It was found that by comparing the yield per nucleon in a proton collision with a neutron-rich target such as tungsten with that for an isoscalar nucleus, the resulting ratio would also be sensitive to the $\bar{d} - \bar{u}$ difference. However, it has since been argued by Eichten et al. [119] that this too may not be a sensitive enough experiment for a small non-zero $\bar{d} - \bar{u}$ difference to be discernable from no difference.

Perhaps the experiment that is most sensitive to the light sea quark distributions was that recently proposed by Ellis & Stirling [120], who suggested measuring the asymmetry between the pn and pp Drell-Yan production (i.e. $pN \to l^+l^-X$) cross-sections at zero rapidity,

$A_{DY} = (\sigma^{pp} - \sigma^{pn})/(\sigma^{pp} + \sigma^{pn})$, where $\sigma^{pN} \propto d^2\sigma^{pN}/d\sqrt{\tau}dy|_{y=0}$. Neglecting terms involving annihilation of sea quarks in the (beam) proton and (target) nucleon, the cross-sections can be written

$$A_{DY} = \frac{(4\lambda_V - 1)(\lambda_S - 1) + (\lambda_V - 1)(4\lambda_S - 1)}{(4\lambda_V + 1)(\lambda_S + 1) + (\lambda_V + 1)(4\lambda_S + 1)} \tag{125}$$

where $\lambda_V = u_V/d_V$ and $\lambda_S = \bar{u}/\bar{d}$. The advantage of measuring this ratio is that it would be free from any nuclear dilution effects, and the complete asymmetry could be determined from ratios of valence and sea quark distributions alone. Since the d_V/u_V ratio is well determined, A_{DY} would then serve as an accurate indicator of λ_S. In Fig.19 we plot this Drell-Yan asymmetry as a function of $\sqrt{\tau} = \sqrt{Q^2/s}$ with $s \sim 1500$ GeV^2 (corresponding to a proton beam energy of about 800 GeV) calculated using the quark and antiquark distributions of the meson model (with $\Lambda = 700$ MeV). This is compared with the asymmetry arising from the parameterisation of Morfin & Tung [109] for the valence quarks (dotted curve), and from the d_V/u_V ratio fixed at $0.57(1-x)$ [25] (dashed curve), with $\lambda_S = 1$ in both cases. It is clear that even small deviations of $\bar{u}/\bar{d}$ from unity will have a big impact upon A_{DY}.

An extension of this idea was discussed in ref.[121], where it was argued that one could directly measure the difference $\bar{d} - \bar{u}$ by going to large projectile momentum fractions x_1, but small target fractions x_2. In that case the term in A_{DY} involving the product of projectile sea and target valence distributions could be neglected and the asymmetry reduced to

$$A_{DY} \approx \frac{(4\lambda_V - 1)(\lambda_S - 1)}{(4\lambda_V + 1)(\lambda_S + 1)}. \tag{126}$$

Unfortunately, there are as yet no data on A_{DY}, although a proposal has been made [122] for an experiment to measure the Drell-Yan cross-sections for hydrogen and deuterium targets. Such data would be eagerly anticipated.

Finally, an interesting observation was made by Levelt, Mulders and Schreiber [123], who found that semi-inclusive charged-hadron production could be used to obtain information on the integrated $\bar{d} - \bar{u}$ difference. Following earlier work by Gronau et al. [124] and Field and Feynman [111] on the parton model for semi-inclusive DIS, Levelt et al. showed that the integrated difference should be proportional to the measured difference between the charged pion and kaon production rates from DIS on protons and neutrons. However, the available data from the EM Collaboration at CERN on semi-inclusive charged-meson production [125] are not yet sufficiently accurate to discriminate between SU(2) flavor symmetry and asymmetry.

However, the most important impact on the question of SU(2) flavor symmetry in the proton sea, and certainly the stimulus for the close attention this question has received in recent times, has come from the measurement by the NMC of the difference between F_{2p} and F_{2n} [58], and the consequent determination of the Gottfried sum rule. We will now discuss the issues involved in this experiment more fully.

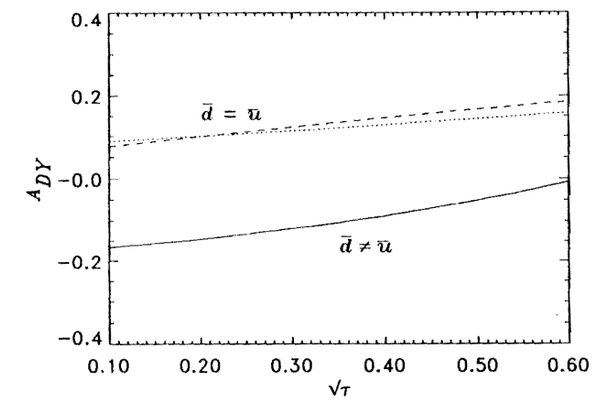

Figure 19: Asymmetry for pp and pn Drell-Yan production. The $\bar{u} = \bar{d}$ predictions, with the valence quark parameterisation of Morfin and Tung [109] (dotted) and with a fixed valence ratio $d_V/u_V = 0.57(1-x)$ [25], are compared with the meson model calculation with $\bar{u} \neq \bar{d}$ (for $\Lambda = 700$ MeV).

6.2 Gottfried Sum Rule

The Gottfried sum rule [57] is perhaps the most famous consequence of SU(2) flavor symmetry of the sea. Because this measures the x-integrated difference between the proton and neutron structure functions, it is sensitive only to the non-singlet SU(2) content of the nucleon. Let us firstly define the quantity

$$S_G(x,1) = \int_x^1 \frac{dx'}{x'}(F_{2p}(x') - F_{2n}(x')). \tag{127}$$

Relating the proton and neutron structure functions to the quark distributions in the proton (i.e. using charge symmetry), we have

$$S_G(x,1) = \frac{1}{3}\int_x^1 dx' \left(u(x') + \bar{u}(x') - d(x') - \bar{d}(x')\right) \tag{128}$$

$$= \frac{1}{3}\int_x^1 dx' \left(u_V(x') - d_V(x')\right) - \frac{2}{3}\int_x^1 dx' \left(\bar{d}(x') - \bar{u}(x')\right) \tag{129}$$

where the valence quark distributions are defined by $q_V \equiv q - \bar{q}$. Since the number of valence quarks in a hadron does not change, we obtain the Gottfried sum rule

$$S_G \equiv S_G(0,1) = \frac{1}{3} \qquad \text{[QPM]} \tag{130}$$

provided we make the additional assumption $\int_0^1 dx\, \bar{d} = \int_0^1 dx\, \bar{u}$, as would be expected in the simple quark-parton model (QPM).

The early experimental data for $S_G(x,1)$ did in fact suggest a value lower than 1/3, but with errors large enough to be consistent with it. However, armed with the theoretical expectation

of SU(2) flavor symmetry, most authors believed that S_G would tend to 1/3 as the accuracy of the data improved. To the surprise of many, the recent, accurate determination of S_G by the NMC appears to support the idea that $\bar{u} \neq \bar{d}$ [58, 126]. Neglecting nuclear effects, the NMC found

$$S_G(x_{min}, 1) = 0.229 \pm 0.0157 \tag{131}$$

where $x_{min} = 0.004$. Included in (131) is an extrapolation from $x = 0.8$ to 1, the contribution from which was estimated to be 0.002 ± 0.001 if a smooth extrapolation of F_{2p}/F_{2n} to 1/4 at $x = 1$ is assumed. From the unmeasured region ($x < 0.004$), using the extrapolation

$$F_{2p}(x) - F_{2n}(x) \longrightarrow \alpha\, x^{\beta} \qquad \text{as } x \to 0 \tag{132}$$

with $\alpha = 0.21, \beta = 0.62$, the contribution was found to be $S_G(0, x_{min}) = (\alpha/\beta)\, x_{min}^{\beta} = 0.011$. With the conventional Regge theory assumption that $\beta = 0.5$, $S_G(0, x_{min})$ would be 0.014. The combined integral over the whole range of x was therefore

$$S_G \;=\; 0.240 \pm 0.016 \qquad \text{[NMC]} \tag{133}$$

with errors added in quadrature. [4] Although not the only one, the most natural explanation for the smaller than expected value of S_G is that $\bar{d}(x) \neq \bar{u}(x)$ (see later for a discussion of other possibilities). Taken at face value, the NMC result would imply that

$$\int_0^1 dx\, (\bar{d}(x) - \bar{u}(x)) \;=\; 0.14 \pm 0.06. \tag{134}$$

The various mechanisms discussed in sect.5.2 are then potential candidates for generating such a difference. Before turning to more exotic explanations, it seems more sensible that the simplest possibilities should be exhausted first. The most compelling, and most economical from the theoretical point of view, appear to be those based on the Pauli exclusion principle, and on the presence of a small pion (and perhaps other meson) cloud.

We therefore examine the consequences of both of these mechanisms on the $p - n$ structure function difference and the Gottfried sum rule. Firstly note that because the non-strange baryon recoil contributions to the quark and antiquark distributions are related by

$$\delta^{(MB)}u(x) = \delta^{(MB)}\bar{d}(x), \qquad \delta^{(MB)}d(x) = \delta^{(MB)}\bar{u}(x) \qquad [M = \text{non} - \text{strange}] \tag{135}$$

the contributions to S_G from DIS from pions or vector mesons would cancel. Furthermore, since the strange content of the proton and neutron should be the same, contributions from kaons and hyperons to S_G should also vanish. However, the Pauli blocking effect should be present in DIS from virtual K^0, K^+ and Σ^+, since these contain unequal numbers of $u(\bar{u})$ and $d(\bar{d})$ quarks. It will not be present in DIS from Σ^0 or Λ^0. This raises the interesting possibility that we may pick up a non-zero strange quark contribution to S_G from the Pauli principle, if the

[4] From a very recent re-evaluation of the ratio F_{2n}/F_{2p} based on newly measured values of F_{2D} the NMC found a slightly larger value for S_G, namely $S_G = 0.258 \pm 0.017$ [127], although this is still consistent with the original value.

Pauli effect in DIS from K with Σ recoil and in DIS from Σ with K recoil are different (and in principle they should be), which would spoil the cancellation of these components. Still, having seen that the role of strange mesons in the DIS process is negligible, we can be fairly confident that by dropping the strange contributions our results will not be significantly affected.

What may be more significant is the possibility that the shape of the Pauli $\bar{d} - \bar{u}$ contribution from DIS off a virtual Δ, with π or ρ recoil (labelled $p_\Delta(x)$) may differ from the shape of the Pauli difference from DIS off a nucleon with a π or ρ recoil, $p_N(x)$. In principle these should be different because the spins of the 4-quark intermediate states (which arise when the $\bar{u}$ or $\bar{d}$ quarks are probed) in the nucleon and Δ are different. This means that, for example, while a quark inserted into a (spin 1/2) proton can produce a state with spin 0 or 1, one inserted into a (spin 3/2) Δ^+ could produce either a spin 1 or spin 2 intermediate state. One way to make spin 0, 1 or 2 four-quark states is to construct them from spin 0 or spin 1 diquarks, and since a vector diquark is more massive than a scalar diquark (see ref.[20]), and therefore has a softer x-distribution, the result is that the Pauli blocking function $p_\Delta(x)$ should have a softer shape than $p_N(x)$. Furthermore, the integral over $p_\Delta(x)$ (denoted $\mathcal{P}_\Delta$) need not necessarily equal $\mathcal{P}_N$. Having said this, it is probably also true that the uncertainty introduced in taking these to be the same will be much smaller than the overall uncertainty in the absolute normalisation of $\bar{d} - \bar{u}$ due to Pauli blocking in the nucleon.

The final expression for $F_{2p} - F_{2n}$, including meson and Pauli effects, is

$$\begin{aligned}
F_{2p}(x) - F_{2n}(x) \;=\;& \frac{Z}{3}\left(x u_V(x) - x d_V(x) - 2x p_N(x)\right) \\
&- \frac{1}{9}\int_x^1 dy'\; \left(f_{N\pi}(y') + f_{N\rho}(y') - 3 f_{N\pi}(y')\right) \\
&\qquad \times \left(x_B u_V(x_B) - x_B d_V(x_B) - 2x_B p_N(x_B)\right) \\
&+ \frac{5}{9}\int_x^1 dy'\; \left(f_{\Delta\pi}(y') + f_{\Delta\rho}(y')\right)\left(x_B d_V(x_B) - 2x_B p_\Delta(x_B)\right) \\
&+ \frac{4}{9}\int_x^1 dy' f_{\Sigma K}(y')\left(\frac{1}{2} x_B u^{\Sigma^+}(x_B) - 2x_B p_\Sigma(x_B)\right) \\
&- \frac{1}{9}\int_x^1 dy\; \left(f_{K\Sigma}(y) - 3 f_{K\Lambda}(y)\right)\left(x_M V^M(x_M) - 2x_M p_K(x_M)\right).
\end{aligned} \tag{136}$$

Making the above approximations, we plot the resulting x distribution in Fig.20. Note that kaons and ω mesons contribute to the structure functions themselves, even though their contributions will cancel when the structure functions are integrated over x. (We include the K and ω contributions only for the sake of completeness, as dropping them altogether has numerically negligible consequences.)

The most noticeable consequence of the meson cloud is a decrease in the peak value of $F_{2p} - F_{2n}$ at $x \sim 0.3$. Since here the parameterisation clearly overestimates the NMC data, the effect of mesons is to move the curve in the right direction. At the same time, however, the structure function difference becomes larger for $x \lesssim 0.1$. Here, the action of the πN states is to decrease $F_{2p} - F_{2n}$ at small x, while adding the $\pi\Delta$ tends to do the opposite. However, it is only with the addition of the vector mesons that there is an increase over the parameterisation in this region. Because the parameterisation is already too large in this region compared with the NMC data, it's clear that mesons alone cannot improve the fit at small x.

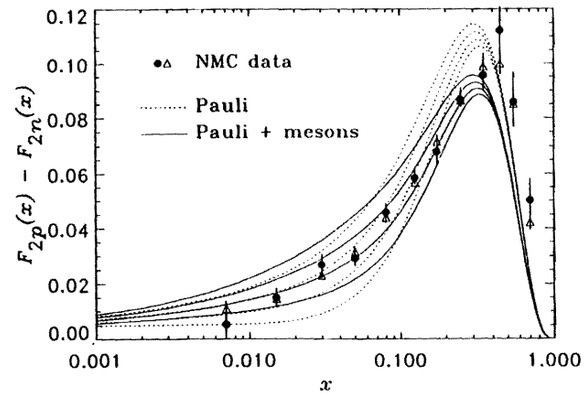

Figure 20: Effect of the Pauli exclusion principle on the proton – neutron structure function difference, as a function of x. The dotted (without meson corrections) and solid (with $\Lambda = 700$ MeV meson corrections) curves are for $\mathcal{P} = 0$ (largest curves) 0.05, 0.1, and 0.15 (smallest curves).

At large x the meson-corrected curves consistently lie beneath the NMC data points. This is a consequence of the original parameterisation [109] underestimating the NMC $F_{2p} - F_{2n}$ results (in fact most other parameterisations [25, 108] also have this property). If we had a parameterisation which could better reproduce the large-x data, the quality of the fits for the corrected curves would naturally improve. We should add, however, that the NMC did not report much data at $x \gtrsim 0.4$. In any case, the discrepancy between the NMC data and the quark parameterisations at large x is unrelated to the failure of the Gottfried sum rule, and is therefore not our primary concern.

The Pauli correction is largest in the small-x region, for $0.01 \lesssim x \lesssim 0.1$. By reducing the absolute value of $F_{2p} - F_{2n}$ at small x the Pauli correction brings the parameterisation (with $\bar{d} = \bar{u}$) into better agreement with the data in that region. However, for larger x ($0.1 \lesssim x \lesssim 0.3$) the peak in the distributions is still too large to be consistent with the NMC data. On the other hand, when combined with a small mesonic correction (for $\Lambda = 700$ MeV), a very good fit is possible with $\mathcal{P}_N \approx 0.1$.

Integrating the structure function difference between x and 1, we plot in Fig.21 the function $S_G(x,1)$ including both meson and Pauli effects. The parameterisation is clearly too large for $x \lesssim 0.1$. With the addition of the meson correction, the fit is clearly improved, but still overestimates the NMC data at very small x. This is partly remedied when a small Pauli blocking correction is added. In particular, the apparent saturation of the sum rule below $x \approx 0.01$ is better fitted by including the Pauli term. (In a more recent experiment, the E665 Collaboration at Fermilab reported an even more dramatic saturation of the Gottfried sum rule for $x \lesssim 0.125$, $\int_{0.001}^{0.125} dx(F_{2p} - F_{2n})/x = -0.07 \pm 0.07$ [128].) In the intermediate-x region

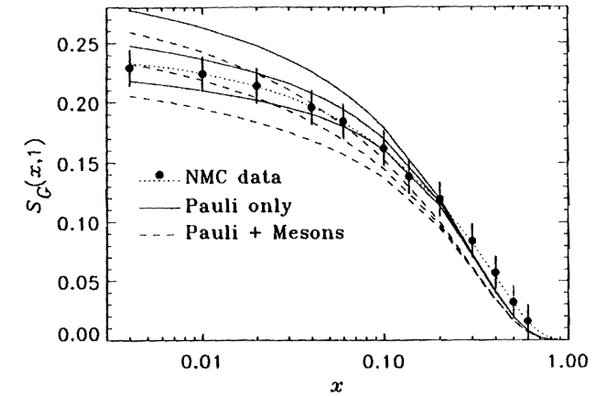

Figure 21: Effect of Pauli blocking on the Gottfried sum integrand with no mesons (solid curves), and with mesons for $\Lambda = 700$ MeV (dotted curves). The three curves in each case are for $\mathcal{P}_N = 0$ (largest curves), 0.05 and 0.10 (smallest curves).

($x \gtrsim 0.3$) the meson-corrected curves appear to underestimate the NMC data. This can be understood from the shape of the original $F_{2p} - F_{2n}$ distributions in Fig.20, where for x above ~ 0.3 the curves tend to lie beneath the NMC data points.

For the Gottfried sum, from equs.(136) and (119) we obtain

$$\begin{aligned} S_G &= S_G^{MB}\,(1 - 2\,\mathcal{P}_N) + \frac{10}{9}(\mathcal{P}_N - \mathcal{P}_\Delta)\left(\langle n\rangle_{\Delta\pi} + \langle n\rangle_{\Delta\rho}\right) \\ &+ \frac{2}{9}(3\mathcal{P}_N + \mathcal{P}_K - 4\mathcal{P}_\Sigma)\,\langle n\rangle_{\Sigma K} + \frac{2}{3}(\mathcal{P}_N - \mathcal{P}_K)\,\langle n\rangle_{\Lambda K} \end{aligned} \tag{137}$$

where

$$S_G^{MB} = \frac{1}{3}\left(1 - \frac{4\langle n\rangle_{N\pi}}{3} - \frac{4\langle n\rangle_{N\rho}}{3} + \frac{2\langle n\rangle_{\Delta\pi}}{3} + \frac{2\langle n\rangle_{\Delta\rho}}{3}\right). \tag{138}$$

is the sum rule with meson/baryon corrections only. Dropping the negligible strange contributions, and assuming that the difference between the Pauli blocking in the nucleon and Δ is not large, only the first term in equ.(137) remains. In Fig.22 we show the variation of S_G with both Λ and $\mathcal{P}_N$. It is clear that the net effect of the virtual meson–baryon states is to decrease S_G. The πN state alone can reproduce the quoted value of S_G for $\Lambda \sim 1.3$ GeV. The addition of $\pi\Delta$ components would require a slightly larger cut-off (since this produces an excess of $\bar{u}$ over $\bar{d}$, which cancels some of the $\bar{d}$ excess generated by the πN states). Including the ρN state however restores, and actually enhances, the $\bar{d}$ excess, although some of this is again cancelled by the $\rho\Delta$ states. With all components included, the NMC value of S_G can be reproduced with $\Lambda \approx 1.1 - 1.2$ GeV. For $\Lambda \lesssim 700$ MeV, as suggested by the antiquark data in the previous section, mesons can generate only about half of the asymmetry required to satisfy the experi-

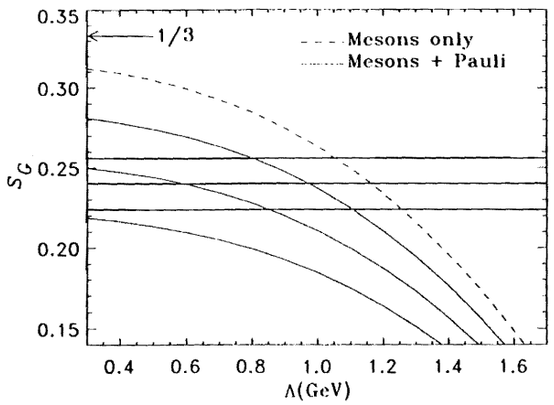

Figure 22: Gottfried sum rule with mesonic and Pauli corrections. The solid curves represent Pauli normalisation of $\mathcal{P}_N = 0.05$ (largest), 0.1 and 0.15 (smallest).

mental sum rule. For $\Lambda \approx 0.7$ GeV, the experimental sum rule can be obtained with $\mathcal{P}_N \approx 0.1$. Thus various phenomenological constraints seem to imply the need for both mechanisms.

Before finishing this discussion, we should mention some alternative explanations for the Gottfried sum rule violation. It was suggested by Martin, Stirling and Roberts [114] that there may not be any violation of the quark-parton model S_G prediction at all, if large contributions to the Gottfried integral come from the unmeasured, $x < 0.004$, region. By parameterising their valence quark distributions to be more singular at small x than what would otherwise be expected from Regge theory (namely, $q_V \sim x^{-0.5}$), and also compared with what the NMC used in their $x \to 0$ extrapolation, it was shown in ref.[114] that a value of 1/3 could be recovered. Although this more singular behaviour seems rather artificial, without data at such small x it remains a possibility. However, one problem with this hypothesis of late onset (in the sense of decreasing x) of Regge behaviour is the data from the E665 Collaboration [128], which suggests early saturation of the Gottfried sum rule, and would therefore tend to rule out this option.

It was also suggested by Kaptari and Umnikov [129] that nuclear effects in deuterium may introduce errors in the extraction of the neutron structure function from the deuteron DIS data. In particular, it was claimed that meson exchange currents in the deuteron could lead to substantial antishadowing corrections, so that F_{2n} extracted in a naive manner would be overestimated. With this correction taken into account, it was argued that a value roughly consistent with 1/3 could again be recovered. Furthermore, although expected to be small, genuine nuclear shadowing in deuterium could also introduce corrections to the naively-extracted neutron structure function [130, 75]. In ref.[131] the nuclear effects in deuterium were investigated for a variety of deuteron models. It was found that the combined effects of shadowing resulted in an increase for F_{2n} of $\lesssim 1-2\%$ for $x \sim 0.004$. Consequently, including shadowing corrections

would mean that the experimental value for S_G should be lowered from 0.24 to ≈ 0.22 when the "true" neutron structure function is used. Within the above model such a decrease can easily be accommodated by increasing the Pauli blocking correction from $\mathcal{P}_N \approx 0.1$ to ≈ 0.15, if the meson—baryon form factor cut-off is kept at the same value ($\Lambda \approx 0.7$ GeV). Of course a larger Λ could also produce a smaller S_G, but, as we saw in the preceding sections, increasing Λ would also produce a depletion in $F_{2p} - F_{2n}$ at intermediate x, together with an increase at small x. This would be contrary to the behaviour of the shadowing-corrected proton—neutron structure function difference seen in Fig.20. A reduction of $F_{2p} - F_{2n}$ at $x \lesssim 0.3$ can only be explained by a larger Pauli blocking correction, such as the one required to reproduce the corrected S_G.

6.3 The EMC Spin Effect

In the past few years a great deal of attention has focussed on the QCD improved parton model as a result of the EMC spin effect (or proton "spin crisis"). The EMC [32] extended the earlier SLAC measurement [132] of the structure function $g_{1p}(x, Q^2)$ of the polarised proton to smaller x and hence improved the accuracy with which the first moment was determined. In the naive parton model g_1 is written as:

$$g_{1p}(x) = \frac{1}{2}\sum_q e_q^2 \Delta q(x) \tag{139}$$

where

$$\Delta q(x) = (q^\uparrow + \bar{q}^\uparrow)(x) - (q^\downarrow + \bar{q}^\downarrow)(x) \tag{140}$$

is the polarised quark distribution. It is helpful to rewrite $g_{1p}(x)$ in terms of the SU(3) flavor combinations:

$$\Delta u(x) - \Delta d(x), \qquad \Delta u(x) + \Delta d(x) - 2\Delta s(x) \tag{141}$$

and

$$\Delta u(x) + \Delta d(x) + \Delta s(x). \tag{142}$$

Then the first moment of the flavor singlet piece is related to the fraction of the proton's spin which is carried by its quarks. After a smooth Regge ($x \to 0$) extrapolation of their data ($g_{1p} \sim x^{-0.12}$) EMC determined this quantity to be [32]

$$\Delta u + \Delta d + \Delta s = 0.120 \pm 0.094(stat.) \pm 0.138(syst.) \tag{143}$$

which is consistent with zero and two standard deviations from the Ellis-Jaffe hypothesis, which says that strange quarks should not play a significant role. Our present discussion closely follows that of Bass and Thomas [39], in which a detailed review of the EMC spin experiment and its theoretical interpretation was given.

This result is a violation of Zweig's rule in the flavor singlet channel [133]. As this is the only one of the three SU(3) flavor combinations which can involve the U(1) axial anomaly it seems

highly likely that this might be the source of the spin effect. If this is the case, and we strongly suggest that it is, it is clearly an important experimental problem to map out the x dependence of the axial anomaly in the inclusive DIS cross-section. We wish to discuss how important information may be obtained about this in current and future experiments, in particular we examine the (C-odd) spin dependent structure function $g_{3p}(x)$ and also the polarised deuteron structure function $g_{1d}(x)$.

As discussed in sect.3, in QCD the inclusive deep-inelastic process is described by the operator product expansion (OPE) and the renormalisation group. The interesting physics of g_{1p} is in the flavor singlet part, which receives contributions from both quark and gluon partons, viz.

$$g_{1p}(x,Q^2)\Big|_S = \frac{1}{3}\sqrt{\frac{2}{3}}\int_x^1 \frac{dz}{z}\left[\Delta q_0(z,Q^2)C_S^q(\frac{x}{z},\alpha_s(Q^2)) + \frac{1}{\sqrt{6}}\Delta g(z,Q^2)C_S^g(\frac{x}{z},\alpha_s(Q^2))\right] \quad (144)$$

The C-even, spin dependent quark $\Delta q_0(x,Q^2)$ and gluon $\Delta g(x,Q^2)$ distributions are defined with respect to the operator product expansion. Their odd moments project out the target matrix elements of the renormalised, spin odd, composite operators

$$2Ms_+(p_+)^{2n}\int_0^1 dx\, x^{2n}\Delta q_k(x,Q^2) = \langle p,s|[\overline{q}(0)\gamma_+\gamma_5(iD_+)^{2n}\frac{\lambda^k}{2}q(0)]^{GI}_{Q^2}|p,s\rangle_c, \quad (145)$$

and

$$2Ms_+(p_+)^{2n}\int_0^1 dx\, x^{2n}\Delta g(x,Q^2) = \langle p,s|[\mathrm{Tr}\; G_{+\alpha}(0)(iD_+)^{2n-1}\tilde{G}^{\alpha}_{+}(0)]^{GI}_{Q^2}|p,s\rangle_c \quad (n\geq 1). \quad (146)$$

¿From unpolarised DIS experiments we know that the gluon distribution is concentrated at small x. In polarised DIS the hard photon scatters from a gluon via a quark-antiquark pair, described in $C^g(x,\alpha_s)$. This dissipates the gluon's already small momentum so that $\Delta g(x,Q^2)$ is relevant to g_{1p} only at small x ($x \leq 0.03$) [134]. It makes a negligible contribution to the measured sum rule between $x = 0.01$ and 1, where the three constituent quarks are expected to dominate.

The clue to understanding the spin effect lies in the identification of the axial-vector current (and the higher spin axial tensors in equ.(145)) with spin. Classically the axial vector current looks like a gauge invariant operator, with the quark field operator transforming as

$$q(x) \to U(x)q(x) \quad (147)$$

and

$$\overline{q}(x)\gamma_\mu\gamma_5 \to \overline{q}(x)\gamma_\mu\gamma_5 U^\dagger(x) \quad (148)$$

under a given gauge transformation U. On the other hand, in quantum field theory the axial vector current operator is not just $\overline{q}(0)\gamma_\mu\gamma_5$ multiplied by $q(0)$. It is a composite operator which has to be renormalised and there are extra divergences which are intrinsic to the operator itself. It turns out that one cannot renormalise the axial tensor operators in a gauge invariant way so that they describe spin at the same time. In general, for a given choice of renormalisation

prescription R, the renormalised axial tensor operator differs from the gauge invariant operator by a multiple of a gauge-dependent, gluonic counterterm $k_{\mu\mu_1\ldots\mu_{2n}}$, viz.

$$\left[\overline{q}(0)\gamma_\mu\gamma_5 D_{\mu_1}\ldots D_{\mu_{2n}}q(0)\right]^R_{Q^2} = \left[\overline{q}(0)\gamma_\mu\gamma_5 D_{\mu_1}\ldots D_{\mu_{2n}}q(0)\right]^{GI}_{Q^2} + \lambda_{R,n}\left[k_{\mu\mu_1\ldots\mu_{2n}}\right]_{Q^2} \quad (149)$$

where the coefficients $\lambda_{R,n}$ are fixed by the choice of renormalisation prescription. This axial anomaly was discovered for the axial vector current in QED [135, 136].

Not only does the axial anomaly lead to a difference between the renormalised axial currents which preserve gauge invariance and chiral symmetry, but in addition the gauge invariant axial current is scale dependent (in this case the scale is Q^2). (The anomalous dimension of the first moment, Δq_0, was first calculated in QCD by Kodaira [137].) This means that one cannot derive the generators of the spin algebra SU(2) from it. It follows [138] that the gauge invariant axial-vector current and the higher spin operators which appear in equ.(145) do not describe a distribution of quark spin in the proton. One can construct a distribution which does measure spin. It differs from the physical distribution $\Delta q(x,Q^2)$ which is measured in deep-inelastic scattering by by a gauge dependent gluonic term related to the $k_{\mu\mu_1\ldots\mu_{2n}}$ in equ.(149) — the anomaly. In other words, one can say that the gauge symmetry screens the spin of the quarks.

We now compare g_1 with the other structure functions measured in deep-inelastic scattering. The axial anomaly is not relevant to the unpolarised quark distributions, which are described in OPE language by the operators $\overline{q}(0)\gamma_+(iD_+)^n q(0)$. Nor is it relevant to g_3, which is the polarised version of F_3. Since g_3 is odd under charge conjugation, and gluons are C-even, it can have no anomalous gluonic contribution. This means that it does make sense to talk about F_1, F_3 and g_3 in terms of quarks with explicit spin degrees of freedom — the clash of symmetry between gauge invariance and spin does not manifest itself in these structure functions.

It is clearly an important problem to map out the x dependence of the anomaly in g_{1p}, and a comparison between g_{1p} and g_{3p} would be the ideal way to do it. Unfortunately, the cross-section for DIS with a neutrino beam and proton target is very small — enough to make direct measurements of g_{3p} impracticable at the present time. However, if one assumes that the quark fragmentation functions are spin independent it may be possible to extract the C-odd distribution from the g_{1p} measurements by detecting fast pions from among the final state hadrons [139]. This experiment is planned by the HERMES collaboration at HERA [140].

Important information about the x dependence of the axial anomaly in polarised deep-inelastic scattering will also come from measurements of $g_{1n}(x,Q^2)$. The axial anomaly occurs only in the flavor singlet part of g_1 and therefore it will be present equally in g_{1p} and g_{1n} as a function of x. If the anomaly acts to screen the quark spin at large x in g_{1p} it follows that the same should be true in g_{1n}. The combination appearing in the Bjorken sum rule ($g_{1p} - g_{1n}$) has no flavor singlet component and is anomaly free. On the other hand, the flavor singlet component is enhanced in the deuteron structure function $g_{1d} = (g_{1p} + g_{1n})/2$, which has no isotriplet piece $\Delta q_3(x,Q^2)$. Thus the deuteron structure function g_{1d} is an ideal place to test model predictions about how the anomaly should contribute in the nucleon structure function $g_1(x,Q^2)$.

As we saw in sect.4.1 the usual quark model calculations, which do not include the anomaly, suggest that g_{1n} will change sign and become small and positive at large x [141, 20, 22]. To the

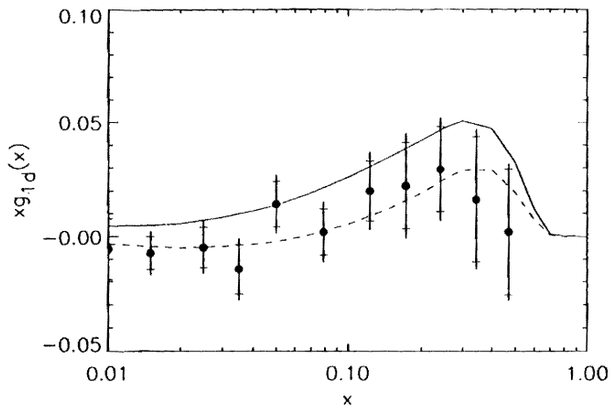

Figure 23: Prediction for the structure function of the deuteron [41] based on the bag model (with $R = 0.8$ fm) – solid curve. The dashed line shows the effect of adding a phenomenological term representing the effect of the axial anomaly on both the proton and the neutron. The data is from SMC [143].

extent that these models do not include any OZI violation, a large-x anomaly would tend to render g_{1n} negative at large x. As a specific example we consider the quark model calculation of the structure functions described in sect.4.1. As we have seen these calculations provide reasonable agreement with the unpolarised structure function data. However the bag model has not yet been extended to satisfy the U(1) chiral Ward identity. That is, it does not include an OZI violation induced by the anomaly. On the other hand it does seem reasonable that these model calculations for $g_1(x)$ might describe $g_3(x)$ at large x — i.e. correspond to a world without the OZI violations due to the anomaly.

As we saw in Fig.6 the bag model prediction for $g_{1p}(x)$ overestimates the data throughout all of the large-x region. Hence, it is tempting to associate the difference between the model results and the data as that associated with the anomaly. In this case, the same flavor singlet correction should therefore be applied to the neutron. In recent work Bass and Thomas [41] have added a purely phenomenological correction to the bag model results to fit the proton data. Adding the same correction to the prediction for the neutron and combining them to get the deuteron structure function they obtained the result shown in Fig.23. (For the present purposes we make the simple approximation that $g_{1d} = (g_{1p} + g_{1n})/2$, thus ignoring corrections due to shadowing, Fermi-motion and the D-state probability of the deuteron. These are expected to be important at the few-percent level [142, 130, 131] — well below the present experimental accuracy.) The corrected curve is in good agreement with the recent SMC measurement of the deuteron spin structure function $xg_{1d}(x, Q^2)$ [143].

To summarise the results of this section, we have discussed how one could map out the x

dependence of the axial anomaly in g_1. If the anomaly is a large-x effect then it can be isolated as a finite difference between g_1 and g_3 in the large-x bins. If it is purely a small-x effect the anomaly would be lost among the sea and gluon distributions which dominate the data at small x (say ≤ 0.1). We stress that the comparison with g_3 is the only definitive experimental test of whether the anomaly is a large or a small x effect. Certainly, it is an intrinsic part of the spin dependent quark distribution and there is no good theoretical reason to believe that it is confined to small x. We strongly urge that consideration be given to the challenging experimental problem of how to measure g_3. In the interim it would be very useful to obtain more data (with reduced errors) on the deuteron spin structure function g_1^d. This deuteron data will help constrain theoretical models of the structure functions.

6.4 Nuclear structure functions

Since the discovery by the EMC that the structure functions of nuclei did not all have the same shape [144-146] there has been considerable further investigation. On the experimental side some features of the data, like the apparently dramatic increase in the sea with mass number, have become much less distinct. Other new features such as shadowing at small x have become apparent. However the outstanding feature of the data, namely the softening of the valence quark distribution below $x = 0.7$ (at which point Fermi motion takes over) has not changed much [32, 147, 148]. In our discussion of the nuclear EMC effect in this section we will closely follow Saito et al. [149, 150].

While one would eventually like a unified theoretical treatment of all the features of the EMC data, we shall concentrate on the softening of the valence quark distribution, which is possibly its most surprising feature. Early attempts to understand this aspect of the data were based upon conventional ideas like nucleon binding, calculated in impulse approximation (IA) [151-154] — for a review see Bickerstaff and Thomas [155]. Other ideas included a possible enhancement of the cloud of virtual pions around a nucleon in a nucleus [156, 157, 68]. More exotic proposals included the possibility of multi-quark clusters [158-160] and quark percolation through the nucleus [161]. Extensive work has also been put into the idea that the nucleon may swell in the nucleus (dynamical rescaling) [162]. Our approach has been to extend to nuclei the same technique that has been successfully used to calculate free nucleon structure functions for the MIT bag model — see sect.4.1.

An earlier investigation by Thomas et al. [163] used the Guichon model [164], in which nuclear matter consists of non-overlapping bags bound in mean-field-approximation (MFA) by the self-consistent exchange of scalar (σ) and vector (ω) mesons. The results emphasised that the EMC effect provides information on the momentum *and* energy distribution of *quarks* in nuclei. In particular the usual impulse approximation based on nuclear binding was shown to significantly overestimate the suppression of the nuclear valence quarks because of the neglect of the binding of the quarks that are spectators to the hard collision. This conclusion remains valid in the more recent work which is significantly more sophisticated [149, 150]. Moreover, in that treatment it is possible to understand the experimental data quantitatively for finite nuclei.

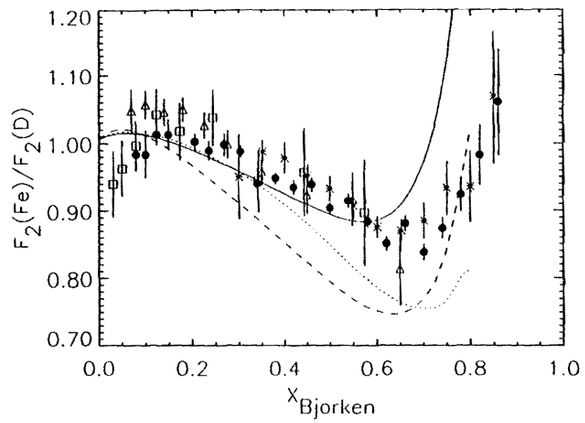

Figure 24: Local density model for the ratio of the structure functions of Fe and D. See the text for details - from ref.[150].

Because it is the energy *and* momentum distribution of quarks that matters one needs a quark model for nuclear matter. At the present stage of development such models are necessarily quite crude. We have used both the Guichon model *and* a further development along the lines of the Boguta model [165] — which enables us to fit not only the binding energy and saturation density of nuclear matter, but also its surface energy and thickness. In order to apply these models to finite nuclei we have used the local density approximation

$$q_A^{(2)}(x,\mu^2) = \int d\vec{r}\ \rho(r) \int_x dy\ f(y,\rho)\ q_N^{(2)}(\frac{x}{y},\rho,\mu^2). \tag{150}$$

Here ρ is the nuclear density distribution, $f(y,\rho)$ accounts for Fermi motion and $q_N^{(2)}$ is the twist-2 quark distribution of the bound nucleon. Note that the recent discovery that convolution fails in a more sophisticated treatment of the off-shell behaviour of the nucleon structure function — c.f. sect.4.2 — has not yet been incorporated in any calculation of the EMC effect.

In Fig.24 the solid curve is the complete calculation for the ratio of the structure functions of Fe and D (at $10GeV^2$), for the case where the free bag radius, R_0, is 0.6 fm. (There is in fact little sensitivity to R_0 [150].) For comparison we also show the most recent data from EMC, BCDMS and SLAC [32, 147, 148]. Clearly the calculation provides a semi-quantitative description of the data. Notice that one cannot use the local density approximation for deuterium. Instead a conventional convolution model which allowed for 8 MeV binding and recoil was used. The nucleon momentum distribution in the deuteron was given by the Paris potential. This particular calculation of the nuclear structure functions included no nucleon momenta higher than about 1.3 fm^{-1}. Therefore a cut-off (p_c) at 1.3 fm^{-1} was also imposed on the deuteron momentum wave function. In fact, this only affects the EMC ratio at large x [150].

The Guichon model [164] predicts the ratio shown by the dotted curve in Fig.24 which is

not quite as good. From the phenomenological point of view it is important to know whether our earlier conclusion about the inaccuracy of the impulse approximation remains true. The dashed curve in Fig.24 shows the effect of ignoring the interaction of the residual two-quark bag with the nucleus. Clearly it dramatically overestimates the EMC effect. On physical grounds this makes good sense. Deep-inelastic scattering measures the energy-momentum distribution of the struck *quark*, not the struck nucleon.

Let us now briefly summarise our conclusions and comment on what remains to be done. It is very satisfying that a quark level description of nuclear matter, together with the local density approximation and a microscopic method of calculating twist-two structure functions does give a reasonable fit to the EMC data on Fe. Although it is disappointing in some ways that the impulse approximation fails, we have seen that there is a sound physical reason for this failure, namely that it effectively assigns the binding of an entire nucleon to a single struck quark. On the positive side we can be sure that nuclear deep-inelastic scattering does tell us about the binding of quarks in nuclei.

Of course, having achieved this much one necessarily wants much more. One would like to go beyond the local density approximation which would require a quark model for the structure of finite nuclei. It is also unsatisfactory to be limited to a mean-field approximation for non-overlapping bags. Even though σ- and ω-exchange may be viewed at least partly as a macroscopic treatment of more complicated short distance processes (perhaps involving quark and gluon exchange) one would like to do better.

The MIT bag model is also a fairly crude representation of nucleon structure. One should explore the consequences of using more sophisticated models — e.g. with a more reasonable surface, a better treatment of c.m. motion and perhaps a pion cloud. (The latter might eventually help us understand why there is no evidence for an enhancement in the pion field of the nucleus in recent Drell-Yan data [166].) As we have explained elsewhere [167], we are limited to leading order QCD unless the model used has a well defined connection to QCD.

In view of our findings in sect.4.2 [43] it will be crucial to go beyond the convolution model in the treatment of nucleon Fermi motion. Finally, our analysis has not yet had anything new to say about the nuclear sea or shadowing at small x. Eventually one may hope to understand all the features of the data within a single unified theory.

7 CONCLUSION

In these lectures we have covered an enormous amount of ground, beginning with elementary kinematics, and finishing with some of the exciting problems that remain unsolved. Along the way we have seen how we can make a clear connection between familiar low-energy quark models and the parton distributions measured in high-energy deep-inelastic scattering. This is a very exciting and enouraging step along the way to meeting the ultimate challenge of nuclear physics — understanding the relationship between QCD and low-energy nuclear physics.

We have seen in detail that pions and possibly heavier mesons are needed if we are to make sense of some of the recent deep-inelastic scattering data. Certainly it is quite likely

that a meson cloud around the proton is at least partially responsible for the observed flavor asymmetry in the proton sea. In addition, a meson cloud may also play a role in the spin structure of the proton, since some of the spin (as well as flavor) quantum numbers may actually be carried by the cloud.

While still not a completely understood subject, it is clear that a fully consistent description of the spin structure of the nucleon requires a thorough re-examination of the very foundations of the parton model. To shed some light on this fundamental question we eagerly anticipate new data on the polarised structure functions of protons and neutrons with which we can compare some of the model predictions.

Finally, we have touched briefly on the important question of how the nuclear medium affects the properties of quarks inside nucleons. In particular, we now understand that microscopic structure is indeed crucial to any quantitative description of nuclear properties as seen by high-energy probes. Furthermore, improvements in calculating nuclear structure functions by incorporating relativistic effects also indicate the necessity of including both quark and nuclear degrees of freedom within a fully consistent treatment.

If we have succeeded in passing on on some of the excitement we feel about this field, then the effort of preparing the lectures has been worthwhile. With an energy upgrade underway at SLAC, new experiments planned at CERN and Fermilab, CEBAF about to come on line and ELFE (in Europe) a real possibility, this is a field that is just beginning to flower.

ACKNOWLEDGEMENTS

We would like to thank the organisers of the Shimoda meeting, particularly Professors T.Yamazaki, S.Homma, Y.Akaishi and K.Yazaki for their generous hospitality. Financial support from the JSPS, INS and the Inoue Foundation is greatfully acknowledged. We would also like to thank S.Bass, K.Saito, A.W.Schreiber, A.I.Signal and F.M.Steffens for their contributions to our understanding of the issues discussed here. This work was supported by the Australian Research Council.

References

[1] A.W.Thomas, in *Progress in Nuclear and Particle Physics*, ed. D. Wilkinson, Vol.11 (1984) 325-378.

[2] A.W.Thomas, in *Progress in Particle and Nuclear Physics*, ed. A. Faessler, Vol.20 (1988) 21-46.

[3] F.E.Close, *At Introduction to Quarks and Partons*, Academic Press, New York (1979).

[4] E.Leader and E.Predazzi, *An Introduction to Gauge Theories and the New Physics*, Cambridge (1982).

[5] T.Muta, *Foundations of Quantum Chromodynamics*, World Scientific, Singapore (1987).

[6] C.T.Sachrajda, in *Gauge Theories in High Energy Physics*, North Holland, Amsterdam (1983).

[7] F.Yndurain, *Quantum Chromodynamics*, Springer, Berlin (1983).

[8] J.L.Alonso and R.Tarrach (eds.), *Quantum Chromodynamics*, Springer, Berlin (1980).

[9] G.Altarelli, *Phys.Rep.* **81** (1982) 1.

[10] N.S.Craigie et al., *Phys.Rep.* 99 (1983) 69.

[11] J.D.Jackson, G.G. Ross and R.G. Roberts, *Phys.Lett.* **B226** (1989) 159.

[12] S.Dasu et al., *Phys.Rev.Lett.* **64** (1988) 2591.

[13] J.G.Morfin, talk given at New Directions in Neutrino Physics at Fermilab, Illinois, Sep.1988, published in *Fermilab Neutrino Phys.* **13** (1988).

[14] H.Abramowicz et al. (CDHS Collaboration), *Z.Phys* **C15** (1982) 19; **C17** (1983) 1283.

[15] M.Lissia, M.-C.Chu, J.W.Negele and J.M.Grandy, *Nucl.Phys.* **A555** (1993) 272.

[16] C.T.Sachrajda, plenary talk given at Annual Lattice Conf., Lattice '88, Batavia, IL, Sep. 1988, published in *Fermilab Lattice* **121** (1988).

[17] R.L.Jaffe, *Nucl.Phys.* **B229** (1983) 205.

[18] C.H. Llewellyn Smith, in *Proc. 1988 CAP-NSERC Summer Institute* (Singapore, World Scientific).

[19] A.I.Signal and A.W.Thomas, *Phys.Rev.* **D40** (1989) 2832.

[20] F.E.Close and A.W.Thomas, *Phys.Lett.* **B212** (1988) 227.

[21] A.W.Schreiber, A.W.Thomas and J.T.Londergan, *Phys.Lett.* **B237** (1989) 120.

[22] A.W.Schreiber, A.W.Thomas and J.T.Londergan, *Phys.Rev.* **D42** (1990) 2226.

[23] D.W.Duke and J.T.Owens, *Phys.Rev.* **D30** (1984) 49.

[24] A.D.Martin, R.G.Roberts and W.J.Stirling, *Phys.Rev.* **D37** (1988) 1161.

[25] E.Eichten, I.Hinchliffe, K.Lane and C.Quigg, *Rev.Mod.Phys.* **56** (1984) 579.

[26] M.Diemoz, F.Ferroni, E.Longo and G.Martinelli, *Z.Phys.* **C39** (1988) 21.

[27] M.Glück, E.Reya and W.Vogelsang, *Nucl.Phys.* **B329** (1990) 347.

[28] A.W.Thomas, *Nucl.Phys.* **A518** (1990) 186.

[29] A.W.Schreiber, P.J.Mulders, A.I.Signal and A.W.Thomas, *Phys.Rev.* **D45** (1992) 3069.

[30] A.Schafer, *Phys.Lett.* **B208** (1988) 175.

[31] G.Farrar and D.Jackson, *Phys.Rev.Lett.* **35** (1975) 1416.

[32] J. Ashman et al., *Phys.Lett.* **B206** (1988) 364; *Nucl.Phys.* **B328** (1990) 1.

[33] J.Ellis and R.L.Jaffe, *Phys.Rev.* **D9** (1974) 1444.

[34] A.W.Schreiber and A.W.Thomas, *Phys.Lett.* **B215** (1988) 141.

[35] H.Hogaasen and F.Myhrer, *Phys.Lett.* **B214** (1988) 123.

[36] F.Myhrer and A.W.Thomas, *Phys.Rev.* **D38** (1988) 1633.

[37] G.Altarelli and G.G.Ross, *Phys.Lett.* **B212** (1988) 391.

[38] R.D.Carlitz et al., *Phys.Lett.* **B214** (1988) 229.

[39] S.D.Bass and A.W.Thomas, *J.Phys.* **G 19** (1993) 925.

[40] R.L.Jaffe and A.V.Manohar, *Nucl.Phys.* **B337** (1990) 509; A.V.Manohar, *Phys.Rev.Lett.* **66** (1991) 289; S.D.Bass, B.L.Ioffe, N.N.Nikolaev and A.W.Thomas, *J.Moscow Phys.Soc.* **1** (1991) 317.

[41] S.D.Bass and A.W.Thomas *Phys. Lett.* **B312** (1993) 345.

[42] C.J.Benesh and G.A.Miller, *Phys.Lett.* **B222** (1989) 476.

[43] W.Melnitchouk, A.W.Schreiber and A.W.Thomas, Adelaide/PSI preprint ADP-93-210/T128, PSI-PR-93-13 (1993).

[44] P.J.Mulders, A.W.Schreiber and H.Meyer, *Nucl.Phys.* **A549** (1992) 498.

[45] V.M.Belayev and B.L.Ioffe, *Nucl.Phys.* **B310** (1988) 548.

[46] G.E.Brown and M.Rho, *Phys.Lett.* **82B** (1979) 177.

[47] A.W.Thomas, *Adv.Nucl.Phys.* **13** (1984) 1.

[48] S.Theberge, G.A.Miller and A.W.Thomas, *Can.J.Phys.* **60** (1982) 59.

[49] R.F.Alvarez-Estrada and A.W.Thomas, *J.Phys.* **G9** (1983) 161.

[50] J.D.Sullivan, *Phys.Rev.* **D5** (1972) 1732.

[51] A.W.Thomas, *Phys.Lett.* **126B** (1983) 97.

[52] A.I.Signal, A.W.Schreiber and A.W.Thomas, *Mod.Phys.Lett.* **A6** (1991) 271.

[53] E.M.Henley and G.A.Miller, *Phys.Lett.* **B251** (1990) 497.

[54] S.Kumano and J.T.Londergan, *Phys.Rev.* **D44** (1991) 717.

[55] W.-Y.P.Hwang, J.Speth and G.E.Brown, *Z.Phys.* **A339** (1991) 383; A.Szczurek and J.Speth, *Nucl.Phys.* **A555** (1993) 249.

[56] W.Melnitchouk, A.W.Thomas and A.I.Signal, *Z.Phys.* **A340** (1991) 85.

[57] K.Gottfried, *Phys.Rev.Lett.* **18** (1967) 1174.

[58] P.Amaudruz et al. (New Muon Collaboration), *Phys.Rev.Lett.* **66** (1991) 2712.

[59] M.Lusignoli and Y.Srivastava, *Nucl.Phys.* **B138** (1978) 151.

[60] G.G.Arakelyan, K.G.Boreskov and A.B.Kaidalov, *Sov.J.Nucl.Phys.* **33** (1981) 247.

[61] M.T.Jeong and Il-T.Cheon, *Phys.Rev.* **D43** (1991) 3725.

[62] A.W.Thomas, *Prog.Theor.Phys.Supp.* **91** (1987) 204.

[63] L.L.Frankfurt, L.Mankiewicz and M.I.Strikman, *Z.Phys.* **A334** (1989) 343.

[64] S.Kumano, *Phys.Rev.* **D43** (1991) 59; 3067.

[65] W.Rarita and J.Schwinger, *Phys.Rev.* **60** (1941) 61.

[66] M.Benmerrouche, R.M.Davidson and N.C.Mukhopadhyay, *Phys.Rev.* **C39** (1989) 2339.

[67] V.Dmitrašinović and R.Tegen, *Phys. Rev.* **C46** (1992) 1108.

[68] E.L.Berger, F.Coester and R.B.Wiringa, *Phys.Rev.* **D29** (1984) 398.

[69] R.L.Jaffe, in *Relativistic Dynamics and Quark-Nuclear Physics*, ed. M.B.Johnson and A.Pickleseimer (Wiley, New York, 1985).

[70] T.Hippchen, J.Haidenbauer, K Holinde and V.Mull, *Phys.Rev.* **C44** (1991) 1323.

[71] B.Kämpfer, A.I.Titov and E.L.Bratkovskaya, *Phys.Lett.* **B301** (1993) 123.

[72] A.Bodek and J.L.Ritchie, *Phys.Rev.* **D23** (1981) 1070.

[73] G.Dunne and A.W.Thomas, *Phys.Rev.* **D33** (1986) 2061.

[74] F.Güttner, G.Chanfray, H.J.Pirner and B.Povh, *Nucl.Phys.* **A429** (1984) 389.

[75] V.R.Zoller, *Z.Phys.* **C54** (1992) 425.

[76] S.Weinberg, *Phys.Rev.* **150** (1966) 1313.

[77] S.D.Drell, D.J.Levy and T.M.Yan, *Phys.Rev.* **D1** (1970) 1035.

[78] W.Melnitchouk and A.W.Thomas, *Phys.Rev.* **D47** (1993) 3794.

[79] R.Machleidt, K.Holinde and Ch.Elster, *Phys.Rep.* **149** (1987) 1.

[80] G.N.Khachatryan and Yu.G.Shakhnazaryan, *Sov.J.Nucl.Phys.* **29** (1979) 73; G.I.Gakh and A.P.Korzh, *Ukr.J.Phys.* **26** (1981) 480.

[81] R.V.Reid, Jr., *Ann.Phys.* **50** (1968) 411.

[82] M.M.Nagels, Th.A.Rijken and J.J.de Swart, *Phys.Rev.* **12** (1975) 744.

[83] M.Lacombe et al., *Phys.Rev.* **D12** (1975) 1495; *Phys.Rev.* **C21** (1980) 861; *Phys.Lett.* **101B** (1981) 139.

[84] A.D.Jackson, D.O.Riska and B.Verwest, *Nucl.Phys.* **A249** (1975) 397.

[85] G.E.Brown and A.D.Jackson, *The Nucleon-Nucleon Interaction* (North-Holland, Amsterdam, 1976).

[86] S.Deister, M.F.Gari, W.Krumpelmann and M.Mahlke, *Few Body Systems* **10** (1991) 1.

[87] A.W.Thomas and K.Holinde, *Phys.Rev.Lett.* **63** (1989) 2025.

[88] K.Holinde and A.W.Thomas, *Phys.Rev.* **C42** (1990) R1195.

[89] B.G.Yu and Il-T.Cheon, *J.Korean Phys.Soc.* **25** (1992) 571.

[90] U.G.Meissner, N.Kaiser and W.Weise, *Nucl.Phys.* **A466** (1987) 685; C.Schuren, E.Ruiz Arriola and K.Goeke, Ruhr University preprint RUB-TPII-01-92 (1992).

[91] We thank K.Holinde for a discussion relating to this point.

[92] T.Uematsu and T.F.Walsh, *Nucl.Phys.* **B199** (1982) 93; P.Hoodbhoy, R.L.Jaffe and A.Manohar, *Nucl.Phys.* **B312** (1989) 571; F.E.Close and S.Kumano, *Phys.Rev.* **D42** (1990) 2377.

[93] D.Allasia et al. (BEBC Collaboration), *Z.Phys.* **C28** (1985) 321.

[94] A.I.Signal and A.W.Thomas, *Phys.Lett.* **B191** (1987) 205.

[95] B.Betev et al. (NA10 Collaboration), *Z.Phys.* **C28** (1985) 15.

[96] M.Glück, E.Reya and A.Vogt, *Z.Phys.* **C53** (1992) 651.

[97] P.J.Sutton, A.D.Martin, R.G.Roberts and W.J.Stirling, *Phys.Rev.* **D45** (1992) 2349.

[98] S.J.Brodsky and R.Blankenbecler, *Phys.Rev.* **D10** (1974) 2973; S.J.Brodsky and G.Farrar, *Phys.Rev.Lett.* **31** (1975) 1193.

[99] P.D.B.Collins, *An Introduction to Regge Theory and High Energy Physics* (Cambridge University Press, 1977).

[100] J.Badier et al., *Phys.Lett.* **93B** (1980) 354.

[101] J.R.Bergervoet et al., *Phys.Rev.* **C41** (1990) 1435; R.Machleidt and F.Sammarruca, *Phys.Rev.Lett.* **66** (1991) 564; R.L.Workman, R.A.Arndt and M.M.Pavan, *Phys.Rev.Lett.* **68** (1992) 1653; 2712.

[102] R.Koch and E.Pietarinen, *Nucl.Phys.* **A336** (1980) 331.

[103] G.Hohler and E.Pietarinen, *Nucl.Phys.* **B95** (1975) 210.

[104] W.Grein and P.Kroll, *Nucl.Phys.* **A338** (1980) 332.

[105] O.Dumbrajs et al., *Nucl.Phys.* **B216** (1983) 277.

[106] P.M.M.Maessen, Th.A.Rijken and J.J.de Swart, *Phys.Rev.* **C40** (1989) 2226; B.Holzenkamp, K.Holinde and J.Speth, *Nucl.Phys.* **A500** (1989) 485.

[107] G.E.Brown and W.Weise, *Phys.Rep.* **C22** (1975) 281.

[108] J.F.Owens, *Phys.Lett.* **B266** (1991) 126.

[109] J.G.Morfin and W.K.Tung, *Z.Phys.* **C52** (1991) 13.

[110] D.A.Ross and C.T.Sachrajda, *Nucl.Phys.* **B149** (1979) 497.

[111] R.D.Field and R.P.Feynman, *Phys.Rev.* **D15** (1977) 2590.

[112] J.F.Donoghue and E.Golowich, *Phys.Rev.* **D15** (1977) 3421.

[113] A.D.Martin, W.J.Stirling and R.G.Roberts, *Phys.Rev.* **D47** (1993) 867.

[114] A.D.Martin, W.J.Stirling and R.G.Roberts, *Phys.Lett.* **B252** (1990) 653.

[115] S.Leone et al. (CDF Collaboration), presented at Rencontres de Moriond, Les Arcs, 1991, in *Moriond 1991: Electroweak*, p.13.

[116] A.S.Ito et al., *Phys.Rev.* **D23** (1981) 604.

[117] G.G.Arakelyan and K.G.Boreskov, *Sov.J.Nucl.Phys.* **41** (1985) 267.

[118] M.Ericson and A.W.Thomas, *Phys.Lett.* **148B** (1984) 191.

[119] E.J.Eichten, I.Hinchliffe and C.Quigg, *Phys.Rev.* **D47** (1993) R747.

[120] S.D.Ellis and W.J.Stirling, *Phys.Lett.* **B256** (1991) 258.

[121] S.Kumano and J.T.Londergan, *Phys.Rev.* **D46** (1992) 457.

[122] G.T.Garvey et al., *Measurement of* $\bar{d}(x)/\bar{u}(x)$ *in the Proton*, Fermilab Proposal P866.

[123] J.Levelt, P.J.Mulders and A.W.Schreiber, *Phys.Lett.* **B263** (1991) 498.

[124] M.Gronau, F.Ravndal and Y.Zarmi, *Nucl.Phys.* **B51** (1973) 611.

[125] M.Arneodo et al. (EM Collaboration) *Nucl.Phys.* **B321** (1989) 541.

[126] G.Preparata, P.G.Ratcliffe and J.Soffer, *Phys.Rev.Lett.* **66** (1991) 687.

[127] M.Arneodo et al. (NM Collaboration), CERN-PPE/93-117 (July 1993).

[128] M.R.Adams et al. (E665 Collaboration), Fermilab preprint (Sep. 1991).

[129] L.P.Kaptari and A.Yu.Umnikov, *Phys.Lett.* **B272** (1991) 359.

[130] B.Badelek and J.Kwiecinski, *Nucl.Phys.* **B370** (1992) 278.

[131] W.Melnitchouk and A.W.Thomas, *Phys.Rev.* **D47** (1993) 3783.

[132] G.Baum et al., *Phys.Rev.Lett.* **51** (1983) 1135.

[133] G.Veneziano, Okubofest lecture, CERN preprint TH-5840/90 (1990).

[134] S.D.Bass and A.W.Thomas, *Nucl.Phys.* **A527** (1991) 519c; J.Ellis, M.Karliner and C.Sachrajda, *Phys.Lett.* **B231** (1989) 497; S.D.Bass, N.N.Nikolaev and A.W.Thomas, Adelaide preprint ADP-90-133/T80 (1990).

[135] J.S.Bell and R.Jackiw, *Nuov.Cim.* **51A** (1969) 47.

[136] S.L.Adler, *Phys.Rev.* **177** (1969) 2426.

[137] J.Kodaira, *Nucl.Phys.* **B165** (1980) 129.

[138] S.D.Bass, Cavendish preprints HEP 92/11 (1992) and 93/2 (1993).

[139] L.L.Frankfurt et al., *Phys.Lett.* **B320** (1989) 141.

[140] HERMES Proposal, K.Coulter et al., DESY/PRC 90-1 (1990); M.Veltri et al., *Proc.Physics at HERA*, Vol. 1, 447 (1991).

[141] R.Carlitz and J.Kaur, *Phys.Rev.Lett.* **38** (1977) 673; A.Schafer, *Phys.Lett.* **B208** (1988) 175.

[142] R.M.Woloshyn, *Nucl.Phys.* **A496** (1989) 749.

[143] The SMC Collaboration, *Phys.Lett.* **B302** (1993) 533.

[144] J.J.Aubert et al. (EM Collaboration), *Phys.Lett.* **B123** (1983) 275.

[145] J.J.Aubert et al. (EM Collaboration), *Nucl.Phys.* **B293** (1983) 740.

[146] R.G.Arnold et al., *Phys.Rev.Lett.* **52** (1984) 727.

[147] A.C.Benvenuti et al. (BCDMS), *Phys.Lett.* **B189** (1987) 483.

[148] S.Dasu et al., *Phys.Rev.Lett.* **64** (1988) 2591.

[149] A.W.Thomas, K.Saito and A.Michels, *Aust.J.Phys.* **46** (1993) 3.

[150] K.Saito, A.Michels and A.W.Thomas, *Phys.Rev.* **C46** (1992) R2149.

[151] S.V.Akulinichev, S.Shlomo, S.A.Kulagin and G.M.Vagradov *Phys.Rev.Lett.* **55** (1985) 2239.

[152] S.V.Akulinichev and S.Shlomo, *Phys.Rev.* **C33** (1986) 1551.

[153] G.Dunne and A.W.Thomas, *Nucl.Phys.* **A455** (1986) 701.

[154] T.Uchiyama and K.Saito, *Phys.Rev.* **C38** (1988) 2245.

[155] R.P.Bickerstaff and A.W.Thomas, *J.Phys.* **G15** (1989) 1523.

[156] C.H.Llewellyn Smith, *Phys.Lett.* **128B** (1983) 107.

[157] M.Ericson and A.W.Thomas, *Phys.Lett.* **B128** (1983) 112.

[158] A.Krzywicki, *Phys.Rev.* **D14** (1976) 152.

[159] H.J.Pirner and J.P.Vary, *Phys.Rev.Lett.* **46** (1981) 1376.

[160] K.Saito and T.Uchiyama, *Z.Phys.* **A322** (1985) 299.

[161] O.Nachtmann and H.J.Pirner, *Z.Phys.* **C21** (1984) 277.

[162] F.E.Close, R.L.Jaffe, R.G.Roberts and G.G.Ross, *Phys.Rev.* **D31** (1985) 1004.

[163] A.W.Thomas, *Nucl.Phys.* **A532** (1989) 177.

[164] P.A.M.Guichon, *Phys.Lett.* **B200** (1988) 235.

[165] J.Boguta, *Phys.Lett.* **B106** (1981) 255.

[166] G.T.Garvey, *Nucl.Phys.* **A532** (1991) 119c.

[167] A.W.Thomas, *Nucl.Phys.* **A532** (1991) 177c.

SALGADO
8910
122
RETURN TO FERMILAB LIBRARY